Università degli Studi di Padova

Dipartimento di Ingegneria Industriale

SCUOLA DI DOTTORATO DI RICERCA IN INGEGNERIA INDUSTRIALE

INDIRIZZO IN INGEGNERIA DELL'ENERGIA

CICLO XVIII

Modeling and management of active electric distribution networks

Direttore della scuola: Ch.mo Prof. Paolo Colombo
Coordinatore d'indirizzo: Ch.ma Prof.ssa Luisa Rossetto
Supervisore: Ch.mo Prof. Roberto Turri

Dottorando: Massimiliano Coppo

31 Gennaio 2016

Abstract

In modern electricity distribution networks the vertically integrated grid paradigm is rapidly changing due to the ever growing presence of generation sources connected at lower voltage levels. These units, although having each a small size respect to the main generation plants connected to the bulk grid, in the last years are becoming more and more relevant due to their high number.

If on one hand the connection of distributed generators is encouraged by the reduction of their cost and the incentives for renewable energy policies, on the other hand this process is resulting in serious concerns on the power system's stability and security. From the bulk grid standpoint, for example, the increasing share of distributed generation in the power generation mix is becoming a key issue as regards the system's frequency regulation. Concerning the operation of the distribution system, the presence of renewable intermittent generation resources (e.g. photovoltaic) and new storage-capable loads (e.g. plug-in hybrid electric vehicles), commonly referred to as Distributed Energy Resources (DERs) is often cause of undesired voltage and current unbalances and higher network losses.

To face the mentioned issues, several national and international standard bodies stated new technical requirements for the generators connected to the distribution network with the aim of improving their integration in the grid regulation. A remarkable share of generators being connected to the distribution grid use static converters as an interface to the system: with the new standards these units need to be capable of changing their operating point supporting the grid regulation either on a local basis (e.g. frequency and Volt/Var control), as a response to remote signals from the DSO or remaining connected in presence of transient fault conditions (fault-ride-through).

As clearly appears from the decisions being taken updating the grid codes, the integration of DGs and in general of distributed energy resources (DERs) will have a key role in the future electrical grids, both for security reasons and to improve the system's efficiency. For this reason, other than the technical requirements for the grid regulation support, decisions at regulatory level are going to be taken in order to path the way towards the "smart-grid".

The mentioned challenges related with the integration of distributed resources in the grid operation highlight the importance of modelling with higher detail a distribution

network in order to represent correctly all the active users which may participate to its regulation. Having suitable simulation tools, scenarios of integration of these resources may be studied proposing strategies for their management. These aspects are addressed in this thesis in which active distribution networks are studied both from the representation and management points of view.

This thesis presents a methodology to represent distribution systems and, in general, multi-conductor networks enabling the consideration of asymmetrical systems, even in presence of specific grounding options and of circuits with different number of phases. From the management point of view, this thesis proposes a decentralised energy management system suitable for Medium Voltage networks aiming at involving DERs in the network's regulation. A coordinated control is also presented for the management of DERs connected in Low Voltage distribution networks, aiming both at limiting the voltage unbalance and aggregating services to be provided to the upstream MV grid.

Both the modelling methodology and the management strategies are simulated in several case studies to demonstrate the applicability of the proposed tools to different power systems.

Sommario

Nelle attuali reti elettriche di distribuzione, la struttura verticalmente integrata sta rapidamente cambiando a causa della crescente presenza di fonti di generazione connesse ai più bassi livelli di tensione. Queste unità, pur avendo dimensioni ridotte rispetto alle centrali tradizionali connesse alla rete di alta tensione, negli ultimi anni stanno diventando sempre più rilevanti a causa del loro elevato numero.

Se da un lato la connessione di generatori distribuiti è incoraggiata dalla riduzione del loro costo e gli incentivi per politiche a sostegno delle energie rinnovabili, d'altra parte questo processo si ripercuote sulla stabilità e la sicurezza del sistema elettrico. Dal punto di vista della rete di trasmissione, la crescente percentuale di energia prodotta nelle reti di distribuzione rispetto ai quella proveniente dalle centrali elettriche tradizionali sta diventando una questione di importanza fondamentale nel risolvere problemi come la regolazione di frequenza.

Per quanto riguarda il funzionamento del sistema di distribuzione, la presenza di risorse di generazione rinnovabile e intermittente (ad esempio fotovoltaico) e nuovi utenti in grado di accumulare energia (ad esempio veicoli elettrici connessi alla rete), comunemente indicati come Distributed Energy Resources (DER) è spesso causa di squilibri indesiderati di tensione e corrente e incremento delle perdite di rete.

Per affrontare i suddetti problemi, diversi enti normativi nazionali e internazionali hanno aggiornato i requisiti tecnici per i generatori connessi alla rete di distribuzione, con l'obiettivo di favorire la loro integrazione nella regolazione di rete.

Una quota rilevante di questi generatori connessa alla rete di distribuzione utilizza convertitori statici per interfacciarsi con il sistema elettrico: con le nuove norme, queste unità devono prevedere la possibilità di modificare il proprio funzionamento per contribuire alla regolazione di rete attraverso controlli basati su logica locale (ad esempio controllo di frequenza e tensione), sulla base di segnali inviati da remoto dal Distributore e rimanendo connessi in presenza di condizioni di guasto transitorie (fault-ride-through).

Come appare evidente dalle decisioni prese sul piano normativo per aggiornare i codici di rete, l'integrazione dei DER avrà un ruolo predominante nella futura gestione delle reti elettriche, sia da un punto di vista della sicurezza che nel migliorare l'efficienza energetica. Per questo motivo, oltre all'aggiornamento dei requisiti di connessione per la partecipazione al supporto di rete, decisioni a livello regolatorio dovranno essere prese per

favorire il passaggio alle cosiddette “smart-grid”.

Le suddette problematiche associate all’integrazione delle risorse distribuite nella gestione delle reti elettriche evidenziano l’importanza di rappresentare con elevato livello di dettaglio la rete di distribuzione, in modo da includere modelli di generatori distribuiti che possono partecipare alla regolazione. Avendo strumenti di simulazione adeguati, scenari di integrazione di queste risorse possono essere studiati, proponendo strategie per la loro gestione. Questa tesi affronta emntrambi i temi, trattando sia la rappresentazione della rete che la sua gestione.

Questa tesi presenta una metodologia per la rappresentazione di reti di distribuzione e, in generale, di reti multi-conduttore, includendo sistemi asimmetrici anche in presenza di particolari configurazioni di messa a terra e di sezioni con diverso numero di conduttori. Dal punto di vista della gestione del sistema, in questa tesi viene proposta una strategia decentralizzata per la gestione di reti di media tensione con l’obiettivo di coinvolgere i DER nella regolazione di rete. Un controllo coordinato viene proposto anche per la gestione di DER connessi alla rete di bassa tensione, con il duplice obiettivo di limitare lo squilibrio di tensione e aggregare i contributi delle risorse distribuite per fornire servizi ancillari.

I criteri di rappresentazione e gestione delle reti di distribuzione sono stati applicati ad alcuni casi studio per dimostrarne l’applicabilità in diversi sistemi elettrici.

Acknowledgements

I would like to thank my supervisor, Prof. Roberto Turri, who supported and trusted me during the past years. I really appreciated his patience and guidance, besides his friendship.

Many thanks to all my colleagues, past and present, at the Department of Industrial Engineering, especially to Riccardo and Antonino for the fruitful discussions and the good time spent together at the office and outside.

Special thanks to Mattia and to the people of the Center for Electric Power and Energy at the DTU who made possible my external stay in Denmark: it was a very fruitful and exciting opportunity to get to know other researchers while, of course, enjoying the Friday Bar.

I can't find the words to thank my parents, Fiorenzo and Monica, who believed in me from the beginning and who motivated and supported me all of these years. I can only hope to have their same strength and determination in my future.

Finally, I want to thank Anna, with whom I shared several years now and would like to spend many more. I dedicate this work to her and I hope I'll be able to return the support I received from her, along with all the time that took to bring me to this point.

Contents

List of Figures

List of Tables

List of abbreviations and symbols

The main abbreviations and symbols used in the thesis are listed below. Other less frequent notations are defined in the text.

Abbreviations

AD	Active Demand
AVR	Automatic Voltage Regulation
DER	Distributed Energy Resource
DG	Distributed Generator
DMS	Distribution Management System
DSI	Demand Side Integration
DSO	Distribution System Operator
EES	Electric Energy Storage
EMS	Energy Management System
EV	Electric Vehicle
GC	Generation Curtailment
ICT	Information and Communication Technologies
LV	Low Voltage
LVNC	Low Voltage Network Controller
MAS	Multi Agent System
MV	Medium Voltage
NS	Network Supervisor
OLTC	On Load Tap Changer
OPF	Optimal Power Flow
$P_{3\Phi}$	Three-phase power
PCC	Point of Common Coupling
PHEV	Plug-in Hybrid Electric Vehicle
PV	PhotoVoltaic
TCDF	Transmission Congestion Distribution Factors
TSO	Transmission System Operator
V2G	Vehicle-to-Grid
VPP	Virtual Power Plant
VUF	Voltage Unbalance Factor (negative sequence)
VUF_O	Voltage Unbalance Factor (zero sequence)

Matrices and vectors

$\mathbf{Y_{Branch}}$	Branch element admittance matrix
$\mathbf{Y_{Prim}}$	Primitive admittance matrix
$\mathbf{A}$	Incidence matrix
$\mathbf{B}$	Topology matrix
$\mathbf{B}_(\mathbf{P}, \mathbf{S}, \mathbf{T})$	Topology sub-matrices for Primary, Secondary and Tertiary windings
$\mathbf{Y_T}$	Transformer's admittance matrix
$\mathbf{Y_0}$	Open-circuit losses admittance
$\mathbf{Y_O}$	Common node O admittance
$[\mathbf{I}]$	Identity matrix
$[\mathbf{0}]$	Zeros matrix
$\mathbf{Y_{Prim(f)}}$	Full primitive admittance matrix (including the common node O)
$\mathbf{A_{(f)}}$	Full incidence matrix (including the common node O)
$\overline{\mathbf{Y_{T(f)}}}$	Full transformer's admittance matrix (including the common node O)
$\overline{\mathbf{Y_T}}$	Unconnected transformer's admittance matrix
$\mathbf{C}$	Turns ratios matrix
$\mathbf{Y_{network}}$	System's admittance matrix
$\mathbf{E}$	Voltages vector
$\mathbf{I}$	Currents vector
$\mathbf{I_{SL}}$	Slack-bus currents
$\mathbf{E_{SL}}$	Slack-bus voltages
$\mathbf{\Delta I_{SH}}$	Shunt-elements correction-currents
$\mathbf{E_{SH}}$	Shunt-elements voltages
$\mathbf{I_G}$	Generator buses currents (including slack-bus and PV buses)
$\mathbf{\Delta I_L}$	Load buses currents (PQ buses)
$\mathbf{E_G}$	Generator buses voltages (including slack-bus and PV buses)
$\mathbf{E_L}$	Load buses voltages (PQ buses)
$\mathbf{\Delta I_{PV}}$	Correction-currents at PV buses
$\mathbf{E_{PV}}$	PV buses voltages
$\mathbf{B_{1ph}}$	Topology matrix for 3-phase to 2-phase transformer in single-phase configuration
$\mathbf{B_V}$	Topology matrix for 3-phase to 2-phase transformer in V-configuration
$\mathbf{B_{Scott}}$	Topology matrix for 3-phase to 2-phase transformer in Scott-configuration
$\mathbf{ed}$	Electrical distance matrix
$\mathbf{\Delta V_j}$	Voltage variations at buses $j = 1 \dots n$
$\mathbf{\Delta I_B}$	Balancing currents triplet
$\mathbf{\Delta I_C}$	Corrected balancing currents triplet
$\mathbf{\Delta I_P}$	Currents triplet for active power constraint

Symbols

$X*$	Complex conjugate
X^T	Transposed vector/matrix
k_Z	Shunt-element's constant impedance share
k_I	Shunt-element's constant current share
k_P	Shunt-element's constant power share
$m_{P,S,T}$	Turns ratio for Primary, Secondary and Tertiary windings
ΔP_j	Active power variation at bus j
$k_{amp\%}$	Percent ratio between actual and nominal currents
$\Delta \mathrm{P_{av}}$	Active power variation availability
$\Delta \mathrm{P_{cap}}$	Active power variation capability
$\Delta \mathrm{Q_{av}}$	Reactive power variation availability
$\Delta \mathrm{Q_{cap}}$	Reactive power variation capability
$\mathrm{S_n}$	Rated apparent power
$\mathrm{P_{act}}$	Actual active power
$\Delta \mathrm{P_{TOT}}$	Total active power variation
$\Delta \mathrm{P_{p1,p2}}$	Active power variation at different prices p1 and p2
obj_V	Voltage regulation objective
$I_{\%}$	Maximum allowed line loading
ΔP_{req}	Request for active power regulation
ΔQ_{req}	Request for reactive power regulation
Δp	Price variation
$\mathrm{P_n}$	Nominal active power
$\mathrm{Q_n}$	Nominal reactive power
$\mathrm{k_u}$	Utilisation factor
$\mathrm{k_{day}}$	Power profile on daily basis
$\mathrm{k_{week}}$	Power profile on week basis
$\mathrm{k_{month}}$	Power profile on month basis
$\mathrm{k_{year}}$	Annual growth factor
$\mathrm{P_i}$	Instantaneous active power
$\mathrm{Q_i}$	Instantaneous reactive power
I_{inv}	Inverter's injected currents
I_m	Measured currents
ΔS_k	Complex power variation on phase k ($k = a, b, c$)
E_{PCC_k}	Phase-neutral voltage on phase k ($k = a, b, c$)
V_d	Direct-axis voltage
V_q	Quadrature-axis voltage
I_d	Direct-axis current
I_q	Quadrature-axis current
V_{set}	Voltage set-point for MV regulation
$\Delta V_{set-point}$	Voltage variation set-point for local control

Chapter 1

Introduction

Due to the renewable energy encouraging policies applied by many countries in the last decade, the number of distributed generators (DG) has strongly increased, leading to a change in the network paradigm. As a consequence, electrical distribution networks have become more and more active, meaning that increasing shares of energy are produced in these system. This process is involved in the transition from the passive distribution networks to *smart grids*, for which a number of new standards and technologies will be necessary in order to tackle the challenge of controlling those systems. In this chapter, some of the concepts related to active networks are recalled focusing on the actual trends in the DG development in the electricity systems. An overview of the regulatory context and the recent updates in the grid codes both at national and international level are summarized to discuss the actions taken from the standard bodies to face the DG integration challenge. A brief summary of the ongoing projects on the smart grid development in Europe is also reported with some data taken from up-to-date reports. Finally, the case of the Italian regulatory resolution aimed at increasing the integration of DGs in the ancillary services provision is recalled to give an example of future pathway to the smart-grid exploitation in the energy market environment.

1.1 Distribution networks evolution

Since the electricity market liberalisation process started, about a decade ago, electric power systems are undergoing a clear change of paradigm from the traditional vertically integrated structure in which few large scale generation plants provide the production for a mainly passive grid to a system where generators are embedded in the distribution network, closer to the loads.

While the diffusion of Distributed Generators (DGs) increases, new challenges arise from the grid operation standpoint and from the economic point of view too. Given the increased environmental awareness, a growing attention is being paid to the electricity supply efficiency and sustainability, other than economics.

Distributed generators usually have sizes between few kWs to few MWs, therefore they are going to be connected near the loads in distribution networks and typically are associated with renewable energy sources like photovoltaic or wind which can be unpredictable. Among other sources, photovoltaic, due to the modules price decline and the intensification of incentives for the connection of new units to the grid, has seen an exceptional increase in its power production, reaching a total world installed power of 178 GW, of which 88 GW in Europe alone [1,6].

As reported in Figure 1.1, the strongest effort in installing new PV plants was made in European countries, but a strong increase of the Asian market already started, where Japan set a national goal of 60 GW of PV capacity by 2030 [7].

A challenge to the electrical power systems operation is given by the fact that a large share of the installed capacity is connected to Low Voltage networks, also due to a reduction of the installation price. For instance, [7] reports a 70% share of PV installations in the Low Voltage network in Germany.

In Italy a similar situation is observed, standing the statistical report on photovoltaic released in 2014 by the Italian Energy Services Manager (GSE in Italian) [2]. In Figure 1.2, taken from the report, it could be seen that the number of installed units increased dramatically starting from 2011 (when the number of PV plants more than doubled the one from the previous year). As reported in the chart and further expressed by Table 1.1, the average power of the units installed in Italy is in the range of few kW, especially those in the last two years of this analysis, confirming the fact that most of DGs powered by this technology are installed in LV networks.

Table 1.1: Average installed PV power in Italy cumulative and per year from 2008 to 2014 [2].

	2008	**2009**	**2010**	**2011**	**2012**	**2013**	**2014**
Average P [kW]	13.9	16.5	22.3	39.2	34.6	30.5	28.7
Average P (year) [kW]	13.5	18.2	27.5	53.4	25.9	13.0	8.1

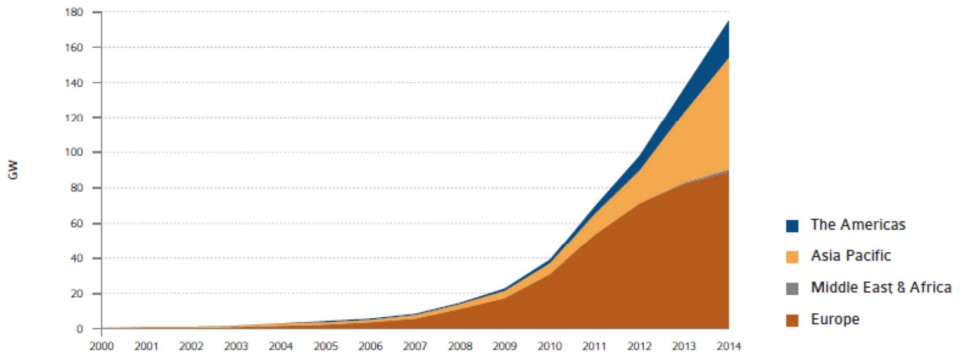

Figure 1.1: Installed PV capacity in the world by country [1].

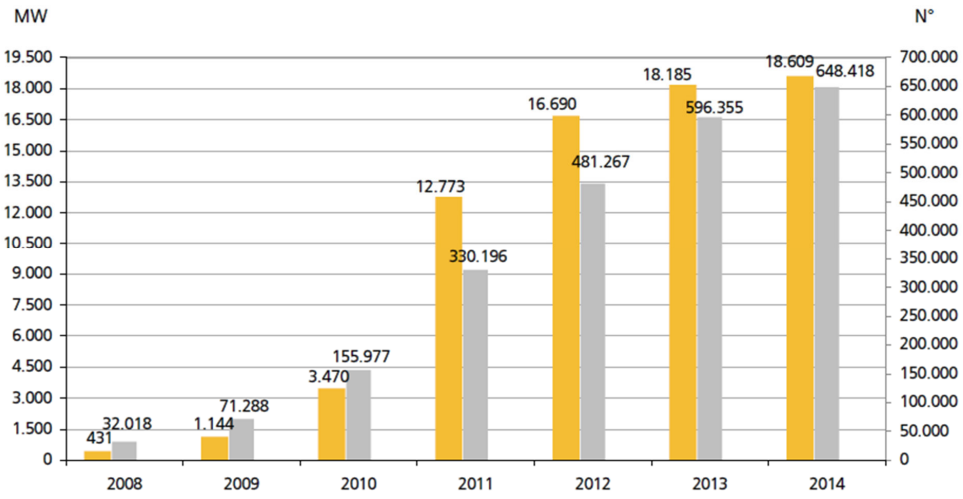

Figure 1.2: Evolution of the PV installed capacity in Italy between 2008 and 2014 [2].

1.2 Grid connection rules for Distributed Generation

As a result of the high increase in Distributed Generation (DG) penetration in Medium and Low Voltage systems, several challenges arise regarding either technical, commercial and regulatory standpoints [8].

On the technical point of view, modern power systems are likely to experience issues regarding voltage deviation, power quality (e.g. voltage sags, harmonic distortion), protection (e.g. loss of selectivity, unintentional islanding) and stability.

In order to support the development of active distribution networks towards a mature smart-grid scenario, innovative concepts for the system management need to be implemented involving signals communication to the active users connected. This process involves the activation of new market frameworks in which the distributed resources may offer ancillary services but at the same time requires a coordination among the regulatory actions taken by the standard bodies updating the rules for connection to the network.

Starting few years ago, several national and international standard bodies updated their grid codes with new technical specifications which introduced additional requirements to the distributed generators connected to distribution networks, especially those interfaced through static converters.

Although those requirements may be slightly different from one case to another, all of the updated standards share a common objective that is making DGs more responsive to the actual working conditions of the network, participating to its management by supporting voltage and frequency and even considering the control by remote signals.

A summary of the common requirements to distributed generators stated by the latest updates in the grid codes are reported in Table 1.2, focusing in particular on the Italian and German cases and on the decisions taken at European level by CENELEC [9–15]. The table lists several of the requirements for generators, which can be summarized as:

Table 1.2: Requirements for generators interfaced with the network through static converters.

	Europe	**Germany**	**Italy**	**Europe**	**Germany**	**Italy**	**Europe**
Standard	EN 50438	VDE-AR-N 4105	CEI 0-21	EN 50549-1	BDEW Technical Guideline	CEI 0-16	EN 50549-2
Applicability	I $\leq$ 16A	LV	LV	LV	MV/HV	MV/HV	MV
enlarged f range	✓	✓	✓	✓	✓	✓	✓
P(f)	✓	✓	✓	✓	✓	✓	✓
fixed p.f.	✓	P$\leq$3.68 kVA	3 kW$\leq$ P $\leq$6kW	✓	✓	✓	✓
p.f. (P)	✓	P>3.68 kVA	P$\geq$ 3kW	✓	✓	✓	✓
Q (V)	✓	×	P>6 kW	✓	✓	✓	✓
P remote	×	P>100 kW	P>6 kW	✓	✓	P>100 kW	✓
Remote trip	×	×	✓	✓	✓	✓	✓
LVRT	×	×	✓	✓	✓	✓	✓
OVRT	×	×	×	✓	×	✓	✓

* The meaning of the first column abbreviations can be found in the text below.

- Frequency regulation action, acted by enlarged frequency operative range and with P(f) droop characteristics;
- Voltage support action, performed by a reactive power provision either with fixed p.f., active-power-dependant p.f. or reactive power as a function of the local voltage (Q(V) droop);
- Remote control availability, obtainable through signals communication by the DSO, for active power management (i.e. P curtailment) or protection trip on remote signal;
- Transient voltage deviations tolerance, identified as Ride-Through capabilities, both in case of reduction (LVRT) or increase (OVRT).

The necessity of integrating the distributed generators in the grid support strategy was highlighted in 2011 by the German VDE-FNN committee with a study about the consequences of restrictive frequency thresholds to Low Voltage generators [16]. The study pointed out that without a change in the rules for connection of active users, in case of frequency values exceeding 50.2 Hz all of the LV connected DGs were going to be automatically disconnected, causing an instantaneous power loss estimated in about 20 GW just from photovoltaic generators in the German area. Such event could seriously compromise the system stability, so the updates in the German standard for connection to LV networks [11], requiring grid supporting actions from DGs, were necessary, as it was the

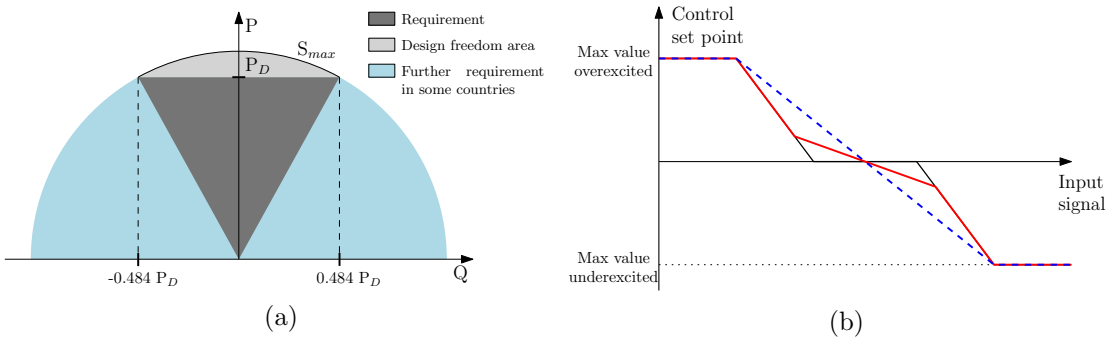

Figure 1.3: Capability areas (a) and characteristic (b) for reactive power provision by DGs as stated by the standard EN50549.

retrofitting of generators already connected to the grid (the VDE-FNN study estimated 315 000 units that needed to be converted).

After the updates in the German grid code to face the mentioned "50.2 Hz problem", other countries updated the respective standards, especially in Europe. Among others, the Italian Electrotechnical Committee (CEI, in Italian) released, starting from 2012, very innovative rules for the connection of generators to LV and MV distribution networks, adding several requirements for the DGs aiming at an increase in their network support action. The latest update was released in September 2014 and included, among other prescriptions, the requirements listed in Table 1.2. It should be noted that respect to the German situation, converters interfacing DGs in Italian LV networks already need to be capable to perform a Volt/Var regulation on a local basis and to deal with external signals coming from the DSO for the active power curtailment or for protection tripping.

At European level, CENELEC released updated requirements for generating units connected to MV [15] and LV networks [13,14] (note that the latter covers LV installations with phase current below 16 A). The technical specifications 50549 (divided in two parts, for MV and LV level respectively) were released at the start of 2015, requiring a complete set of actions to be available from DGs. These specifications trace the guidelines for the development of the national grid codes revision, setting the control characteristics to implement the grid supporting actions. Converters are expected to remain connected to the grid with an enlarged frequency range between 47.5-51.5 Hz (maximum values are set at 47-52 Hz but not mandatory), with a droop function causing an active power reduction, when frequency overcomes the 50.2 limit, with a slope between 2% and 12%. Along with the stability support action, reactive power provision for Volt/Var local regulation is also considered, adopting the capability areas depicted in Figure 1.3a and control function of the type in Figure 1.3b, which can be used, with suitable control variables to be selected by the DSO, for the requested regulation mode (e.g. Q or p.f. as function of V or P).

In the United States, IEEE has amended the standard IEEE 1547 regulating the DER interconnection systems, permitting the converters to remain connected to the grid with wider voltage and frequency ranges for ride-through purposes and voltage support [17].

In [3] the state-of-the-art of the services that may be provided by inverter-interfaced PV units, reported in Figure 1.4, is discussed, in compliance with the new grid codes. It should be noted that many of the functionalities offered by the converters are already taken into account in the rules for connection above mentioned, but in most of the cases the adoption of these controls is up to the local DSO discretion [3].

Regarding the grid forming capability of the converters connected to a distributed source as in the example depicted in Figure 1.4, a recent update of the mentioned rules for connection of DGs to the LV system in the Italian grid was released in December, 2014, stating new requirements for units equipped with storage as reported in Figure 1.5 [4]. In Figure 1.5a the capability area required for bi-directional converters connecting storage units to the LV grid is reported, showing possibly different active power capabilities for charging and discharging (P_{CMAX} and P_{DMAX} respectively) and the required range of variation of the reactive power respect to the actual working point. While other requirements set for all the DGs discussed above are still valid, a new frequency regulation action, shown in Figure 1.5b, needs to be accounted for by storage units: with the generators convention, if the storage is absorbing power from the grid for recharging (negative P semi-plane) but the frequency falls below 49.7 Hz, the converter is required to change gradually the active power exchanged, even changing its sign, up to the capability range for the discharging function.

1.3 Active networks management

Standing the actual trends in the generating sources diffusion in distribution networks and the updates in the grid codes discussed previously, going into the future a key role in the network's management will be played by the coordinated control of those units. A term that has been widely used to define modern electrical distribution power systems is "active network".

An active distribution network should allow the connection of generators and loads

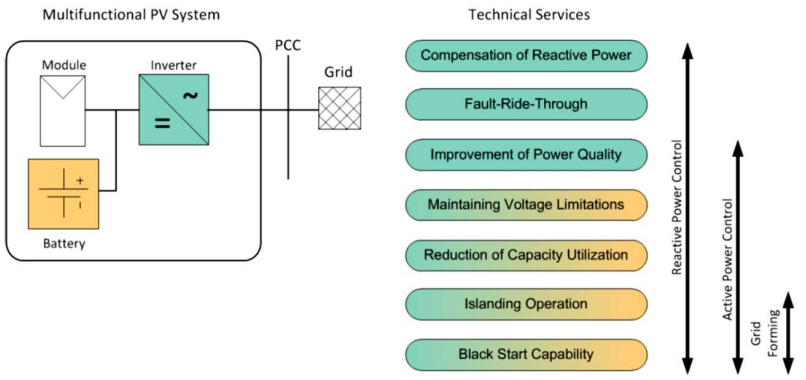

Figure 1.4: Technical services from inverter-interfaced active users [3].

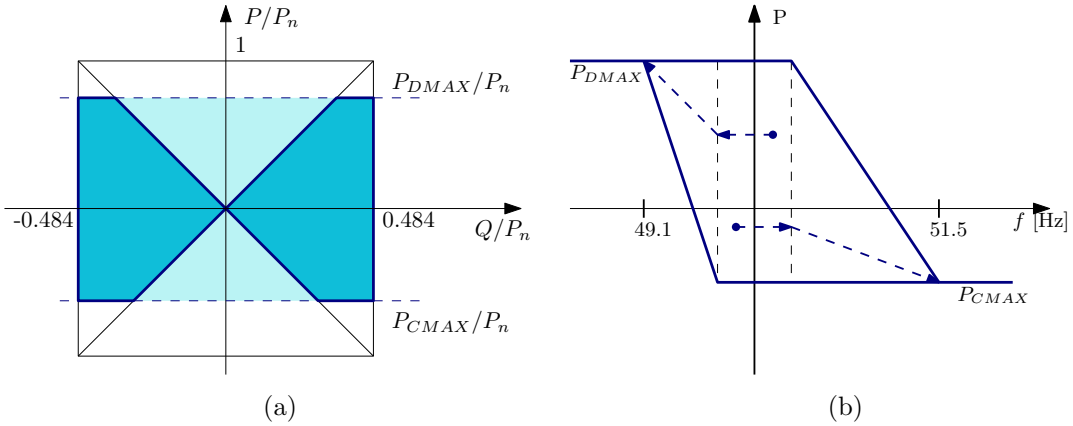

Figure 1.5: Capability area (a) and P(f) (b) for storage capable units stated by the CEI-021 update of 2014 [4].

that take decisions in real time about their operation [18]. To implement this concept, electrical systems will need to increase the connectivity between the DSO and the users through Information and Communication Technologies (ICT). As a result, in the future networks it is expected that the system management will be implemented coordinating the bulk grid operation with the local actions taken at distribution level by aggregates of distributed energy resources (DERs). In [18] the concept of virtual utility is used to define an infrastructure integrating several DGs for the provision of energy (electricity and heat), controlled by a central unit called Energy Management System (EMS). By running an optimization of the DERs working point, a virtual utility can participate to the energy market, possibly competing with traditional plants for the provision of ancillary services. The same concept is used in [8], speaking about Virtual Power Plants (VPP) which should have the function of aggregating DGs and loads in order to participate to the market. In this perspective, the multi-microgrid concept is introduced, consisting in a set of secondary substations connected to the same Medium Voltage network and acting like active cells in a hierarchical control architecture.

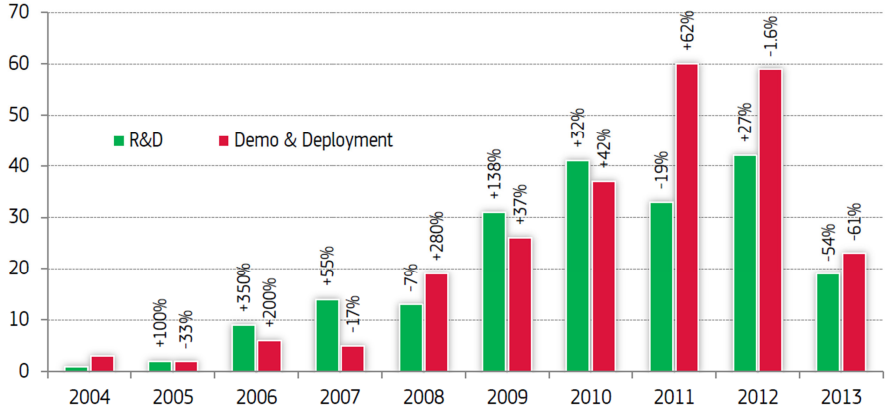

Figure 1.6: Number of smart grid projects in Europe and stage of development per year [5].

Given the challenges and opportunities associated with the increasing amount of DERs, a large number of research projects are being developed in Europe. The 2014 outlook on Smart Grid projects released by the European Commission Joint Research Centre (JRC) [5] reported a total of 459 R&D and Demo & Development projects averaging a budget of 7.5 M€ each and involving 578 sites of implementation.

In the UK several projects about smart grids have been funded by Ofgem during the period 2010-2015 through the Low Carbon Networks (LCN) Fund. Those projects, sponsored by the distribution network operators (DNOs) propose potential technical and commercial solutions to face some of the challenges in distribution networks [19]. An example is the Customer-led Network Revolution (CLNR) project resulted in the deployment of an Active Network Management system for the control of Electrical Energy Storage (EES), voltage regulation, real-time thermal rating and Demand Side Response interventions [20]. Another project dealing with the management of distribution networks is the Accelerating Renewable Connections (ARC) project aimed at improving the integration of DGs through novel commercial and technical approaches [21].

As could be seen from the chart reported in Figure 1.6 taken from the 2014 JRC's outlook, the number of smart grid projects per year dramatically increased starting from 2009, registering a prevalence of Demo & Development ones, indicating that some of the smart-grid technologies involved reached a mature stage, ready for implementation. This increase is ascribable to large publicly-funded projects like those mentioned above regarding the Low Carbon Network Fund in the UK.

Smart grid applications considered in those projects mainly involve the following areas:

- Smart network management: increase of flexibility of the electricity grid though *observability* (e.g. smart metering, real-time monitoring, fault identification) and *controllability* (e.g. voltage and frequency controls, controllable inverters, auto-reconfiguration of the network, voltage conditioning MV/LV transformers);

- Integration of large scale RES: integration of renewable energy sources in the transmission grid (e.g. planning tools for market integration, ancillary services from DSOs to TSOs and forecast tools);

- Integration of DERs: improving the control of DERs for enhancing their integration in the system (e.g. ancillary services provision, production forecast, advanced protection devices and new control architectures centralised or decentralised for their integration);

- Aggregation (VPP and Demand Response): implementation of VPP and Demand Response concepts to face grid constraints and market signals;

- Smart customers and smart home: proposal of appliances and tariff schemes for active participation of consumers;

- Electric Vehicles (EVs) and Plug-in Hybrid Electric Vehicles (PHEVs) integration in the electricity network, considering Vehicle-to-Grid (V2G) services;
- Smart metering: investments for the installation of smart meter devices on the network.

The map reported in Figure 1.7 from [5] shows the number of implementation sites weighted with the respective budget in the European countries. It could be seen that EV and V2G projects are mainly being implemented in central Europe and in the continent extremities (e.g. Italy, Spain, Ireland, Finland) while Smart Customer projects have larger shares in the west-side and northern part of Europe. Large budget shares are devoted to DERs integration projects especially in countries with availability of wind (Denmark) or solar (Italy, France) resources.

1.4 Regulatory context for active users participation to grid management

In the previous two sections the technical aspects related with the power systems improvements were addressed, regarding respectively the grid codes update and projects testing new approaches to the grid operation. These solutions, in order to be effective in the transition towards the smart-grids, need necessarily to be supported by regulatory decisions aimed at integrating the resources in a modern energy market context. Nowadays, RES

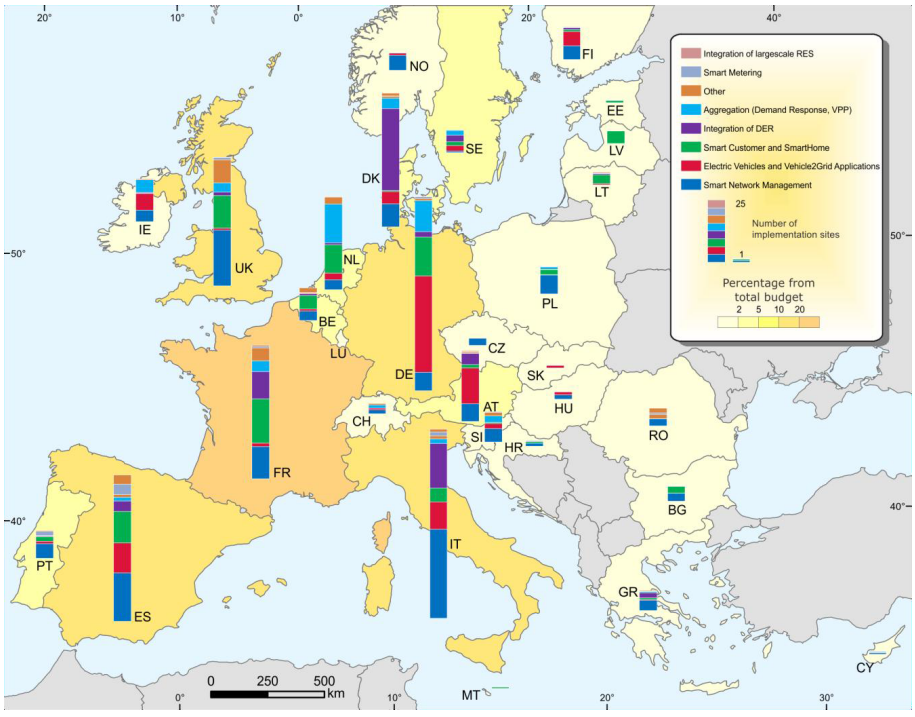

Figure 1.7: European map of implementation sites of smart grid projects per application respect to the respective budget [5].

feed significant shares of energy demand, resulting in a reduction of the market energy price and, on the other side, a consistent increase of expenditures for ancillary services due to RES inherent not programmability.

This is the reason why the Italian Regulatory Authority for Electricity Gas and Water (AEEGSI) started analyzing the different options towards the implementation of a future regulatory framework where distributed generators and loads are expected to play an active role in supporting bulk system balancing and could therefore compete with traditional power plants in offering ancillary services. The Italian Authority with a specific resolution (DCO 354/13 [22]) proposed three possible market models for enabling the provision of ancillary services by DGs connected to the distribution network, pictorially shown in Figure 1.8.

The first market model, depicted in Figure 1.8a assumes that the DG units connected to the distribution network have the possibility to participate directly to the Ancillary Services Market (ASM) presenting offers to the TSO, while the local services are managed through the DSO's direct call. The DSO verifies the sustainability of the modified power flow and in case of contingencies requests local ancillary services to the DGs.

In the second market model, shown in Figure 1.8b, the DSO aggregates the contributions coming from the active users connected to the distribution network verifying the technical feasibility of the solution and makes an offer to the ASM, therefore TSO should not act directly on the DGs connected on the distribution network. This model assumes the presence of an Ancillary Services Market for Distribution network (ASM-D) through which the users present their offers.

The third market model, reported in Figure 1.8c, hypothesizes that the DSO is responsible for maintaining a scheduled power profile at the HV/MV interface, without offering ancillary services on the ASM. The solution of contingencies occurring within the distribution network is performed by the DSO through an ASM-D like in the previous case. In this way the bulk system services operated by the TSO are separated from the local services for which the DSO is in charge, so reducing the volumes traded on ASM.

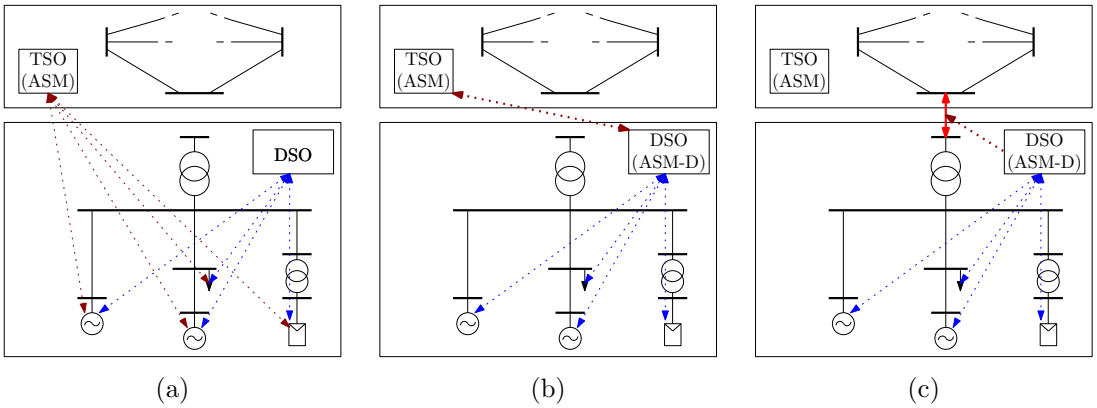

Figure 1.8: Market models for the integration of ancillary services from DGs as for AEEGSI DCO 354/13.

As highlighted by the decision taken by the Italian Authority, the provision of services for the power system is both an opportunity and a necessity. The share of not programmable energy sources that are making the balance between load and generation more expensive and risky causes the necessity. The opportunity is represented by the availability of more flexible resources embedded in the system that increase the number of players in the market and make it possible a wider participation of customers. For this reason, aspects like representing in more detail the distribution grid and proposing solutions for its management are becoming of fundamental importance in order to continue the study of more efficient and reliable ways of operating the system.

1.5 Thesis objectives and overview

The issues related with distribution networks operation in presence of an ever growing share of distributed generators are addressed by this thesis which has the aim of developing a methodology for the representation of multi-conductor networks (enhancing the detail level in the network modelling) and proposing controls for the Medium Voltage and Low Voltage networks management aiming at allowing DERs to provide ancillary services.

The second chapter presents in detail a power flow methodology developed to consider generic multi-phase circuits, including the possibility of interconnecting systems with different voltage level and number of phases. The latter feature is made possible with a self-developed generalized approach for the representation of multi-phase transformers, allowing to model a unit connecting a generic number of buses each with a generic number of phases. Some applications are shown including the results of collaborations with other Institutions contributing to the final development of the methodology.

A management strategy for Medium Voltage active networks is presented in the third chapter. It consists in a decentralised Distribution Management System in which a central unit evaluates a suitable set-point for the On-Load-Tap-Changer (OLTC) in Primary Substation and active and reactive power requests to the DERs clustered through an adaptive-area selection. This procedure, in part developed within the Italian research project "ATLANTIDE", was applied to several case studies presenting possible scenarios of implementation.

In the fourth chapter, a management scheme for Low Voltage networks is proposed, considering a central unit, placed at the PCC which evaluates P and Q signals for the DERs in order to pursue the voltage unbalance mitigation and, in case, the provision of ancillary services to the MV grid. The applications of this methodology highlight the importance of suitably coordinate the local intervention of each DER.

The two management strategies are then simulated together in an example of coordinated DMS for MV and LV networks regulation in the fifth chapter.

Finally, the most important achievements and perspectives for future developments are discussed in the sixth chapter.

The case studies considered throughout this research were implemented in several network models (duly detailed in the Appendices) in order to further demonstrate the applicability of the methodologies to systems with different characteristics and peculiarities.

Chapter 2

Multi-conductor power flow analysis

Large part of the ever-growing Distributed Generation (DG) diffusion is taking place in Low Voltage networks, which generally have an asymmetrical structure with customers' powers unevenly distributed on the phases. For this reason, in order to study the effect of the DG penetration in these systems, it's important to rely on a computational tool capable of dealing with a generic number of phases mutually coupled. Furthermore, an important feature to be considered is the flexibility in allowing the implementation of customized control strategies, which may be included in a smart grid. This chapter firstly discusses the state of the art in the power flow calculation for distribution networks, then the development of a network analysis tool allowing the computation of the steady-state power flows in a generic multi-phase asymmetric network is presented, considering also an original generalized approach to the transformer modelling.

2.1 Power flow solution methods for distribution grids

Given the growing importance that low voltage networks play in the modern power systems, several research works were presented lately regarding the improvement of existing methods for the power flow calculation, dealing with the peculiarities of the distribution networks [23]. These systems may arise several challenges when considered for power flow calculation, for example modelling of single-phase appliances, voltage control equipments, asymmetrical lines and specific transformer connections. A tool capable of dealing with all the cited features can offer the support needed in studying the behaviour of the whole distribution grid, helping the research of new solutions to include the small-scale distributed generators (DGs) in innovative network management strategies. A wide number of algorithms have been developed to date, but they are generally classified in three groups: backward/forward (BF) sweep, Newton-type and Gauss-Seidel (or fixed-point) methods. In the following, a brief recall of the main algorithms for the power flow solution

in distribution networks is made.

2.1.1 Backward-forward sweep method

This kind of algorithm is widely suggested as the preferred solution in case of distribution networks with the necessity of considering multi-phase circuits because of its robustness and simplicity of implementation. The BF sweep method was initially developed for radial systems [24] and then further refined to solve weakly meshed systems [25]. Its application was also proposed to solve a three-phase power flow problem [26] and also including four-wire systems [27].

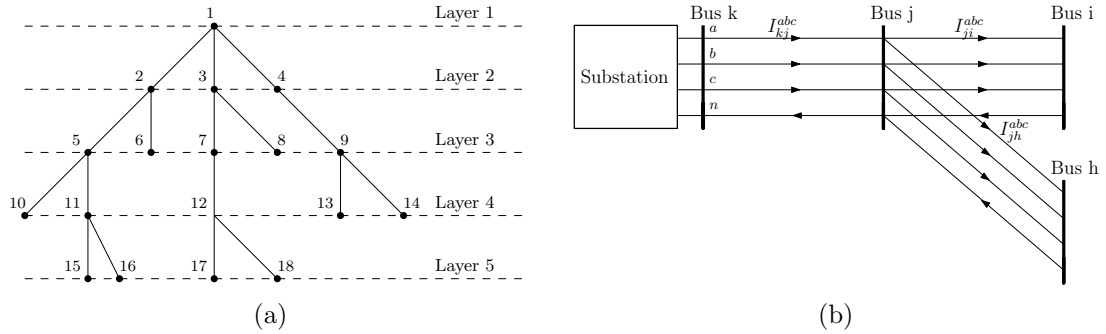

(a) (b)

Figure 2.1: Backward/Forward sweep method: busbar numbering (a) and circuit design (b).

This kind of formulation relies on the approach used in power system design, by a sequential application of the Kirchhoff's voltage and current laws to the network branches. The first requirement for the BF sweep application is the initialization of the busbar layers in a structure which can be seen in Figure 2.1a. With the system defined in such a way, the following steps are followed to calculate the power flow:

1. calculation of the branch impedance matrix (in case of multi-phase circuit like the one in Figure 2.1b)

2. the nodal currents are calculated starting from the complex powers of loads or generators. For the bus k the currents associated to each phase is:

$$I_k^{abc} = \frac{S_k^{abc}}{E_k^{abc\ *}} \tag{2.1}$$

   where S is the complex power and E^* is the complex conjugate of the phase-neutral potential, in each phase (a, b and c).

3. *Backward-sweep*: calculation of the branch currents summing the nodal contributions starting from the bottom layer up to the root node. For the generic branch $k - j$, the flowing current can be calculated as:

$$J_{kj}^{abc} = I_k^{abc} + \sum_{m \in \Omega} J_m^{abc} \tag{2.2}$$

where J^{abc} is the total current flowing in a branch and Ω is the set of branches connected to branch $k-j$.

4. *Forward-sweep*: calculation of the busbar voltages starting from the upmost layer towards the bottom one. For example, for bus j the voltage is given by:

$$V_j^{abc} = V_k^{abc} - Z_{kj} J_{kj}^{abc} \tag{2.3}$$

5. Convergence is checked for each of the bus voltage magnitudes and angles comparing them with the previous iteration values. If not reached, the procedure returns to step 2.

As could be seen in Figure 2.1b and described in a generalized form above, the algorithm is easily applied to multi-phase systems, after the network's impedance matrix is calculated. Beyond the basic implementation described by the 5 aforementioned steps, some solutions were presented to deal with unbalanced loading [28–30] and in particular with the necessity of calculating the effects on the neutral conductor [27]. Especially in the latter one, the scope is to allow the calculation of neutral-wire and ground-return currents by adding a fifth conductor to the scheme shown in Figure 2.1b and performing a so-called *voltage correction* before the convergence check, in order to compute the actual neutral potential depending on the current flowing through the grounding impedance. This kind of solution, although solving the problem of representing the neutral potential shifting with different grounding options, introduces elaborations on the result of the voltage drop calculated at step 4 which may lead, in particularly ill-conditioned systems, to convergence problems, depending on the grounding conditions and couplings between the conductors and earth.

2.1.2 Newton-Raphson method

The Newton-Raphson method has been applied widely to solve the power flow calculation on electrical networks, given its robustness and fast approach to the solution. Power flow algorithms based on this method solve a non-linear system of equations in the form:

$$P_j = \sum_{j=1}^{n_{PQ}+n_{PQ}} |V_j||V_k| \left(G_{ij}\cos\theta_{jk} + B_{ij}\sin\theta_{jk}\right) \tag{2.4}$$

$$Q_j = \sum_{j=1}^{n_{PQ}+n_{PQ}} |V_j||V_k| \left(G_{ij}\sin\theta_{jk} - B_{ij}\cos\theta_{jk}\right) \tag{2.5}$$

for any bus j, with G_{jk} and B_{jk} conductance and susceptance between buses j and k, θ_{jk} phase angle difference between the two buses voltages V_j and V_k. Depending on the bus type (i.e. PQ or PV for fixed P and Q or fixed P and V magnitude), active and

reactive powers P_j, Q_j and the bus voltage magnitude V_j may be known or unknown, while voltage is fixed in magnitude and angle at the slack buses (usually one).

To solve the power flow problem, the Newton-Raphson method requires to set the Jacobian matrix by the form in equation 2.6, including by the partial derivatives of equations (2.4) and (2.5) respect to the voltage magnitude and angle, computed at each iteration until the convergence given by a variation on the power balance staying within a given threshold.

$$\begin{bmatrix} \mathbf{\Delta P} \\ \\ \mathbf{\Delta Q} \end{bmatrix} = \begin{bmatrix} \dfrac{\boldsymbol{\partial \mathbf{P}}}{\boldsymbol{\partial \theta}} & \dfrac{\boldsymbol{\partial \mathbf{P}}}{\boldsymbol{\partial \mathbf{V}}} \\ \dfrac{\boldsymbol{\partial \mathbf{Q}}}{\boldsymbol{\partial \theta}} & \dfrac{\boldsymbol{\partial \mathbf{Q}}}{\boldsymbol{\partial \mathbf{V}}} \end{bmatrix} \begin{bmatrix} \boldsymbol{\Delta \theta} \\ \\ \mathbf{\Delta V} \end{bmatrix} \tag{2.6}$$

Although being one of the most robust and reliable for the solution of the power flow problem, this method may not be suitable when applied to ill-conditioned systems like for example the distribution networks which are characterized ususally by asymmetrical lines with high R/X ratios, unbalanced loading and particular grounding options (especially on the LV side).

To overcome these issues, one of the first proposals for power flow algorithms working on radial distribution feeders has been presented in [31]. In [32] the authors adopted the Newton-Raphson's algorithm to compute the power flow in four-wire systems and was thereafter improved adding specific component models for unbalanced three-phase networks in [33] by composing the Jacobian matrix starting from the current injection equations written in rectangular coordinates.

2.1.3 Gauss $\mathbf{Z_{Bus}}$ method

The Gauss Z_{bus} method is also a well-known approach for the power flow problem solution. It uses a sparse Y_{Bus} matrix to define the network structure, including branch and shunt elements, adopting a current injection technique to solve the power flow problem.

Using the power flow problem definition given in equations (2.4) and (2.5) for the application of the Newton-Raphson algorithm, in this case the system admittance matrix is directly employed in the algorithm, without the necessity of forming the Jacobian matrix. This feature, besides allowing a more flexible approach to the network modelling, may result into a worsening in the convergence ratio, especially with a high number of PV buses. This aspect anyway may be neglected when considering distribution systems, generally composed by PQ buses with a slack bus with voltage reference [34].

Its application has been recently presented as a solution for the calculation of power flow in unbalanced distribution systems in a loop frame of reference and using the current-injection technique [35] and in a phase-decoupled version to improve its computational efficiency [36]. A similar approach has been adopted by EPRI to develop OpenDSS, an open source multi-phase power flow tool [37]. A Gauss-Seidel method is also applied

in GridLab-D, a simulation environment developed by the U.S. Department of Energy (DOE) [38].

2.2 Multi-phase network representation

Starting from the considerations made in the previous paragraphs, an algorithm for the power flow calculation in distribution systems has been developed taking into account the presence of multi-phase circuits with uneven power distribution on the phases, as it often occurs especially in low-voltage networks. The proposed algorithm allows the consideration of customizable voltage dependencies for loads and generators while permitting the inclusion of virtually any number of wires in the system, even the case of different number of phases from one area to another.

The algorithm described in the following is derived from the methodology presented in [39] which proposed the solution of the power flow problem through the application of the current injection technique directly to the system's admittance matrix in which both loads and generators were included as shunt elements. The main advantages given by this method are the simplicity of implementation and robustness respect to particularly ill-conditioned systems, including low-voltage networks with high R/X ratios.

A description of the approach was presented in [40] and further enhanced in [41]. This *correction-current injection* algorithm evolved from the complex admittance matrix power flow methodology described in [39] by including a multi-conductor network structure in order to consider any number of phase and earth conductors. The main feature of this method is the inherent flexibility in how multi-conductor network models and their associated effects are considered. Mutual coupling influences between the phases are computed through a method that was originally developed for calculating electromagnetic coupling of complex conductor geometries [42]. The use of such a multi-conductor approach facilitates accounting for any kind of interaction between phases meaning that any network shunt element connections can be considered in terms of the system's phase and reference potentials and with respect to specific grounding (earthing) options. This feature intrinsically allows to consider any generic network with asymmetrical structure and operating under unbalanced conditions.

Figure 2.2 shows a schematic representation of the distribution system, incorporating network structure, load, generation and grounding elements. The branch element admittance matrix is composed through an incidence matrix approach computing the mutual admittances between the system's buses, which are represented as n-phase ports ("nodes"). The network shunt elements and grounding admittances are connected to these nodes, providing a linkage between the phase potentials and the system ground.

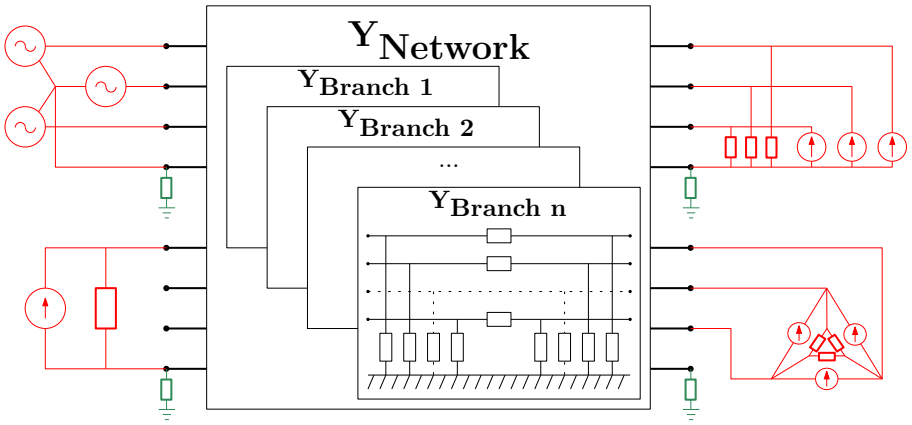

Figure 2.2: Schematic representation of the distribution system in the multi-conductor correction-current-injection power flow algorithm

2.2.1 Branch Elements

Branch elements are included in the network admittance matrix by considering a n-phase π-model. Each branch admittance matrix comprise longitudinal impedance Z and transversal admittance Y_t matrices as described in equation (2.7) and illustrated in Figure 2.3:

$$\mathbf{Y_{Branch}} = \begin{bmatrix} \mathbf{Z}^{-1} + \dfrac{\mathbf{Y_t}}{2} & -\mathbf{Z}^{-1} \\ -\mathbf{Z}^{-1} & \mathbf{Z}^{-1} + \dfrac{\mathbf{Y_t}}{2} \end{bmatrix} \tag{2.7}$$

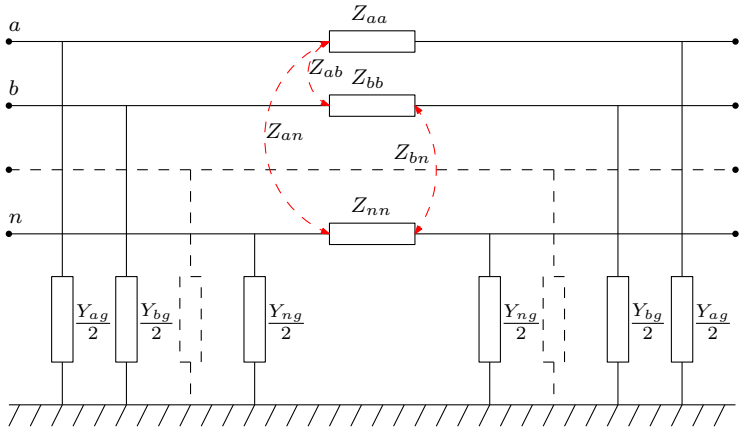

Figure 2.3: Circuital representation of a line section with the multi-phase π-model.

The $\mathbf{Y_{Branch}}$ matrix represents the relationship between currents (positive if entering) and voltages (with respect to a common zero-voltage reference) of the $2n$ ports of the branch element. The construction of the $\mathbf{Z}$ and $\mathbf{Yt}$ sub-matrices within the π-model is obtained using the classical *Carson-Clem* formulation for a n-phase branch as described in [42] also presenting an approximation of the correction terms for the real and imaginary components of the external part of the self and mutual impedance with earth return. It

is important to note that in practical cases these correction terms could be the dominant component in the 4-wire model, especially when considering unbalanced operation. The longitudinal impedance matrix Z contains the self and mutual impedances for each phase. Given two generic circuits i and j those terms are calculated as in equations (2.8-2.9):

$$Z_{ii} = R_i + R_e + j\omega \cdot 2 \cdot 10^{-4} \cdot \ln\left(\frac{D_e}{r_i}\right) \tag{2.8}$$

$$Z_{ij} = R_e + j\omega \cdot 2 \cdot 10^{-4} \cdot \ln\left(\frac{D_e}{d_{ij}}\right) \tag{2.9}$$

where:

R_i: DC resistance [Ω/km];

r_i: phase conductor radius [m];

d_{ij}: mutual distance between conductors i and j [m];

while the terms subscripted with e refer to the earth return path with depth D_e and resistance R_e [42] which takes into account the soil's finite conductivity. Those terms are calculated as for equations 2.10-2.11:

$$R_e = \pi f \cdot 10^{-4} \qquad \left[\frac{\Omega}{\text{km}}\right] \tag{2.10}$$

$$D_e = 659\sqrt{\frac{\rho}{f}} \qquad [\text{m}] \tag{2.11}$$

where:

f: system frequency [Hz];

ρ: soil conductivity [Ωm] (typically 100 Ωm).

The transversal admittance matrix $\mathbf{Y_t}$ represents the capacitive self and mutual susceptances, as evaluated through the Maxwell's potential coefficients. For the power flow problem in LV networks however, these terms have only a marginal effect. Once Y_{Branch} is computed for each longitudinal element, the system's nodal admittance matrix can be easily constructed through an incidence matrix that defines the topology of the network. For an m-bus, n-conductors network, $Y_{network}$ is a square matrix with size $(m \times n) \times (m \times n)$.

2.2.2 Shunt Elements representation

Loads, generators and in general any shunt element, can be represented by a combination of a constant shunt admittance as calculated in 2.12 and, if needed, through suitable

correction current injector as highlighted in Figure 2.4. For a single-phase shunt element connected between nodes k and h, the nominal complex admittance can be calculated as follows:

$$Y_{kh} = \frac{S^*_{kh(0)}}{|U_{kh(0)}|^2}, \qquad (U_{kh} = E_k - E_h) \tag{2.12}$$

where $S_{kh(0)}$ is the shunt element's rated power and E are the potentials of the k and h nodes. The subscript (0) indicates that the values are referred to the initial guess (nominal values). This kind of approach enables the inclusion of the shunt elements within the system admittance matrix allowing the voltage dependency to be customised according to the chosen model. The shunt element apparent power can be described through equation 2.13, which refers to the *i-th* iteration. Separating the constant admittance term facilitates the definition of a correction-current vector ΔI, which allows the introduction of a specific voltage dependency without changing the shunt element's admittance. In this way, the shunt element nominal admittance can be included in the system admittance matrix, which is then composed entirely of constant values as depicted in Figure 2.4.

$$S^*_{kh(i)} = Y_{kh} \cdot |U_{kh(i)}|^2 - U_{(kh(i))} \cdot \Delta I_{(kh(i))} \tag{2.13}$$

Considering equation (2.13) as for the *ZIP* model formulation, the concept of the aforementioned correction-current approach can be applied to separate the contributions of different voltage dependencies as shown in equation 2.14.

$$\begin{aligned} S^*_{kh(i)} &= S^*_{kh(0)} \left[k_Z \left(\frac{|U_{kh(i)}|}{|U_{kh(0)}|} \right)^2 + k_I \left(\frac{|U_{kh(i)}|}{|U_{kh(0)}|} \right) + k_P \right] \\ &= S^*_{kh(i)_Z} + S^*_{kh(i)_I} + S^*_{kh(i)_P}, \; k_Z + k_I + k_P = 1 \end{aligned} \tag{2.14}$$

With regard to the constant impedance part, the ΔI component in equation 2.13 is set to zero. For the constant current part of the *ZIP* model in equation 2.14, which describes a linear voltage dependency, the correction current ΔI can be obtained as for equations (2.15-2.16):

$$S^*_{kh(i)} = k_I \left(\frac{|U_{kh(i)}|}{|U_{kh(0)}|} \right) Y_{kh} \cdot |U_{kh(0)}|^2 = k_I \left(Y_{kh} \cdot |U_{kh(i)}|^2 - U_{kh(i)} \Delta I_{kh(i)_{I\%}} \right) \tag{2.15}$$

with

$$\Delta I_{kh(i)_{I\%}} = k_I \frac{Y_{kh}}{U_{kh(i)}} \left(|U_{kh}|^2_{(i)} - |U_{kh}|_{(i)} \cdot |U_{kh}|_{(0)} \right) \tag{2.16}$$

The constant power share may also be expressed through a suitable correction-current

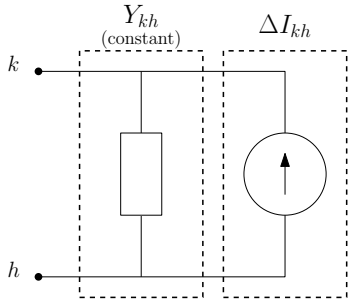

Figure 2.4: Shunt element representation with constant admittance part and correction current term.

term as described in equations (2.17-2.18):

$$S^*_{kh(i)_{P\%}} = k_P Y_{kh} \cdot |U_{kh(0)}|^2 = k_P \left(Y_{kh} \cdot |U_{kh(i)}|^2 - U_{kh(i)} \Delta I_{kh(i)_{P\%}} \right) \tag{2.17}$$

with

$$\Delta I_{kh(i)_{P\%}} = k_P \frac{Y_{kh}}{U_{kh(i)}} \left(|U_{kh}|^2_{(i)} - |U_{kh}|^2_{(0)} \right) \tag{2.18}$$

Finally, equation (2.19) describes the composition of the ZIP model, with an emphasis on the fact that the different voltage dependency shares may be represented by separate current injectors.

$$S^*_{kh(i)} = Y_{kh} \cdot |U_{kh(i)}|^2 - \left(\Delta I_{kh(i)_{I\%}} + \Delta I_{kh(i)_{P\%}} \right) \cdot U_{kh(i)} \tag{2.19}$$

2.2.3 Connections among nodes and grounding

One of the most important features of this kind of power flow calculation is that it allows to customize the connection between network phases and ground at any point of the system. This allows for a consideration of the specific connection layouts and grounding options without the necessity of utilizing the sequences approach. As shown in Figure 2.4 for the shunt elements representation, the system is composed by simply including admittances defining the coupling among conductors. The same approach is applicable for the connection between neutral and ground (green elements in Figure 2.2), which can therefore be represented as a self-admittance at the grounded bus.

2.3 Generalized transformer model

The transformer is a network element whose representation in a multi-conductor environment is quite challenging, especially when dealing with particular phase connections, due to singularities in the admittance matrix. This reason led to the choice of reserving a separate section to the representation of this branch element.

Several works in literature include the transformers in the power system by using reference-frame transformations. For instance, in [43] the $\alpha\beta 0$ stationary reference frame is adopted, while the sequence frame is used in [44]. Although correctly representing the symmetrical system admittance, a more detailed definition of the mutual couplings among the conductors is obtainable working on the Y matrix of the transformer as proposed for example in [45]. The concept was also adopted to develop multi-winding multi-terminal transformer models in [46–48]. Other works were presented to model particular transformer topologies for the connection of traction loads, for instance [49].

This section discusses about a generalized method for modelling transformers in a multi-conductor grid representation in order to allow analysis on asymmetrical networks. The aim is to represent any transformer connection through an incidence matrix approach, knowing the impedance for each single-phase equivalent circuit. Some examples on how to build the model considering several specific connections are given and tested to validate the approach.

The multi-phase transformer model described in this section is built by connecting each single-phase equivalent circuit through suitable incidence matrices in three sequential steps:

1. Definition of the transformer's primitive admittance matrix
2. Calculation of the admittance matrix for the *unconnected* transformer model
3. Application of the connections among the phases to represent the connection and group.

In the following, a detailed description of the approach used to model the multi-phase transformer is given.

2.3.1 Single-phase equivalent circuit

The single-phase circuit defines the impedances associated to one of the transformer's phases, allowing to set the impedances between the primary and secondary side. The most common way to represent it is through the model shown in Figure 2.5a, where the short-circuit and the magnetizing impedances z_{cc} and z_0 are referred to the primary side voltage E_1 which is intended to be the phase-to-ground potential of node h.

Another way to define the self and mutual impedances for the single-phase circuit is to adopt the well-known π-model shown in Figure 2.5b, applicable in the per-unit system, with the admittances defined as:

$$Y' = \frac{1-m}{z_{cc}} \tag{2.20}$$

$$Y'' = \frac{m(m-1)}{z_{cc}} \tag{2.21}$$

$$Y''' = \frac{m}{z_{cc}} \tag{2.22}$$

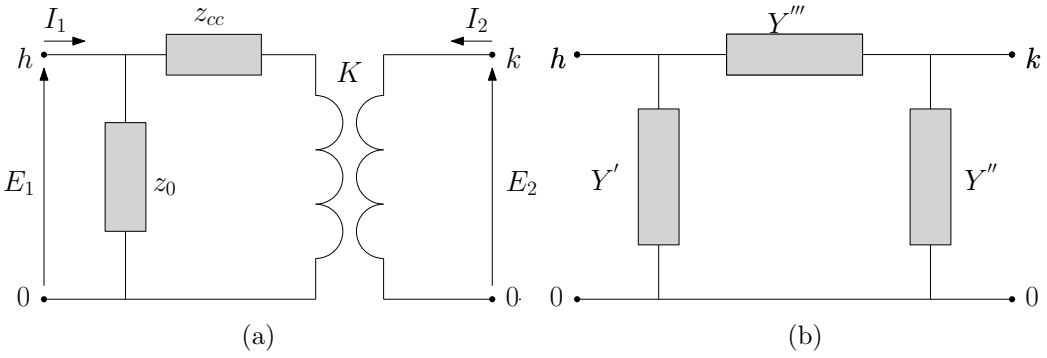

Figure 2.5: Equivalent circuits for a single-phase 2-windings transformer.

where $m = K\dfrac{E_1}{E_2}$ is the transformation ratio and $K = \dfrac{N_1}{N_2}$ is the turns ratio. The z_0 term shown in Figure 2.5a is related to the open-circuit losses and will be added separately since it only involves the primary side bus.

2.3.2 Unconnected n-phase transformer

Once the π-model for each single-phase circuit has been defined, a primitive matrix for the multi-phase system can be built placing on the diagonal the admittance terms defined in equations (2.20-2.22) for each single-phase transformer composing the model, obtaining a square matrix of order $4n$ (where n is the number of phases).

$$\mathbf{Y_{Prim}} = \begin{bmatrix} Y'_a & 0 & \cdots & \cdots & \cdots & \cdots & \cdots & 0 \\ 0 & \ddots & 0 & \cdots & \cdots & \cdots & \cdots & 0 \\ \vdots & 0 & Y''_a & 0 & \cdots & \cdots & \cdots & 0 \\ \vdots & \vdots & 0 & \ddots & 0 & \cdots & \cdots & 0 \\ \vdots & \vdots & \vdots & 0 & Y'''_a & 0 & \cdots & 0 \\ \vdots & \vdots & \vdots & \vdots & 0 & \ddots & 0 & 0 \\ \vdots & \vdots & \vdots & \vdots & \vdots & 0 & Y_{0a} & 0 \\ 0 & 0 & 0 & 0 & 0 & 0 & 0 & \ddots \end{bmatrix} \tag{2.23}$$

The transformer's admittance matrix composition is given by applying a suitable incidence matrix to the primitive matrix defined in equation (2.23). It is worth noting that the definition of the incidence matrix depends on the order used to group the π-model's terms. In this case the incidence matrix is:

$$\mathbf{A} = \begin{array}{c} \\ Y' \\ Y'' \\ Y''' \\ Y_0 \end{array} \begin{array}{c} \begin{array}{cc} (A,B,...) & (a,b,...) \end{array} \\ \begin{bmatrix} [\mathbf{1}] & [\mathbf{0}] \\ [\mathbf{0}] & [\mathbf{1}] \\ -[\mathbf{1}] & [\mathbf{1}] \\ [\mathbf{1}] & [\mathbf{0}] \end{bmatrix} \end{array} \tag{2.24}$$

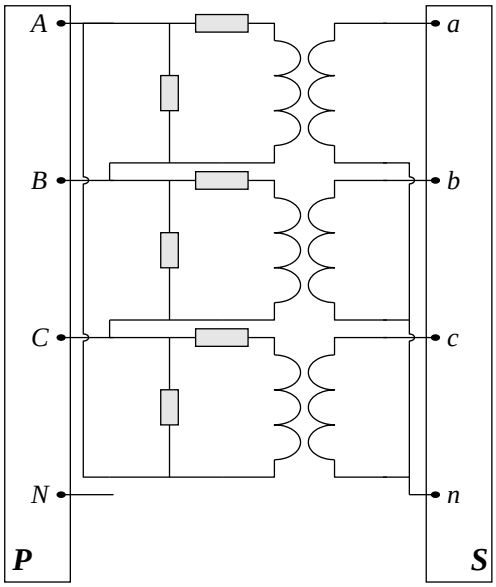

Figure 2.6: Connection scheme of a Delta-Wye three-phase transformer. The P and S letters indicate the Primary and Secondary busbars.

where $[\mathbf{1}]$ is the identity matrix and $[\mathbf{0}]$ is a zeros matrix, each with order equal to the number of phases m. In equation (2.24) the column indexes refer to each phase on the primary side (capital letters) and on secondary side (lower case letters): the number of phases in this system is equal to the single-phase circuit in parallel. For a two-windings, three-phase transformer $\mathbf{A}$ will then be a $[(4 \times n) \times (2 \times n)]$ matrix where $n = 3$ is the number of single-phase circuits in parallel.

2.3.3 Delta-Wye transformer

After the composition of the unconnected transformer, an interface between the transformer ports and the buses at primary and secondary sides is needed. In the following this process is described relating to a *Delta-Wye* connection of a three-phase transformer which is depicted in Figure 2.6.

Once the nodal admittance matrix is built for the three-phase transformer, the topology of the external connections can be set by defining a suitable incidence matrix as shown in equation (2.25).

$$\mathbf{B} = \begin{array}{c} \\ A{-}B \\ B{-}C \\ C{-}A \\ a{-}n \\ b{-}n \\ c{-}n \end{array} \begin{array}{c} \begin{array}{cccccccc} A & B & C & N & a & b & c & n \end{array} \\ \left[\begin{array}{cccccccc} 1 & -1 & 0 & 0 & 0 & 0 & 0 & 0 \\ 0 & 1 & -1 & 0 & 0 & 0 & 0 & 0 \\ -1 & 0 & 1 & 0 & 0 & 0 & 0 & 0 \\ 0 & 0 & 0 & 0 & 1 & 0 & 0 & -1 \\ 0 & 0 & 0 & 0 & 0 & 1 & 0 & -1 \\ 0 & 0 & 0 & 0 & 0 & 0 & 1 & -1 \end{array}\right] \end{array} = \begin{bmatrix} [\mathbf{B_P}] & [\mathbf{0}] \\ [\mathbf{0}] & [\mathbf{B_S}] \end{bmatrix} \tag{2.25}$$

Assuming a 4-wires busbar on the primary side, in (2.25) it could be seen that the

number of elements on the delta-connected side is still kept as 4 with the explicit neutral node to show how the number of phases can be chosen independently from the ports actually used in the model. Considering both the incidence matrices **A** and **B** the transformer nodal admittance matrix is given by:

$$\mathbf{Y_T} = \mathbf{B}^T\{\mathbf{A}^T\ \mathbf{Y_{Prim}}\ \mathbf{A}\}\mathbf{B} \tag{2.26}$$

2.3.4 Three-windings transformer model

To generalize the method discussed so far, this section shows how to represent a three-windings transformer demonstrating how the same approach could be applied to a device connected to multiple busbars, each consisting in a generic number of phases. In this

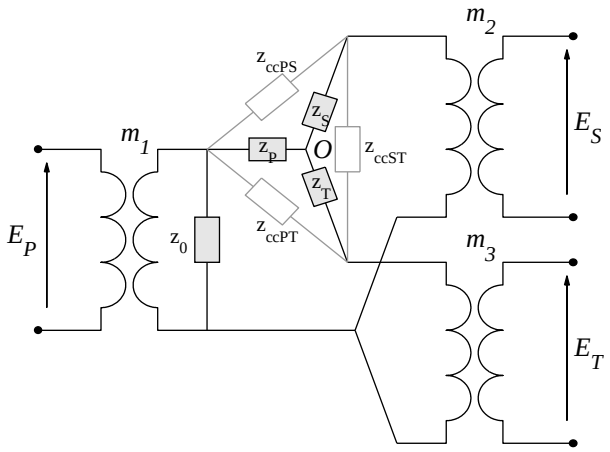

Figure 2.7: Single-phase equivalent circuit of a three-windings transformer.

case, the single-phase equivalent circuit is designed as shown in Figure 2.7: the short circuit impedances are defined for each pair of buses identified as P, S and T (Primary, Secondary and Tertiary sides). The circuit's nodal admittance matrix can be obtained by considering a common node (called O) and then calculating the share of short circuit impedance referred to each side as for equation (2.27).

$$Z_{wye} = \begin{bmatrix} z_P \\ z_S \\ z_T \end{bmatrix} = \frac{1}{2} \begin{bmatrix} 1 & -1 & 1 \\ 1 & 1 & -1 \\ -1 & 1 & 1 \end{bmatrix} \begin{bmatrix} z_{ccPS} \\ z_{ccST} \\ z_{ccPT} \end{bmatrix} \tag{2.27}$$

$$Y_{wye} = \begin{bmatrix} z_P^{-1} \\ z_S^{-1} \\ z_T^{-1} \end{bmatrix} \tag{2.28}$$

The three impedances defined in equation (2.27) compose the star inscribed in the Delta-connected short-circuit impedances. The admittance array calculated as for equation (2.28) can be included in the diagonal of a primitive matrix, as shown in (2.29), while an incidence matrix can be defined as for equation (2.30) setting the connections of each admittance term of the multi-phase transformer.

$$\mathbf{Y_{Prim(f)}} = \begin{bmatrix} [\mathbf{Y_P}] & [\mathbf{0}] & [\mathbf{0}] & [\mathbf{0}] & [\mathbf{0}] \\ [\mathbf{0}] & [\mathbf{Y_S}] & [\mathbf{0}] & [\mathbf{0}] & [\mathbf{0}] \\ [\mathbf{0}] & [\mathbf{0}] & [\mathbf{Y_T}] & [\mathbf{0}] & [\mathbf{0}] \\ [\mathbf{0}] & [\mathbf{0}] & [\mathbf{0}] & [\mathbf{Y_0}] & [\mathbf{0}] \\ [\mathbf{0}] & [\mathbf{0}] & [\mathbf{0}] & [\mathbf{0}] & [\mathbf{Y_O}] \end{bmatrix} \tag{2.29}$$

$$\mathbf{A_{(f)}} = \begin{array}{c} \\ Y_P \\ Y_S \\ Y_T \\ Y_0 \\ Y_O \end{array} \begin{array}{c} \begin{array}{cccc} P(a,b,...) & S(a,b,...) & T(a,b,...) & O(a,b,...) \end{array} \\ \begin{bmatrix} [\mathbf{I}] & [\mathbf{0}] & [\mathbf{0}] & -[\mathbf{I}] \\ [\mathbf{0}] & [\mathbf{I}] & [\mathbf{0}] & -[\mathbf{I}] \\ [\mathbf{0}] & [\mathbf{0}] & [\mathbf{I}] & -[\mathbf{I}] \\ [\mathbf{I}] & [\mathbf{0}] & [\mathbf{0}] & [\mathbf{0}] \\ [\mathbf{0}] & [\mathbf{0}] & [\mathbf{0}] & [\mathbf{I}] \end{bmatrix} \end{array} \tag{2.30}$$

The primitive matrix in equation (2.29) is built by diagonal matrices with order 3 (since there are three single-phase circuits coupled) containing each the respective admittance terms calculated in equation (2.28) shown in Figure 2.7. The open-circuit losses are included by adding the $\mathbf{Y_0}$ term, while it's important to note that a term called $\mathbf{Y_O}$ has been added to introduce a reference to earth for the common node in each circuit. These terms are defined as tiny admittances (in the order of 10^{-10} respect to the short-circuit terms) and are considered only for numerical reasons, in order to prevent from issues when inverting the admittance matrix.

With this reference, the incidence matrix can be easily built by using identity and zeros matrices with order 3 as shown in equation (2.30). In case of a three-phase-three-windings transformer, $\mathbf{Y_{Prim(f)}}$ and $\mathbf{A_{(f)}}$ are matrices with order $(5 \cdot n)$ and $[(5 \cdot n) \times (4 \cdot n)]$ respectively, where $n = 3$ is the number of parallel single-phase circuits.

Since the common node O is not defined in the system's admittance matrix (in which the transformer's one will be included), a reduction is required and obtained through the procedure described in the following:

1. Calculate the nodal admittance matrix for the *unconnected* transformer from the primitive and incidence matrices (2.29-2.30) as for equation (2.31):

$$\overline{\mathbf{Y_{T(f)}}} = \mathbf{A_{(f)}^T}\ \mathbf{Y_{P(f)}}\ \mathbf{A_{(f)}} \tag{2.31}$$

   where the signed term indicates that the nodal admittance matrix doesn't include the connections among the phases

2. Invert $\overline{Y_T}$ obtaining the order 15 impedance matrix with the explicit common node

$$\overline{\mathbf{Z_{T(f)}}} = (\overline{\mathbf{Y_{T(f)}}})^{-\mathbf{1}} \tag{2.32}$$

3. Delete the rows and columns relative to the common node, reducing the impedance matrix to order 12: $\overline{\mathbf{Z_{T(f)}}} \rightarrow \overline{\mathbf{Z_T}}$;

4. Invert $\overline{Z_T}$ to get the reduced admittance matrix for the *unconnected* transformer:

$$\overline{\mathbf{Y_T}} = (\overline{\mathbf{Z_T}})^{-\mathbf{1}} \tag{2.33}$$

With the approach followed in this case, the information about the actual transformation ratio is not directly contained in the impedances definition and it needs to be set separately linking the ports in the 1-Volt-reference system to the external ports of each side. This process is depicted in Figure 2.7 as three couplings with turns ratio defined as:

$$\begin{cases} m_P = k_P \\ m_S = 1/k_S \\ m_T = 1/k_T \end{cases} \tag{2.34}$$

where $k_x = E_{xR}/E_{xBase}$ (with $x = P, S, T$) is the ratio between the winding's rated voltage and the respective busbar's base voltage.

With the turns ratios calculated as for equation 2.34, the nodal admittance matrix of the generic multi-phase transformer can be calculated similarly to the two-windings case shown in section 2.3.3 but adjusting the voltage reference to the actual values of each side. This process is obtained by introducing the matrices **B** and **C**:

$$\mathbf{B} = \begin{bmatrix} [\mathbf{B_P}] & [\mathbf{0}] & [\mathbf{0}] \\ [\mathbf{0}] & [\mathbf{B_S}] & [\mathbf{0}] \\ [\mathbf{0}] & [\mathbf{0}] & [\mathbf{B_T}] \end{bmatrix} \tag{2.35}$$

$$\mathbf{C} = \begin{bmatrix} m_P & 0 & \cdots & \cdots & \cdots & 0 \\ 0 & \ddots & 0 & \cdots & \cdots & 0 \\ \vdots & 0 & m_S & 0 & \cdots & 0 \\ \vdots & \vdots & 0 & \ddots & 0 & 0 \\ \vdots & \vdots & \vdots & 0 & m_T & 0 \\ \vdots & \vdots & \vdots & \vdots & 0 & \ddots \end{bmatrix} \tag{2.36}$$

where the $\mathbf{B_{P\ldots T}}$ sub-matrices contain the topology for each side similarly to equation (2.25), while **C** is a diagonal matrix containing the turns ratios as defined in equation (2.34).

Standing the choice (explained in section 2.3.3) of keeping the full number of phases of the 4-wires system at the external ports, the order of **B** will be $[(3 \cdot n) \times (4 \cdot n)]$ with the same meaning for n, while **C** is a square matrix of order $(4 \cdot n)$ containing the actual turns ratios defined in equation (2.34). The nodal admittance matrix for the multi-phase 3-windings transformer is then given by equation (2.37):

$$\mathbf{Y_T} = \mathbf{B}^T\{\mathbf{C}^T\ \overline{\mathbf{Y_T}}\ \mathbf{C}\}\mathbf{B} \tag{2.37}$$

It is worth noting that the method described in this section to build a three-windings

transformer with a generic number of phases could be as well applied to a model with any number of windings by simply adding new ports to the circuit (and of course computing the impedances in the single-phase circuit accordingly), including the two-windings transformer considered in the previous sections.

2.3.5 Transformers with special connections: Zig-Zag and Scott

The method for representing n-phase transformers with any number of windings has been shown so far, discussing a generalized method for implementing the relations between the phases. In this section the *Zig-Zag* and *Scott* connections are considered as examples on how to realize specific connection schemes through the presented method.

Zig-Zag

The *Zig-Zag* connection is typically used to create a common reference for the neutral conductor in three-phase/three-wires systems or, in general, to reduce the amount of voltage unbalance on the transformer's primary side while feeding an unbalanced load. Figure 2.8 shows the voltage diagrams at both sides referring to the circuit depicted in Figure 2.9.

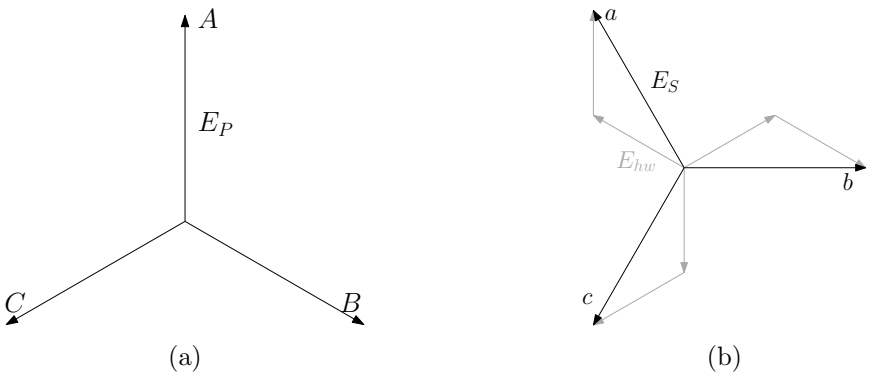

Figure 2.8: Vectorial diagrams for the Primary (a) and Secondary (b) sides of a Wye-ZigZag transformer.

Defining the phase voltages on each side of the transformer as E_P and E_S (similarly to the case shown in section 2.3.3), the turns ratio is given by:

$$\begin{cases} m_P = E_{PBase}/E_{Pn} = 1 \\ m_S = E_{SBase}/E_{Sn} = 2/\sqrt{3} \end{cases} \tag{2.38}$$

where E_{PBase} and E_{SBase} are the base voltages of each side.

Applying the general approach described in section 2.3.4 the impedance related to each side can be obtained as half of the short-circuit impedance introducing the common node, then the same considerations made to calculate the admittance matrix are still valid. In this case, considering both the vectorial diagram and the three-phase circuit shown in Figures 2.8 and 2.9, the incidence matrix of a Wye-ZigZag transformer with group 11 can

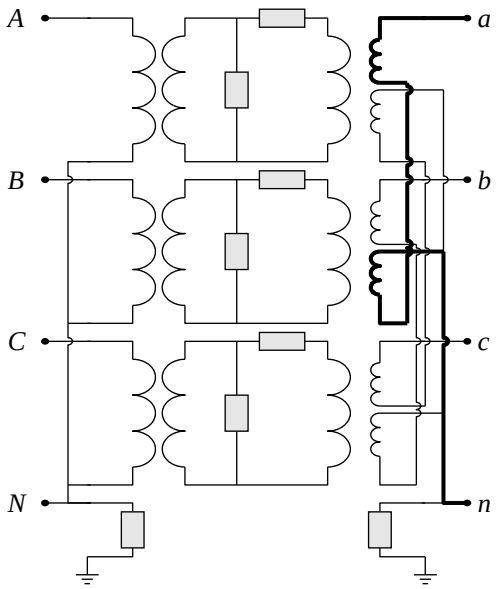

Figure 2.9: Connection scheme of a three-phase Wye-ZigZag transformer. The path for the phase-neutral voltage in phase-a is highlighted at the secondary busbar.

be built as in equation (2.35) with the sub-matrices defined as:

$$\mathbf{B_P} = \begin{bmatrix} 1 & 0 & 0 & -1 \\ 0 & 1 & 0 & -1 \\ 0 & 0 & 1 & -1 \end{bmatrix} ; \quad \mathbf{B_S} = \begin{bmatrix} 0.5 & -0.5 & 0 & 0 \\ 0 & 0.5 & -0.5 & 0 \\ -0.5 & 0 & 0.5 & 0 \end{bmatrix} \tag{2.39}$$

As could be seen from the vectorial diagram in Figure 2.8b, the secondary voltage is obtained as composition of two half-winding voltages E_{hw} taken from different phases. To include this aspect in the incidence matrix definition, the connections among the phases have been set to 0.5 as shown in (2.39).

Scott

The Scott transformer is employed for the connection of traction systems to a three phase network, in order to reduce the amount of unbalance on the three-phase grid due to the asymmetrical nature of the traction system. The main advantage of this configuration is the possibility to maintain balanced voltages at the primary side while feeding a system with 2 phases displaced by 90°. This kind of connection can be represented through the general approach to the n-phase transformer given in the previous sections by simply setting a suitable incidence matrix defining the interaction between the windings, in order to obtain the voltage vectors composition shown in Figure 2.10a.

As for the Zig-zag connection, one of the windings (here on the primary side) is divided in two half-windings, so the incidence matrix will involve fractional terms. Furthermore, since the number of windings is different from the number of phases in the system, the incidence matrix will not be square as in the previous cases and could be built as follows:

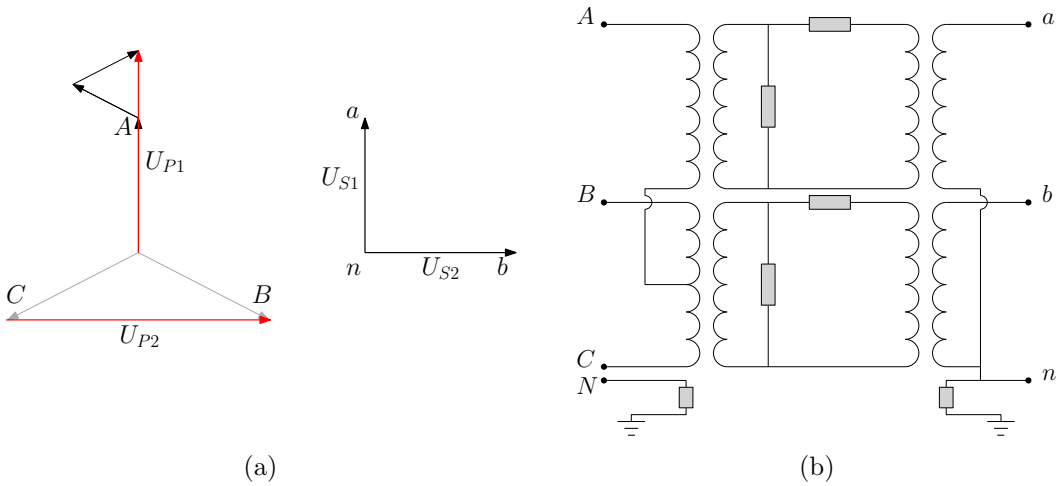

(a) (b)

Figure 2.10: Vectorial diagram (a) and connection scheme (b) of a Scott transformer: in red the voltages applied to each phase-winding on the primary side.

$$\mathbf{B} = \begin{array}{c} \\ P1 \\ P2 \\ S1 \\ S2 \end{array} \begin{array}{c} \begin{array}{ccccccc} A & B & C & N & a & b & n \end{array} \\ \begin{bmatrix} 1 & -0.5 & -0.5 & 0 & 0 & 0 & 0 \\ 0 & 1 & -1 & 0 & 0 & 0 & 0 \\ 0 & 0 & 0 & 0 & 1 & 0 & -1 \\ 0 & 0 & 0 & 0 & 0 & 1 & -1 \end{bmatrix} \end{array} \tag{2.40}$$

From equation (2.40) it could be seen that the number of phases on the primary side is still kept as 4 with the explicit neutral node to show how the number of phases can be chosen independently from the ports actually used in the model. In this scheme, the neutral point needs then to be connected to earth through an external impedance not to cause inversion problems when including the transformer model in the system admittance matrix.

In this case, differently from the previous examples, not only the turns ratio changes from one side to the other, but also from one phase-winding to the other. In particular, for the Scott connection the transformation ratios can be calculated as follows, defining the phases with 1 and 2:

$$\begin{cases} m_{P1} = E_{P1Base}/E_{P1n} = 1/1.5 \\ m_{P2} = E_{P2Base}/E_{P2n} = 1/\sqrt{3} \\ m_{S1} = E_{S1Base}/E_{S1n} = 1 \\ m_{S2} = E_{S2Base}/E_{S2n} = 1 \end{cases} \tag{2.41}$$

NOTE:
An observation that arises from the examples mentioned above is that the incidence matrix **B** includes not only unitary values but in general real ones, depending on the specific connection option. This feature allows basically to obtain any kind of topology, also reducing the number of phases on the transformer's sides.

2.4 Correction-Current-Injection (CCI) power flow algorithm

The power flow algorithm is formulated as a set of non-linear equations which compose the system:

$$\mathbf{I} = \mathbf{Y} \cdot \mathbf{E} \tag{2.42}$$

As proposed in the methodology described in [39], matrices for the mere network structure and shunt elements may be computed separately as discussed in the previous sections and aggregated in the total system admittance matrix, which will include both the busbar connections and shunt elements contributions following the scheme depicted in Figure 2.11. Calling $\mathbf{Y_{network}}$ the system's admittance matrix, the power flow problem can be represented as in Figure 2.12.

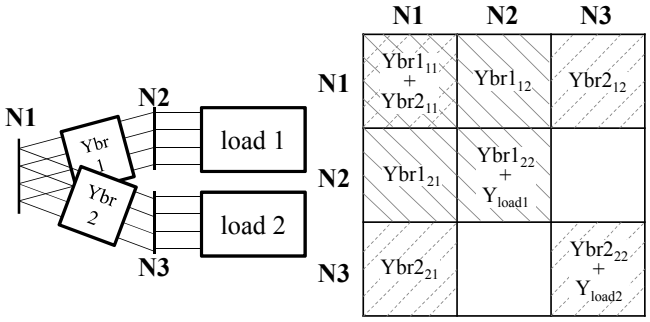

Figure 2.11: Example of admittance matrix composition for a three-bus system.

In Figure 2.12, the system has been partitioned to highlight the components concerning the slack bus (SL). It should be noted that, since the system is made by multi-phase buses, the number of elements composing the current and voltage vectors **I** and **E** is given,for a total number of buses n and phases m, by $[n \times m]$. The partitioned system can be written as:

$$\mathbf{I_{SL}} = \mathbf{Y_{SL-SL}} \cdot \mathbf{E_{SL}} + \mathbf{Y_{SL-SH}} \cdot \mathbf{E_{SH}} \tag{2.43}$$

$$\mathbf{\Delta I_{SH}} = \mathbf{Y_{SL-SH}} \cdot \mathbf{E_{SL}} + \mathbf{Y_{SH-SH}} \cdot \mathbf{E_{SH}} \tag{2.44}$$

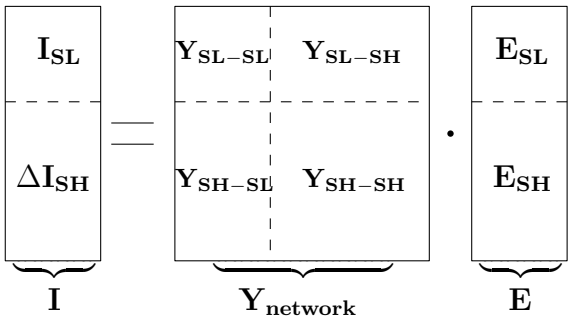

Figure 2.12: Partitioned system for the power flow problem.

Since both the shunt elements' admittance and ground connection matrices are included in $\mathbf{Y_{network}}$, the values composing array $\mathbf{\Delta I_{SH}}$ are defined as *correction-currents* which adapt the power absorption or injection of the shunt elements according to their voltage dependency as discussed in section 2.2.2. Solving equation (2.44) for $\mathbf{E_{SH_{(i)}}}$ yields:

$$\mathbf{E_{SH_{(i)}}} = \mathbf{Y^{-1}_{SH-SH}} \cdot \left(\mathbf{\Delta I_{SH_{(i-1)}}} - \mathbf{Y_{SH-SL}} \cdot \mathbf{E_{SL}} \right) \tag{2.45}$$

in which subscript i stands for the i^{th} iteration. The inclusion of the shunt elements' constant admittance part in the system matrix contributes to increase the calculation speed since it allows to operate the matrix inversion in equation (2.45) only once at the start of the iterative process. In the following, the power flow algorithm is schematically described.

Input: Branches length and connection type, loads and generators active and reactive powers.

Result: Voltage vector $\mathbf{E}$ solving the power flow problem.

Initialize of the admittance matrices:

- calculate the branches sub-matrices as for equation (2.7);
- calculate the ground connection matrix;
- calculate the shunt elements' admittance matrix whose components are calculated as for equation (2.12);

Compose the network admittance matrix $\mathbf{Y_{network}}$ as the sum of the previous matrices;

Invert $\mathbf{Y_{SH-SH}}$;

Initialize the voltage vector $\mathbf{E}$;

$i \leftarrow 0$;

while $|\mathbf{E}| \leq \epsilon_M$ *and* $\underline{/\mathbf{E}} \leq \epsilon_A$ *and* $i <= max_i$ **do**

  $i \leftarrow i + 1$;

  update the shunt elements' currents vector $\mathbf{\Delta I_{SH}}_{(i-1)}$;

  calculate $\mathbf{E}_{(i)}$ as for equation (2.45);

end

Algorithm 1: Correction-Current-Injection (CCI) power flow algorithm

2.5 Generalization of the CCI power flow

The advantage given by the introduction of the correction-currents concept is that any kind of shunt elements' voltage dependency may be considered and suitably taken into account by simply adapting the respective term in the $\mathbf{\Delta I_{SH}}$ array included in equation (2.45).

The ZIP-model described in section 2.2.2 can be used to represent the behaviour of PQ buses, defining the correction-current as a function of the constant admittance part and of the voltage variation. To generalize the approach explained so far, a representation of the PV buses is given in this section. PV busbars are characterized by constant active power and fixed voltage magnitude and are used to represent the presence of traditional generation plants which have the ability to control the voltage magnitude at the connection bus by means of a reactive power variation. This type of operation is obviously related to sections of the power system where the branches' R/X ratio is below 1, leading to a prevalent link between reactive power and voltage magnitude. In this vision a way to adapt the generator currents at PV buses was presented in [39] for the current-injection implementation in the equivalent single-phase system and its application to multi-phase circuits is discussed in the following.

Starting from the power flow problem formulation given by equations (2.43) and (2.44), it is possible to subdivide the system between generators (G) and loads (L) buses considering the first ones connected to Slack and PV buses and the latter ones to PQ buses, obtaining:

$$\mathbf{I_G} = \mathbf{Y_{GG}} \cdot \mathbf{E_G} + \mathbf{Y_{GL}} \cdot \mathbf{E_L} \tag{2.46}$$

$$\mathbf{\Delta I_L} = \mathbf{Y_{GL}} \cdot \mathbf{E_G} + \mathbf{Y_{LL}} \cdot \mathbf{E_L} \tag{2.47}$$

where the terms indicated with subscript G include the slack bus too. Solving equation (2.47) for $\mathbf{E_L}$ yields:

$$\mathbf{E_L} = -\mathbf{Y_{LL}^{-1}Y_{LG}} \cdot \mathbf{E_G} + \mathbf{Y_{LL}^{-1}} \cdot \mathbf{\Delta I_L} \tag{2.48}$$

leading to:

$$\mathbf{I_G} = (\mathbf{Y_{GG}} - \mathbf{Y_{GL}Y_{LL}^{-1}Y_{LG}}) \cdot \mathbf{E_G} + \mathbf{Y_{GL}Y_{LL}^{-1}} \cdot \mathbf{\Delta I_L} \tag{2.49}$$

which can also be written separating the slack and PV buses (i.e. the $\mathbf{E_G}$ array is decomposed in the two components $\mathbf{E_{SL}}$ and $\mathbf{E_{PV}}$) as:

$$\begin{bmatrix} \mathbf{I_{SL}} \\ \mathbf{\Delta I_{PV}} \end{bmatrix} = \begin{bmatrix} \mathbf{A} & \mathbf{B} \\ \mathbf{C} & \mathbf{D} \end{bmatrix} \begin{bmatrix} \mathbf{E_{SL}} \\ \mathbf{E_{PV}} \end{bmatrix} + \begin{bmatrix} \mathbf{Y_{GL}Y_{LL}^{-1}} \end{bmatrix} \cdot \begin{bmatrix} \mathbf{\Delta I_L} \end{bmatrix} \tag{2.50}$$

Finally, the correction-current that needs to be injected at the PV buses is given by:

$$\mathbf{\Delta I_{PV}} = \mathbf{C} \cdot \mathbf{E_{SL}} + \mathbf{D} \cdot \mathbf{E_{PV}} + \mathbf{Y_{GL}Y_{LL}^{-1}} \cdot \mathbf{\Delta I_L} \tag{2.51}$$

where $\mathbf{E_{PV}}$ is the vector of voltages whose magnitude needs to be maintained constant and $\mathbf{\Delta I_L}$ corresponds to the $\mathbf{\Delta I_{SH}}$ array defined in equation (2.44), for the remaining PQ buses.

In a general case in which the neutral point at the PV busbar shifted due to voltage unbalances, the $\mathbf{E_{PV}}$ potentials need to be set in order to obtain a phase-neutral voltage with the desired magnitude and an unmodified angle. An example referred to phase a is shown in Figure 2.13. In the example, since the objective is to obtain the dashed voltage

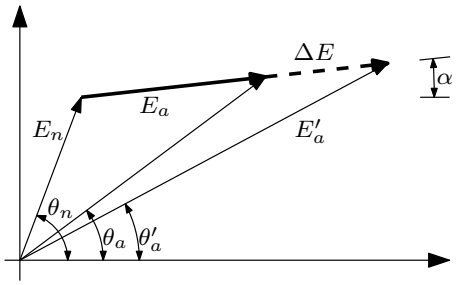

Figure 2.13: Voltage diagram for phase-a of a generic PV bus.

vector variation, phase-a potential $\overline{E'_a}$ needs to be set as:

$$\overline{E'_a} = \overline{E_a} + \Delta E \cdot e^{j\,\alpha} \tag{2.52}$$

where ΔE is the magnitude difference between the actual phase-neutral voltage and the desired one and $\alpha = \theta_a - \theta_b$. Applying the same concept to the other phases, vector $\mathbf{E_{PV}}$ in equation (2.51) is defined for the respective iteration. In order to control the voltage magnitude by means of a reactive power variation, the currents composing the array $\mathbf{\Delta I_{PV}}$ in equation (2.51) need to be set in quadrature with the relative phase-neutral voltage as for the discussion in [39].

2.6 Case study applications of the CCI algorithm

This section reports several applications in the study of the steady-state operation of electrical networks, focusing on different aspects of the CCI power flow algorithm discussed in the previous sections. Case studies are presented to validate the obtained solution compared to other simulation environments and show some of the possible applications of the algorithm.

2.6.1 Analysis of an Irish multiple-grounded 4-wire distribution network

In this case study, the CCI algorithm was adopted to model and simulate the operation of a Low Voltage distribution network including both three-phase and single-phase lines, with multiple ground connections. The system considered below, whose layout is depicted in Figure 2.14, is a suburban distribution network within the city of Dublin, Ireland, which incorporates users' single-phase connections, also provided with neutral connection to earth as well as DG connections.

The system hosts 74 households distributed on a 10-bus feeder radially departing from a 10/0.4 kV Secondary Substation. The neutral conductor is connected to ground in several

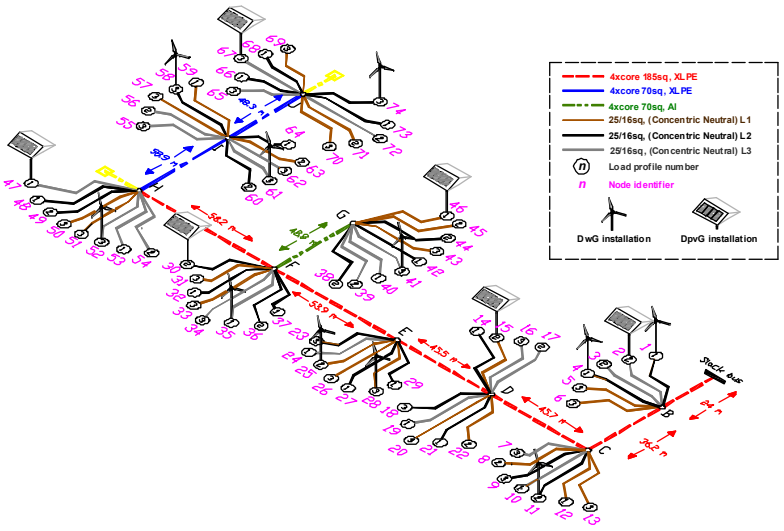

Figure 2.14: Layout of the Irish LV distribution network.

points around the network: each busbar along the main three-phase line (i.e. pillars B-J) have a 1 Ω earth electrode, while customers have distinct earth connections through a 5 Ω impedance. The neutral conductor is grounded at the Secondary Substation (i.e. pillar A).

The sending voltage at the Secondary Substation is varied in accordance with the assumed maximum voltage drop limits as defined in the EN50160 standard for the Irish DSO's distribution code [50], requiring the DSO to deliver electricity in a voltage range of $\pm 10\%(V_n)$. In the application presented in the following, the sending voltage at the feeder bus is fixed at +5% respect to the nominal voltage.

The three-phase branches composing the main feeder, with a maximum extension of 327 m, have three different types as reported in Figure 2.14 although in the analysis discussed below only one cable type was employed to represent all the three-phase connections (i.e. the 185 mm^2 XLPE cable). A complete description of the network's model is given in Appendix A.

Distributed generators are connected to some of the customers as can be seen in Figure 2.14, distinguishing in PV units and micro-wind generators. Daily power profiles are considered for the variation of loads consumption and generators production. In particular, for the customers the power profiles are deduced from a representative year data [51]. Both generators and loads in this analysis have been represented as constant power units in each instance of the 24-hours simulation, so in respect to the ZIP model description in equation 2.14, the value of parameter k_P is 1 (while, of course, $k_P = k_I = 0$).

The network's reaction to variable load/generation over a 24-hour period has been analysed by mixing the three power profiles shown in Figure 2.15 for the loads, referring to different seasons (load 1, 2 and 3 representing Autumn, Winter and Spring respectively) assigned as reported in Figure 2.14. The wind speed, solar irradiance and temperature considered to calculate the DG output power profiles shown in Figure 2.15 refer to recordings

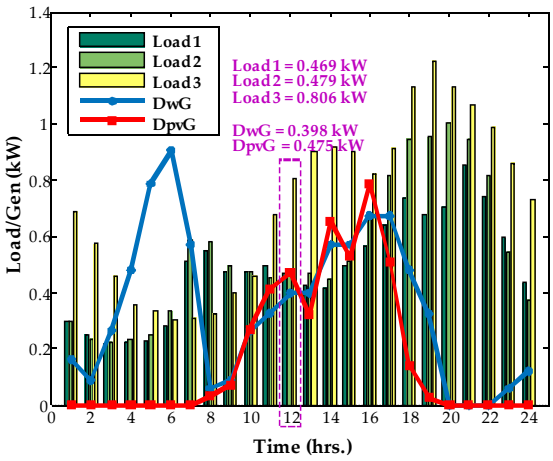

Figure 2.15: Daily power profiles for load and generation in the Irish LV distribution network.

over 24-hours in the Autumn period.

Initially the instance at h. 12 is highlighted for consideration. In this regard, the different load profiles identified in Figure 2.15 lead to total power consumptions of 0.469 kW, 0.479 kW and 0.806 kW (unity power factor) at the assigned consumer connections (as illustrated in Figure 5). The total amounts of power produced by DGw and DGpv in this instance are respectively 0.398 kW and 0.475 kW with power factor 0.95 applicable to both DG types. Table 2.1 reports the results in terms of currents at the PCC and busbar voltages detailed for the connections at pillars B and J (i.e. the extreme ends of the feeder). For the sake of validation, the same analysis has been conducted with the simulation software OpenDSS and DigSilent PowerFactory and the respective results reported in Table 2.2 confirm the correctness of the solution obtained through the CCI algorithm.

The voltage profile along the feeder on the 24-hours period is shown in Figure 2.16a for each phase and the neutral conductor employing the same presentation logic used in Table 2.1. Figure 2.16b illustrates the voltage unbalance at the respective pillars, defined as the ratio of the voltage negative and zero sequence components over the positive one, in percent [52, 53], i.e.:

$$VUF = \frac{V_- \cdot 100}{V_+} \tag{2.53}$$

$$VUF_O = \frac{V_0 \cdot 100}{V_+} \tag{2.54}$$

The maximum voltage drop along the feeder can be quantified as about 2% of the nominal voltage, being similar in each phase, while the pillar voltage unbalance varies from 0.002% to 0.198% and is within the acceptable tolerance (2%). This is mainly due to the distributed neutral grounding throughout the grid (including customer buses) and to

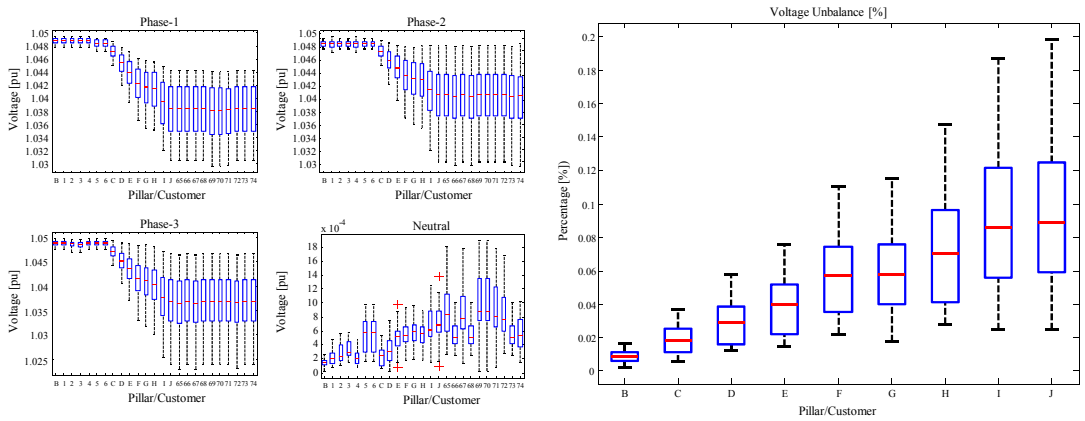

(a) (b)

Figure 2.16: Voltage profile in each phase (a) and VUF (b) in the Irish LV network at h. 12.

the relatively low power flow values, as derived from the reference scenario considered for loads and generators. An analysis of the possible effects coming from an intense growth of DG power installed in this system has been conducted in [40]. It should be also noted that with network configurations like the one considered here, having ground connections at each household besides at the three-phase line pillars, it is unlikely that the voltage unbalance overcomes the statutory limit of 2%. Nevertheless this issue may occur with other network structures having a single grounding point for the neutral conductor at the secondary substation LV busbar, like, for example, in the Italian and Danish LV distribution networks.

Table 2.1: Irish LV network's pillars and customers' bus voltage magnitudes and angles: results of the h. 12 instance.

Bus	V_1 [pu]	$\angle V_1$ [deg]	V_2 [pu]	$\angle V_2$ [deg]	V_3 [pu]	$\angle V_3$ [deg]	$V_{neutral}$ [pu]
B	1.0487	-0.04	1.0493	-120.01	1.0486	119.99	0.0002
1			1.0493	-120.01			0.0002
2					1.0485	119.99	0.0003
3					1.0483	119.99	0.0002
4			1.0493	-120.01			0.0007
5	1.0481	-0.04					0.0007
6	1.0481	-0.04					
C	1.0469	-0.08	1.0483	-120.03	1.0466	119.97	0.0004
D	1.0449	-0.14	1.0472	-120.05	1.0444	119.95	0.0005
E	1.0432	-0.19	1.0463	-120.07	1.0425	119.93	0.0007
F	1.0413	-0.24	1.0453	-120.08	1.0402	119.91	0.0007
G	1.041	-0.25	1.0452	-120.09	1.0399	119.91	0.0007
H	1.0402	-0.28	1.0448	-120.09	1.0385	119.89	0.0008
I	1.0394	-0.3	1.0444	-120.09	1.0373	119.87	0.0008
J	1.0391	-0.31	1.0442	-120.1	1.0369	119.87	0.0008
65					1.0363	119.87	0.0009
66			1.0439	-120.1			0.0006
67					1.0365	119.87	0.0008
68			1.0439	-120.1			0.0006
69	1.0385	-0.32					0.0013
70	1.0385	-0.32					0.0013
71	1.0388	-0.31					0.0011
72					1.0366	119.87	0.0008
73			1.0439	-120.1			0.0006
74			1.0438	-120.1			0.0006

Table 2.2: Results obtained with the simulation software OpenDSS and DigSilent PowerFactory.

	OpenDSS							**PowerFactory**						
	V_1 [pu]	$\angle V_1$ [deg]	V_2 [pu]	$\angle V_2$ [deg]	V_3 [pu]	$\angle V_3$ [deg]	V_n [pu]	V_1 [pu]	$\angle V_1$ [deg]	V_2 [pu]	$\angle V_2$ [deg]	V_3 [pu]	$\angle V_3$ [deg]	V_n [pu]
B	1.0487	0.0	1.0494	-120.0	1.0486	120.0	0.0002	1.0487	0.0	1.0493	-120.0	1.0486	120.0	0.0002
C	1.0469	-0.1	1.0484	-120.0	1.0467	120.0	0.0003	1.0469	-0.1	1.0483	-120.0	1.0467	120.0	0.0004
D	1.0450	-0.1	1.0472	-120.1	1.0445	119.9	0.0005	1.0450	-0.1	1.0472	-120.1	1.0444	119.9	0.0005
E	1.0433	-0.2	1.0463	-120.1	1.0426	119.9	0.0006	1.0433	-0.2	1.0462	-120.1	1.0426	119.9	0.0007
F	1.0415	-0.2	1.0454	-120.1	1.0403	119.9	0.0007	1.0414	-0.2	1.0453	-120.1	1.0403	119.9	0.0008
G	1.0412	-0.3	1.0453	-120.1	1.0400	119.9	0.0007	1.0412	-0.3	1.0452	-120.1	1.0400	119.9	0.0007
H	1.0404	-0.3	1.0449	-120.1	1.0387	119.9	0.0008	1.0403	-0.3	1.0448	-120.1	1.0387	119.9	0.0008
I	1.0396	-0.3	1.0445	-120.1	1.0375	119.9	0.0008	1.0396	-0.3	1.0443	-120.1	1.0375	119.9	0.0008
J	1.0393	-0.3	1.0443	-120.1	1.0371	119.9	0.0008	1.0392	-0.3	1.0441	-120.1	1.0370	119.9	0.0008

2.6.2 Proposal of a decoupled phase-tap-changer transformer

An interesting application of the multi-phase approach on which the CCI algorithm is based is discussed in the following, presenting the case study of a phase-decoupled on-load-tap-changer transformer for voltage management in LV networks [54].

One of the main issues modern distribution networks are facing these days is the voltage management in LV networks. For this reason, some research have been presented lately discussing the possibility of employing on-load-tap-changers even at the MV/LV interface (i.e. the Secondary Substation) to control the voltage magnitude. Some commercial products are already available relaying on electronic switching capabilities [55] and are commonly referred to as *Smart Transformers* [56–59].

As will be deeply discussed in the following chapters, the problem of voltage unbalance mitigation in LV networks may become of fundamental importance going into the future. For this reason, the on-load-tap-changing capability of the transformer has been investigated together with the possibility of independently varying the tap position on the three phases allowing the voltage unbalance regulation at a specific busbar. The possibility to switch the tap position independently on the phases could help to control the uneven voltage drop due to unbalances in the power flow, meaning that, for instance, in case one of the phases is particularly loaded, the transformer will reduce the ratio just on that specific phase, without involving configuration changes of the other two phases.

In Figure 2.18 the control setup is schematically depicted, showing that a remote bus is taken as reference, assuming the presence of a communication infrastructure allowing the voltage measurement signals to be sent to the Secondary Substation. The OLTC operation is run through the control scheme reported in Figure 2.18b where an integral action is shown for the tap changing feature: each time the respective phase-voltage overcomes the Dead-Band (i.e. a voltage range around the nominal value V_{ref}), the tap position is increased or reduced accordingly.

The network considered for application consists in a 12-bus Danish LV feeder connected to the MV network through a 10/0.4 kV Delta-Wye transformer as shown in Figure 2.17 [60]. The short circuit power of the main network is 20 MVA. Measurements on the real system allowed characterizing the power consumption of the 33 single phase loads during a 24-hours interval which resulted to be about 740 kWh, with a mean power of 30.8 kW. For a full description of the network's model, see Appendix B.

As reported in the network layout in Figure 2.17, the controlled bus in this case is Bus 10, placed at the feeder-end. The simulations have been conducted over a 24-hour period under three scenarios:

1. **Synchronized OLTC:** the OLTC is operated simultaneously on the three phases, taking as reference the phase voltage at phase a. The tap-changing ratio is the same adopted for off-load operation in distribution transformers;

2. **Phase-wise OLTC – discrete:** three independent controllers are set referring each

to the respective phase. The control uses the same tap changing ratio used for the synchronized action;

3. **Phase-wise OLTC – continuous:** the independent action of each phase is considered with a higher number of taps with smaller variations.

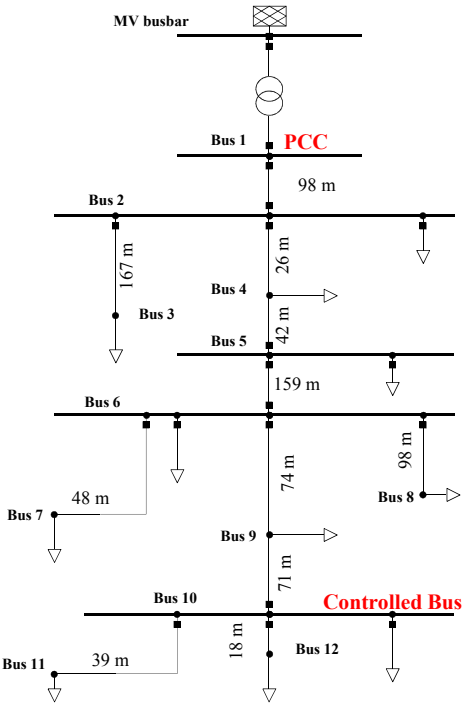

Figure 2.17: Layout of the case study Danish real LV distribution network.

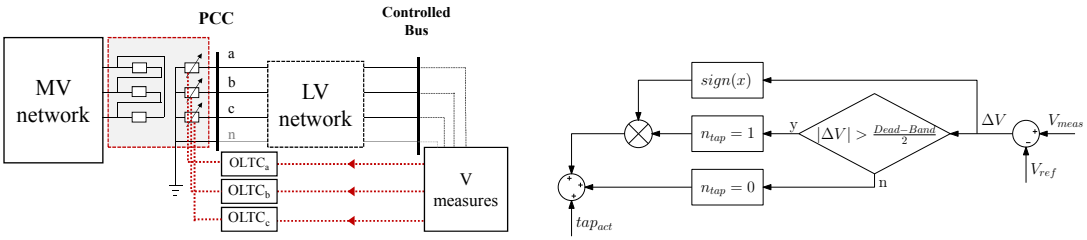

Figure 2.18: Control setup for the implementation of the decoupled OLTC.

The objective of the control is to minimize the voltage deviations respect to the nominal value at the feeder end, considering a Dead-Band of $\pm 2\%(V_n)$, with the possibility by the OLTC to switch on 5 positions for a total $\pm 5\%(V_n)$ variation, i.e. with steps of $\Delta V = 2.5\%(V_n)$. This capability is enhanced in scenario 3 where the total variation range is covered by a finer tap regulation, with steps of $\pm 0.1\%(V_n)$ and a Dead-Band set at $\pm 0.25\%(V_n)$.

The simulation of the Base Case (i.e. the non-regulated case applying the measured power profiles shown in Figure 2.19) resulted in the phase-neutral voltage profiles shown

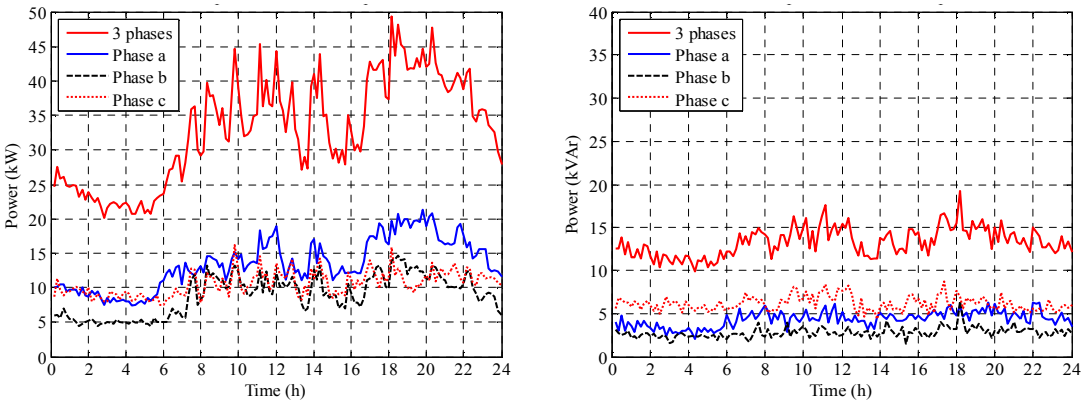

(a) (b)

Figure 2.19: Active (a) and reactive (b) power measured over a 24-hours period for the three-phases and in total on the Danish LV network.

in Figure 2.20a. As it can be seen, the profile follows what is expected in a residential area, with low loading during the night (from 0 to 6 a.m.) and higher absorption by loads in the evening (from 6 to 12 p.m.). The maximum voltage sag could be observed around 8 p.m. in phase a, with 0.955 pu.

In scenario 1, the OLTC operates a synchronous tap variation on the three-phases. By hypothesis, the reference voltage has been considered the one in phase a, so the voltage profile, shown in Figure 2.20b, highlights the ΔV=0.025 pu variations introduced by the tap changes occurring when the phase-a voltage overcomes the Dead-Band limit. Around h. 6 the loads consumption starts intensifying, causing a voltage drop that is faced by a +1 tap variation. The same situation occurs around h. 20 when the load in phase-a is heavier than on the other two, so the tap adjustment causes an undesired voltage rise on phases b and c.

Scenario 2, although still applying the voltage variation per tap considered in the previous one, adopts the decoupled OLTC capability, allowing each phase to be controlled independently. Figure 2.20c reports the voltage profile at bus 6 for Scenario 2, showing that the tap controllers react to the Dead-Band overcoming by the relative voltage in different instants reducing the deviations within the Dead-Band. On the other hand, this operation could possibly adversely affect the voltage unbalance as shown in Figure 2.21, where the Voltage Unbalance Factor (negative sequence) in scenarios 1 and 2 are compared.

In scenario 3, along with the decoupled OLTC operation on the phases, a finer regulation is adopted by considering a higher number of steps. From Figure 2.20d it can be seen that the voltage regulation at bus 6 results more accurate since the Dead-Band region is respected during all the simulated period. In Figure 2.22 the VUF values for scenario 2 and 3 are compared, showing that a continuous tap adjustment may overcome the issue of increasing the VUF due to a discrete control, as highlighted also in Table 2.3 reporting the average values of VUF and phase voltages at Bus 10.

Table 2.3: Average values of VUF and phase voltages at bus 6 during the 24-hours simulation.

	VUF	**Bus 10 Voltage [pu]**		
	[%]	ph a	ph b	ph c
Base Case	0.2760	0.9746	0.9851	0.9819
Synchronized	0.2850	0.9960	1.0062	1.0019
Discrete Phase-wise	0.4500	0.9960	1.0018	1.0048
Continuous Phase-wise	0.2180	0.9996	0.9999	0.9997

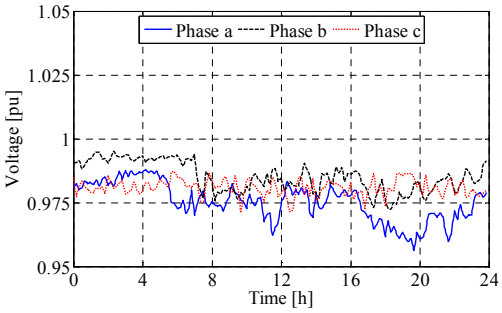

(a) Base Case

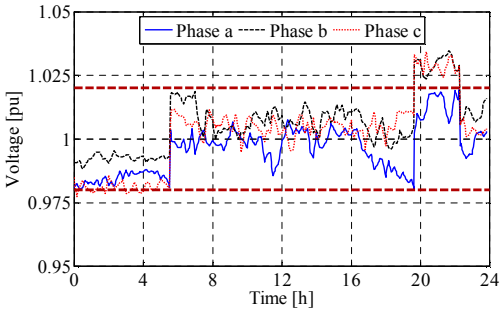

(b) Scenario 1

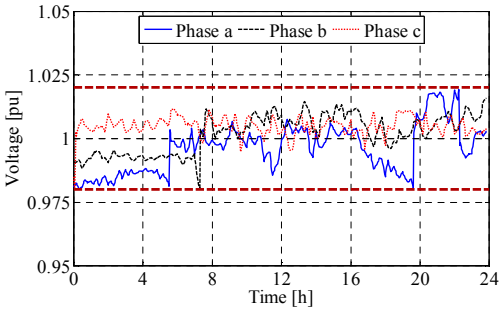

(c) Scenario 2

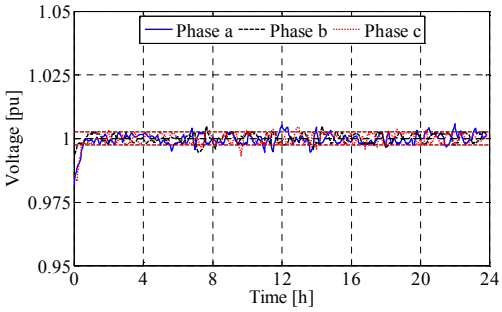

(d) Scenario 3

Figure 2.20: Phase voltage at the controlled bus 6 during the 24-hours simulation in the three scenarios compared with the non regulated Base Case.

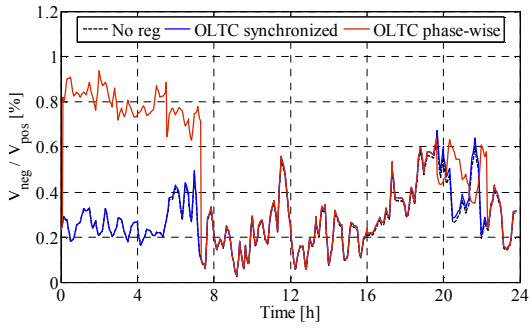

Figure 2.21: Voltage unbalance factor (VUF) in scenarios 1 and 2.

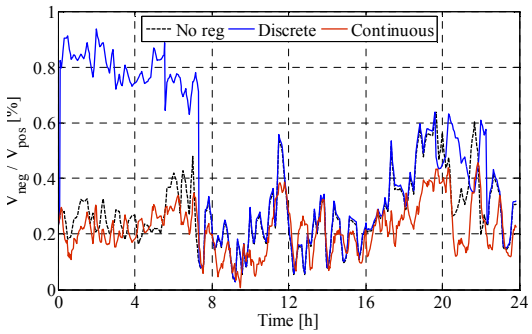

Figure 2.22: Voltage unbalance factor (VUF) in scenarios 2 and 3.

Figure 2.23: Single-phase toroidal transformer with continuous tap selector.

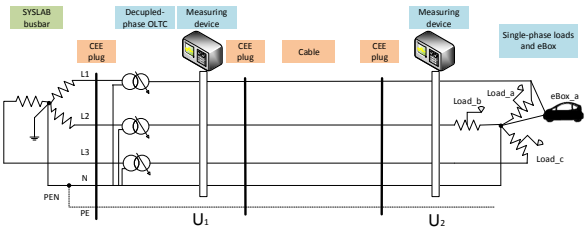

Figure 2.24: Scheme of the experimental setup for the OLTC test.

The research conducted on this topic was part of the Energy Saving by Voltage Management Project (EUDP – Danish project) and included also an application of the discussed OLTC operation in presence of distributed generation on the same LV feeder, even including the reactive power provision by inverters for local voltage support [61, 62].

The model discussed previously has been validated experimentally in the research infrastructure SYSLAB-PowerLabDK, a laboratory facility for the development and test of control and communication technology for active and distributed power systems, located at the DTU Risø campus [63].

The experimental setup, schematically shown in Figure 2.24 includes a cable with impedance equivalent to the one between the LV busbar and Bus 10 in LV network in Figure 2.17, a three-phase controllable load and a power source represented by an Electric Vehicle (EV) performing a Vehicle-to-Grid (V2G) service. The Phase-Decoupled OLTC used for the test has a rated power of 35 kVA and is capable of continuously changing the tap position allowing a voltage regulation in the range $\pm 10\%(V_n)$. A picture of one of the single-phase transformers composing the three-phase OLTC is shown in Figure 2.23.

The results of this activity are still to be published, but the results of two of the tested scenarios are reported here as enlighting examples. The first scenario is a passive case, in which the loads connected to the three phases are increased simultaneously by steps of 1.1 kW from 0 to the rated power per phase (i.e. 11.6 kW). The second scenario considers the presence of the EV as a source injecting active power to the network, connected to phase a as could be seen in Figure 2.24. The controlled bus in this test is the PCC, while loads and generator are connected to the bus at the end of the line. In both scenarios, the OLTC device has demonstrated to behave as expected by the simulation activity, as can be seen from the good agreement between the measured voltages and the simulated ones.

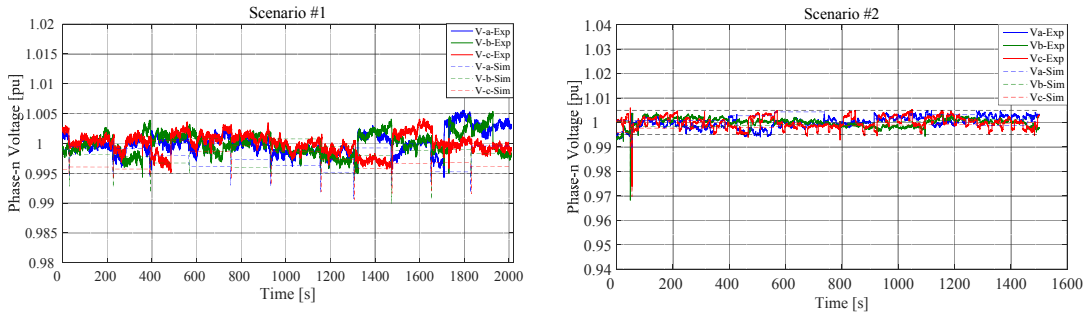

(a) (b)

Figure 2.25: Phase Voltage results for the experimental test and simulation of the Phase-Decoupled OLTC in scenario 1 and 2.

2.6.3 Application of the generalized transformer model

In this section an application of the generalized transformer model discussed in section 2.3 is presented to compare different connection options dealing with load unbalance. This kind of comparison has been presented in [49], which has been used here as a reference for the validation of the model discussed so far.

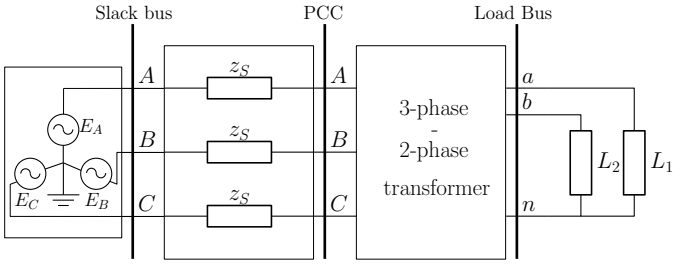

Figure 2.26: Three-phase circuit for the application. Different options are compared changing the 3-phase/2-phase model and testing the effects of different load unbalances.

The circuit considered in this application is shown in Figure 2.26: the main three-phase network feeding the system has been modeled introducing longitudinal impedances between the slack bus (represented as a wye-connected triplet of voltage generators) and the PCC. The loads are connected to the secondary side of the transformer in a 2-phase plus neutral system as in the case of a traction load. In the following, the generalized transformer model described in the previous sections will be applied to obtain three connection options to the Load Bus. Even the source impedance connected between the Slack bus and the PCC can be modeled as a transformer: using the Wye-wye connection with a unitary transformation ratio (in pu), in fact, the result for the branch element will be a three-phase π-model composed by longitudinal impedances only (called z_S in Figure 2.26).

Figure 2.27 shows the connection schemes for the three options considered to connect the Load Bus to the PCC. As could be seen, even if the phase connections on the primary side change, each transformer is composed by two single-phase circuits, meaning that the

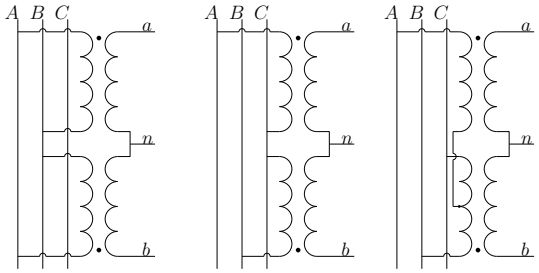

Figure 2.27: Connection scheme for the three options tested in the application: a) single-phase, b) V-connection, c) Scott-connection

order of the corresponding incidence matrix **B** will be $[(2 \times 2) \times (2 \times 3)] = [4 \times 6]$. Its composition for the three cases depicted in Figure 2.27 is shown in equation (2.55), where it should be noted that real values may be used to compose the incidence matrix which contains also the information about the specific topology (as for the Scott connection matrix).

$$\begin{aligned}
\mathbf{B_{1ph}} &= \begin{bmatrix} 1 & -1 & 0 & 0 & 0 & 0 \\ 1 & -1 & 0 & 0 & 0 & 0 \\ 0 & 0 & 0 & 1 & 0 & -1 \\ 0 & 0 & 0 & 0 & 1 & -1 \end{bmatrix} \\
\mathbf{B_V} &= \begin{bmatrix} 1 & 0 & -1 & 0 & 0 & 0 \\ 0 & 1 & -1 & 0 & 0 & 0 \\ 0 & 0 & 0 & 1 & 0 & -1 \\ 0 & 0 & 0 & 0 & 1 & -1 \end{bmatrix} \\
\mathbf{B_{Scott}} &= \begin{bmatrix} 1 & -0.5 & -0.5 & 0 & 0 & 0 \\ 0 & 1 & -1 & 0 & 0 & 0 \\ 0 & 0 & 0 & 1 & 0 & -1 \\ 0 & 0 & 0 & 0 & 1 & -1 \end{bmatrix}
\end{aligned} \tag{2.55}$$

The data for the test circuit shown in Figure 2.26 are taken from [49] and are recalled in the following.

The Slack bus imposes three phase voltages E_{LN}:

$$\begin{cases} E_A = E_{LN} \cdot \exp^{j0} \\ E_B = E_{LN} \cdot \exp^{j\frac{-2\pi}{3}} \\ E_C = E_{LN} \cdot \exp^{j\frac{2\pi}{3}} \end{cases} \tag{2.56}$$

where the subscript LN stands for line-to-neutral. Defining the base values for apparent

power and voltage as S_{Base} and V_{Base} the impedance z_S for each phase is calculated as:

$$z_S = \frac{E_{LL}^2}{S_S} \cdot \frac{S_{Base}}{E_{Base}^2} \quad \text{(p.u.)} \tag{2.57}$$

where:
S_S is the three-phase apparent power for the equivalent source;
E_{LL} is the line-to-line voltage ($E_{LL} = \sqrt{3}E_{LN}$).

The transformer's short-circuit impedance z_T is calculated as:

$$z_T = \frac{E_{sc}}{E_{1R}} \cdot \frac{E_{1n}^2}{S_R} \cdot \frac{S_{Base}}{E_{Base}^2} \quad \text{(p.u.)} \tag{2.58}$$

where:
E_{sc} is the short-circuit voltage in V;
E_{1R} is the rated voltage at the primary side in V;
S_R is the rated apparent power for one phase in VA.

Finally, the load impedance is defined depending on the apparent power:

$$z_L = \frac{E_{LN}^2}{S_{Lx}} \cdot \frac{S_{Base}}{E_{Base}^2} \quad \text{(x=1, 2)} \quad \text{(p.u.)} \tag{2.59}$$

where the E_{LN} term stands for the phase-voltage on the 2-phase system and S_L is the single-phase load power in VA.

In this example, assuming as S_{Base} the transformer's single-phase rated power (S_R) and as E_{Base} the phase-neutral voltage E_{LN}, the magnitudes of the three phase-voltages in (2.56) are 1 pu, while the impedances are calculated considering the following values: S_S = 4000 MVA, S_R = 50 MVA, $E_{1R} = E_{LN}$, $E_{sc} = 8\%(E_{1R})$, $S_{L1} + S_{L2}$ = 50 MW. With this set of data and the mentioned base values, the impedances in the circuit result: $z_S = 0.035$ pu and $z_T = 0.08$ pu.

The three connection options in Figure 2.27 have been tested under different load unbalance conditions obtained by changing the power ratio of each load and not varying the total power S_L:

$$S_{L1} = k \cdot S_L; \qquad S_{L2} = S_L - S_{L1} \tag{2.60}$$

The result of the comparison is shown in Figure 2.28, where it could be seen that the Scott connection is the only one to eliminate the voltage unbalance when the two single phase loads are equal. The results shown here are consistent with the ones in [49], validating the approach discussed so far.

The phase voltage results are reported in table 2.4 for each connection considering three cases of load unbalance and the respective voltage vectors are shown in Figure 2.29. A consideration should be done regarding the neutral point shifting under the different

Table 2.4: Phase voltages under three unbalance conditions with each connection option.

Conn.	k	E_{AB}	E_{BC}	E_{CA}	E_{an}	E_{bn}	E_n
1-ph	0.0	1.728 ∠28.6	1.712 ∠−90.3	1.750 ∠149.6	0.998 ∠28.6	0.995 ∠24.0	0.498 ∠−153.7
	0.5	1.730 ∠28.6	1.713 ∠−90.3	1.750 ∠149.6	0.998 ∠26.3	0.998 ∠26.3	0.499 ∠−153.7
	1.0	1.728 ∠28.6	1.712 ∠−90.3	1.750 ∠149.6	0.995 ∠24.0	0.998 ∠28.6	0.498 ∠−153.7
V	0.0	1.750 ∠29.6	1.728 ∠−91.4	1.712 ∠149.7	0.989 ∠−30.3	0.995 ∠−96.0	0.417 ∠116.7
	0.5	1.732 ∠29.6	1.740 ∠−90.9	1.721 ∠149.1	0.993 ∠−33.2	1.004 ∠−93.2	0.432 ∠116.6
	1.0	1.712 ∠29.7	1.750 ∠−90.4	1.728 ∠148.6	0.995 ∠−36.0	1.010 ∠−90.4	0.446 ∠116.6
Scott	0.0	1.750 ∠29.6	1.728 ∠−91.4	1.712 ∠149.7	1.000 ∠0.0	0.995 ∠−96.0	0.334 ∠132.2
	0.5	1.731 ∠29.3	1.731 ∠−90.7	1.731 ∠149.3	0.999 ∠−3.0	0.999 ∠−93.0	0.353 ∠132.0
	1.0	1.710 ∠29.0	1.732 ∠−90.0	1.748 ∠148.9	0.995 ∠−6.0	1.000 ∠−90.0	0.371 ∠131.9

connections: its deviation, in absolute, decreases from about 0.5 pu with the single-phase connection to about 0.35 pu with the Scott transformer. For the sake of completeness the case with grounded neutral on the load's side is also reported in Figure 2.30.

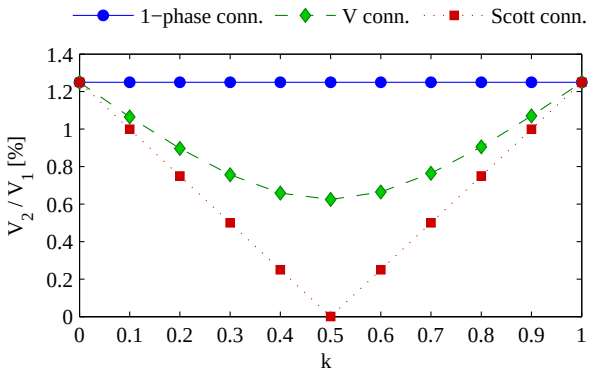

Figure 2.28: Comparison among the three different kind of connections in relation to the load unbalance.

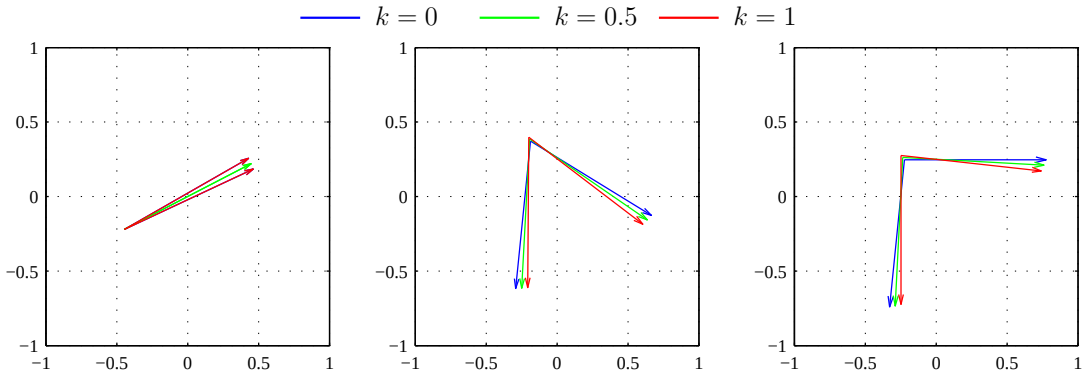

(a) Single-phase connection (b) V-connection (c) Scott-connection

Figure 2.29: Phase voltage on the Load Bus with different connection options and isolated neutral under three load unbalance conditions: $k = 0$ (blue), $k = 0.5$ (green) and $k = 1$ (red).

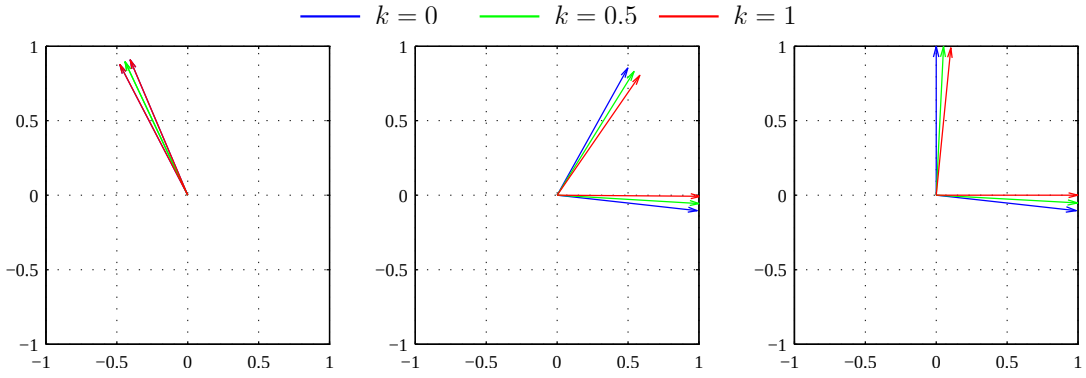

(a) Single-phase connection (b) V-connection (c) Scott-connection

Figure 2.30: Phase voltage on the Load Bus with different connection options and grounded neutral under three load unbalance conditions: $k = 0$ (blue), $k = 0.5$ (green) and $k = 1$ (red).

Chapter 3

Medium Voltage Distribution Management System

Contents

The ever increasing penetration of distributed generation in distribution networks is leading to a significant worsening of the system working conditions. As a result, Distribution System Operators (DSO) may be forced into new investments for network upgrade or to find new solutions to tackle the problem of grid management. To face the challenge represented by the search for suitable management solutions, several strategies can be found in literature, discussing both centralised and decentralised controls aiming at exploiting the DERs capabilities in the network regulation. This chapter approaches the problem of the distribution grid management proposing a strategy for the participation of the distributed resources aiming at regulating contingencies due to voltage magnitude deviations or congestions in the network branches, supposing the presence of a local energy market through which the DERs are allowed to offer and provide ancillary services. Several case studies demonstrate the improvements in power quality obtainable by the application of this strategy and its possible employment as a way to coordinate the MV distribution network to offer ancillary services for the transmission grid management.

3.1 Active users as a resource for the network regulation

Standing the very fast growth of installed generation in distribution networks in the last years, DSOs may consider the application of alternative solutions to the grid reinforcement investments by implementing regulation strategies aimed at exploiting the presence of Distributed Generation (DG), Active Demand (AD) and storage-capable users (e.g. electric vehicles) summarized with the expression "active users" at the scope of increasing the energy efficiency of the system. In [64] the economical benefits deriving from such a coordination strategy are compared with the reinforcement investments.

In literature, several solutions have been presented dealing with the necessity of involving DERs in the network management and they can be summarized in mainly two kind of approaches, distinguishing the centralised and distributed control. The debate between the two approaches is still open even though the vast majority of real applications are based on light decentralised systems with a control system that operates in Primary Substation and controls all the resources spread into the supplied system. The major drawback of such systems is represented by the difficulty to operate in quasi-real time systems with storage capabilities (i.e. electric, thermal and mechanical storage) in real scale applications. On the other hand, simulations and experiments proved that decentralized DMS can significantly reduce the amount of information exchange among players and, thus, be applied in real time applications. Application of both the approaches are presented in [65].

The centralised Energy Management System (EMS) is a concept based on the hypothesis that the DSO is allowed to set the users' operating conditions according to Optimal-Power-Flow (OPF) calculations run by a central unit. The OPF optimizes an objective function summing all the operational costs related to all the active management actions which may be adopted and the distribution system's technical constraints (e.g., line thermal limits, nodal voltage, reserve, etc.). This kind of optimization based on price signals offers the possibility to optimally coordinate the participation of DER in the network regulation while suitably scheduling the cyclic operation of storage units.

An EMS resorts to the following operation options [66], depicted in Figure 3.1:

- Optimization of the On Load Tap Changer (OLTC) position;
- Active power generation curtailment (GC);
- Active power injection from programmable generators;
- Volt/Var regulation with DG and storage;
- Demand Side Integration (DSI), to involve customers that participate to Active Demand (AD) programs, possibly including the payback effect [67]- [68] for a better representation of its real impact;

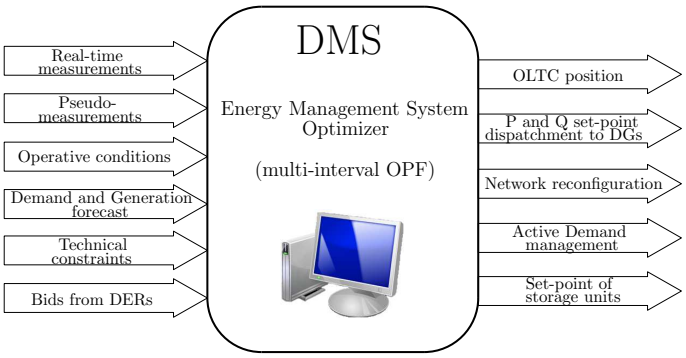

Figure 3.1: Schematic representation of the centralised Distribution Management System (DMS).

- Energy losses minimization to improve the total energy efficiency;

- Storage devices charge and discharge used for load levelling and voltage regulation [69]- [70].

Regarding the decentralised approach to network regulation, most of the research works in literature rely on a Multi Agent System (MAS) to involve users in the network management. The MAS concept for Power Engineering applications is described in [71]: although a number of definitions of *agent* are given in literature, many of them agree to the concept that it is an entity (either software or hardware) capable of autonomously react to changes in the environment (i.e. the external system). As far as the distributed control of a power system is concerned, agents need to be capable of a number of actions such as: working conditions monitoring, manage availability and technical requirements of the users composing it, communicate with other agents.

The MAS is used for instance in [72] and in [73] to coordinate voltage regulation in an active network. Distributed algorithms for the active network management are presented in [74, 75] and [76] to implement the dissemination of control signals among agents in order to obtain ancillary services from the Distributed Energy Resources (DERs) including demand response.

Regardless of the approach chosen for the network control, the transition to a Smart Grid environment needs a substantial improvement of the Information and Communication Technologies (ICT) in the power system, allowing the exchange of signals from and to the users. In [77] the IEC 61850/61499 communication protocols are used for the automation of a distribution system applying the Multi-Agent approach to the fault location and power restoration issues. In the following sections a DMS based on the decentralised approach is presented and applied to several case studies to simulate a distribution network control and coordination for its participation to the ancillary services' market.

3.2 A distributed procedure for active users participation

In the following, a strategy for the management of a distribution grid is presented considering the decentralised solution discussed in the previous section. The main goal of the procedure is to ensure the free choice of any active element to participate or not in network regulation, meaning that each user may decide whether to participate or not to the network management according to power availability, offered remuneration for the regulation service, priority level required and allowed maximum active and reactive power variation set by the system operator. In other words, the aim of the developed procedure is to implement a local energy market for the provision of ancillary services.

As previously mentioned, since the challenge is to involve an ever growing number of distributed resources to the network management, the presence of communication infrastructures is necessary for modern distribution networks, so in this work the exchange of signals among different subjects is assumed to be suitably working. Under this hypothesis, the electrical network management could be imagined to be working as for an internet-like model, using those infrastructures to collect the set of power contributions from the distributed resources.

As proposed in the Multi-Agent-System (MAS) approach, the key feature of the strategy is to decompose the system complexity in separate levels communicating to each other. The problem of managing the network, then, is not solved by a single optimization problem, but rather as a set of sub-problems leading to local optimal solutions. In this perspective, every node can be considered as a separate agent acting independently from the others, just replying to signals received from the network according to its own technical constraints. Furthermore, the entire network system could be considered as a set of sub-systems communicating to a cluster of buses, reducing even more the complexity of the operation.

The procedure developed in this work can be depicted as in Figure 3.2, combining the concepts introduced so far. The architecture of the control is similar to one of the protocols used for computer networks operation, called token-ring [78]. A main network supervisor monitors the grid collecting the remote voltage and current measurements coming from the grid's buses and branches. If a contingency occurs, either violating the voltage objectives is any of the busbars or exceeding the ampacity of one of the branches, the network is decomposed into several regulation areas clustering buses depending on their mutual electrical coupling and on the operating conditions. Suitable signals aiming at obtaining the needed active and reactive power variations are forwarded to each area, where the active users are involved in the regulation though a local market logic, setting prices for the services provision. The Primary Substation Transformer's OLTC is also involved in the strategy, varying the transformation ratio helping to reach the voltage objective.

The multi-level management ensures an overall objective to be achieved, by decomposing the complexity of the management of system into micro-area levels. In the following

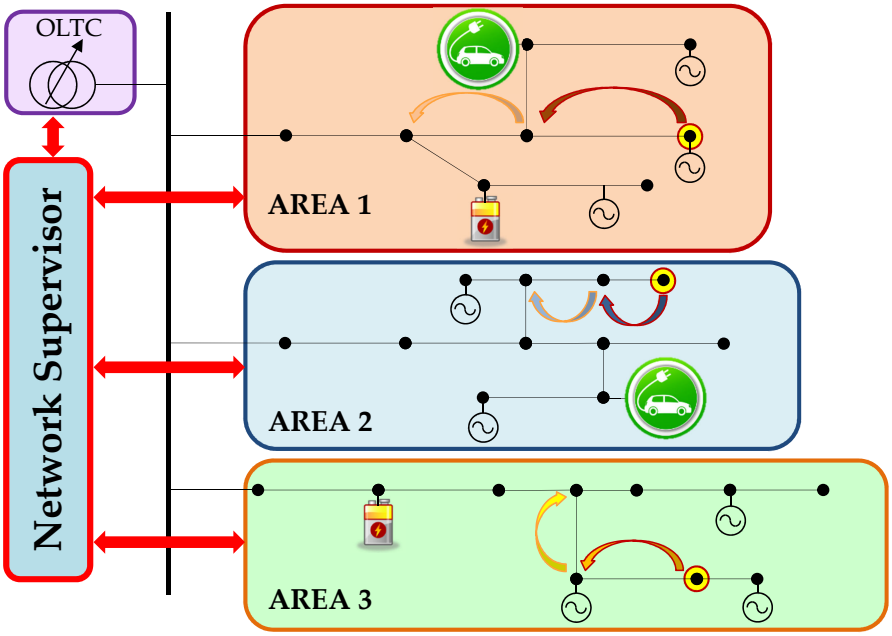

Figure 3.2: Conceptual scheme of the distributed regulation procedure: the network is divided in several areas where the quantity/price signals can circulate, the OLTC is also a subject involved in the control.

the procedure is detailed in each part, describing the operations related to the occurrence of a voltage or current contingency.

3.2.1 Primary Substation's OLTC coordination

Standing the hypothesis of a well developed communication infrastructure, reliable informations about the grid status are expected to be available for the network supervisor (i.e. remote measures or pseudo-measures). In this perspective, the regulation strategy exploits the Primary Substation transformer's On-Load-Tap-Changer ($OLTC$) coordinating it with the requests sent to the local areas in order to help the overall network management.

As a common practice, since generally distribution grids are radial, the OLTC is employed to maintain a fixed voltage magnitude at the MV busbar downstream the Primary Substation, acting in Automatic Voltage Regulation (AVR) mode by varying the transformation ratio to compensate the voltage deviations. This kind of operation works well in case of a passive grid, since the power flows are uni-directional, so changing the initial voltage value will affect the voltage drops on the branches controlling the deviations at the end of the line.

With the presence of distributed generation (DG) the power flow direction may not be known for every feeder departing from the Primary Substation, so the OLTC action as AVR may not be the best choice since the voltage drops are not known. Assuming the availability of remote measurements through real-time communication, a coordination of this device becomes possible aiming at reducing the overall voltage deviation.

The flow chart in Figure 3.3a shows how the remote voltage measurements (once the

maximum and minimum are selected) are used to influence the choice of varying or not the tap position and in which direction. Maximum and minimum thresholds are set in order to evaluate the voltage objectives (they should be the same adopted for the network regulation), then a truth-table combines the input states enabling the tap variation. In particular, the OLTC action is enabled only if just one of the voltage extremes is beyond the objective and even then only if the voltage variation caused by a tap change (indicated with $\Delta V_{\%}$) is less then the distance between the other voltage extreme and the respective objective. This concept is explained pictorially in Figure 3.3b, where an example of voltage profile is shown for a network with two feeders where one is passive (blue) and the other hosts DGs leading to reverse power flow (red). In this case, since only the passive feeder presents a violation of the objective (i.e. 0.95 p.u.), the OLTC action is allowed since the voltage variation introduced by the tap change is lower than ΔV_1 (i.e. the range between the maximum voltage on the other feeder and its objective). From the example it should also be noticed that an *AVR* action by the OLTC, set on the nominal voltage (i.e. 1 p.u.) would have lead probably to a voltage violation on the active feeder (red), confirming the necessity of a coordinated action with remote measurements.

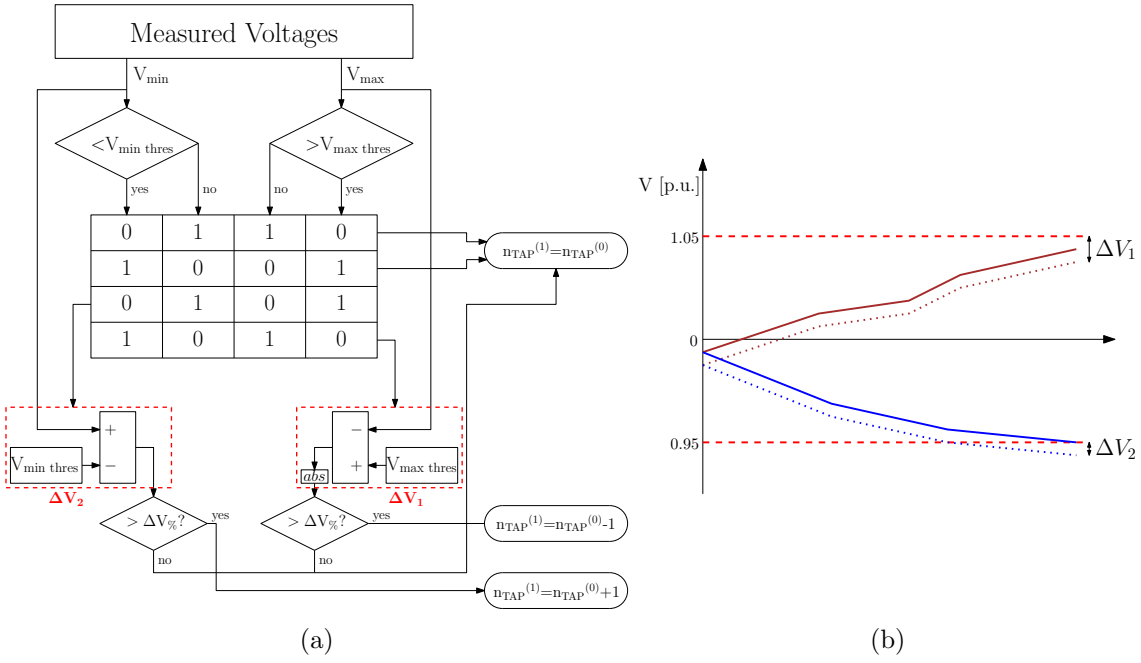

Figure 3.3: Flow chart of the OLTC coordination procedure (a) and example of the voltage trend in two feeders with opposite power flows (b).

3.2.2 Congestions regulation

Before considering any control procedure for the voltage regulation aiming at improving the power quality, a check on the actual network's operating conditions is necessary. In particular, a critical situation which may occur when a considerable amount of generation is connected to the system is that one or more branches overcome their ampacity levels. This would practically result into protections tripping with the consequent disconnection of the overloaded branch and, if the network is radial, of the downstream feeder. To solve this contingency, avoiding the loss of service, a procedure for the compensation of the power flows through active power requests is described in the following.

As mentioned in the description of Figure 3.2, the network supervisor elaborates the request signals based on the remote current measurements acquired from the grid's branches and forwards them to the regulation areas, so the first step of the procedure consists in the areas definition. This process is carried out through the definition of a Transmission Congestion Distribution Factor ($TCDF$) which is an approach initially proposed for High-Voltage grids where the active power flow mainly depends on the voltage angle due to the ratio $R/X \ll 1$ [79]. This assumption may still be valid for many MV networks, especially those connecting in large part rural areas, consisting generally in overhead lines.

The coefficients of the $TCDF$ matrix represent the variation of active power in a line due to a change in the power exchanged at the terminal bus, so for a generic line k connecting buses i and j it can be written:

$$TCDF_i^k = \frac{\Delta P_{i-j}}{\Delta P_i} \tag{3.1}$$

where ΔP_{i-j} is the active power variation on line k, while ΔP_i is the one at the ending bus i.

The active power on line k is given by:

$$P_{i-j} = V_i V_j Y_{ij} cos(\theta_{ij} - \delta_i - \delta_j) - V_i^2 Y_{ij} cos\theta_{ij} \tag{3.2}$$

where δ indicates the voltage angle at the respective bus, θ_{ij} is the phase difference between the two buses and Y_ij is the mutual admittance.

Using Taylor's series approximation and ignoring terms with order higher than 1, equation (3.2) can be written as:

$$P_{i-j} = \frac{\partial P_{i-j}}{\partial \theta_i}\Delta\theta_i + \frac{\partial P_{i-j}}{\partial \theta_j}\Delta\theta_j + \frac{\partial P_{i-j}}{\partial V_i}\Delta V_i + \frac{\partial P_{i-j}}{\partial V_j}\Delta V_j \tag{3.3}$$

then, substituting equation (3.4), defining the voltage phase variation $\Delta\theta$ through the Newton-Raphson Jacobian relationship between voltage phases and active power:

$$\Delta\theta = \frac{\partial\theta}{\partial P}\Delta P = \left(\frac{\partial P}{\partial\theta}\right)^{-1}\Delta P \tag{3.4}$$

in equation (3.3), neglecting the terms coupling active power and voltage magnitude as for the aforementioned hypothesis of having $R/X \ll 1$, it can be written:

$$TCDF_i^k = \frac{\partial P_{i-j}}{\partial \theta_i} \cdot \frac{\partial \theta_i}{\partial P_i} + \frac{\partial P_{i-j}}{\partial \theta_j} \cdot \frac{\partial \theta_j}{\partial P_i} \tag{3.5}$$

The *TCDF* matrix coupling lines and buses allows to set a criterion on which the network buses may be clustered in order to deal with the congestion on a certain branch, identifying which buses may influence the relative power flow. Once the regulation areas have been defined, the active power variation requests are evaluated for each contingency as:

$$\Delta P_j = P_j \frac{(k_{amp\%} - 100)}{100} \tag{3.6}$$

defining the active power variation neeeded at bus j as a linear dependency of the active power with the ampacity level, defined as $k_{amp\%}$, which is the percent ratio between the actual current and the nominal one.

3.2.3 Voltage regulation

Aside from the congestion management described in the previous section, a distributed voltage regulation procedure is also considered, still applying a local area approach similar to the one described for the congestions management.

In this case, the criteria adopted to group the buses is the *electrical distance* which is a measure of the mutual sensitivity among the network buses in relation to reactive power variations [80, 81]. Considering the sensitivity matrix, obtainable inverting the $\partial Q/\partial V$ sub-matrix of the system's Jacobian, the relation among two generic nodes i and j can be expressed as:

$$\Delta V_i = \alpha_{ij} \cdot \Delta V_j = \left[\frac{\partial V_i/\partial Q_j}{\partial V_j/\partial Q_j}\right] \cdot \Delta V_j \tag{3.7}$$

from which the *electrical distance* can be derived in the form:

$$ed_{ij} = -ed_{ij} = -log(\alpha_{ij} \cdot \alpha_{ji}) \tag{3.8}$$

The electrical distance matrix **ed** composed by the terms defined in equation (3.8), having dimension $[n \times n]$ for a system with n nodes, allows to quantify the influence in terms of voltage variations due to the reactive power exchange at a certain bus, then permitting a coherent clustering. This process needs the definition of a so-called *pilot bus*, which consists in the most significant one within the area. In this case, since the objective is to regulate the voltage, the pilot bus for each area is chosen selecting the one with the most deviated voltage. After normalizing the **ed** matrix respect to its maximum value, reducing the coefficients to values between 0 and 1 with 0 on the diagonal, it is possible

to divide the network in areas setting a maximum range for the normalized electrical distance, called *electrical radius* and applying it respect to the coefficient of the pilot bus.

A further criteria adopted to correlate the buses is based on their operative condition, distinguishing, within each area, those with the most similar voltage magnitude. Using the already defined pilot bus as reference, each area is suitably adapted to consider only buses with similar working conditions. In this way, the area selection becomes dynamic, being correlated to the actual power flow state and not only on the network's topology.

Finally, after the definition of the control areas, the voltage regulation is possible using the array of sensitivity coefficients related to the pilot bus and recursively estimating the reactive power exchange at that bus:

$$\mathbf{\Delta V_j} = \left\{ \frac{\partial V_j}{\partial Q_i} \right\} \cdot \Delta Q_i \tag{3.9}$$

where i is the pilot bus and $j = 1 \cdots n$ is the complete list of buses.

3.3 Local market for ancillary services

An important feature to be taken into account when investigating the possibility of an electrical network's distributed management is the availability by the active users to contribute to the regulation. This feature clearly depends on the technical constraints of a relative user, but the decision whether to participate or not is also function of the economic benefits obtainable.

As already mentioned for the centralised management approach in section 3.1, some supply and demand dependency may be set for active users for this method too. In particular, by defining a cost for each active user contribution, a local market approach can be implemented by coupling the active and reactive power variation requests with price signals.

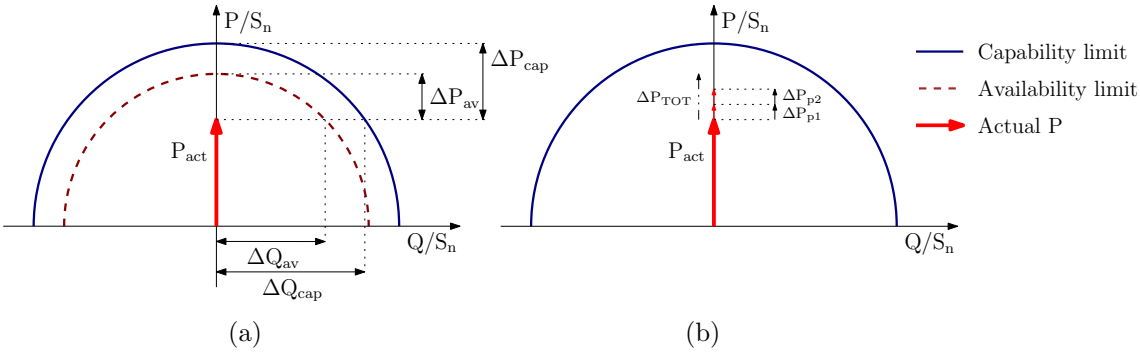

Figure 3.4: Example of participation by an active user: availability limitation for technical contraints (a) and economic considerations respect to the offered price.

An example on how both the technical constraints and economic convenience are considered affecting the decision by a user to participate to the regulation is shown in Figure

3.4, where a capability for the DG production is represented as a semicircular region on the P and Q plane. In Figure 3.4a the dependency of the availability from the technical constraints is shown as a reduction of the active power variation which can be offered due to a decrease of the capability range. How this quantity is offered on the local market is shown in Figure 3.4b, where sequential contributions are considered coming from the user while the price increases.

3.4 Distributed control implementation

The concepts described in section 3.2 regarding the distributed regulation strategy are implemented in a steady-state environment based on the power flow solution with the Newton-Raphson method, recalled in section 2.1.2. In the following, the algorithms developed to implement the procedure are described more in detail.

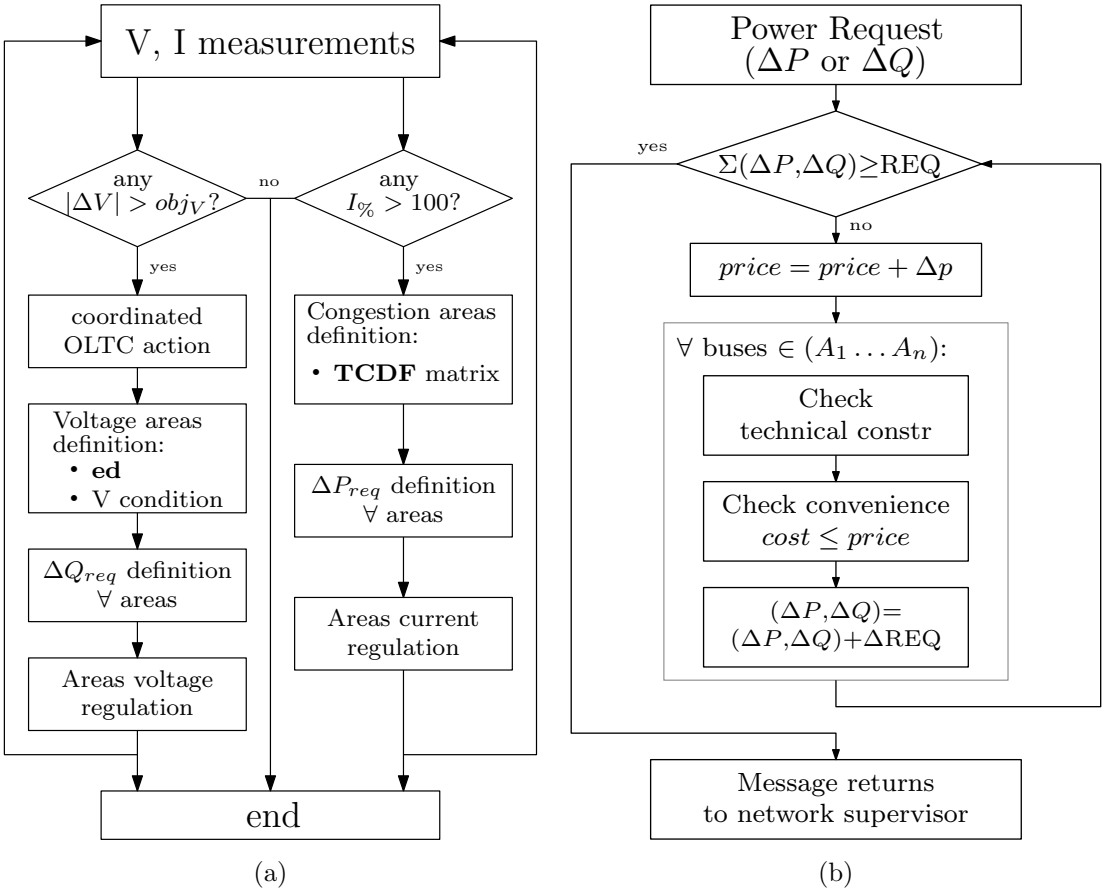

Figure 3.5: Flowcharts of the distributed regulation procedure: Network Supervisor (a) and local-area (b) controls.

Figure 3.5a shows a flowchart of the Network Supervisor control implementation. The whole grid regulation scheme is supposed to be working depending on the requests forwarded by this unit, which collects the remote voltage and current measurements. Once a contingency is detected (one of the buses' voltage or lines' current overcomes the respective objective) the regulation areas are identified adopting the techniques described in sections

3.2.2 and 3.2.3, so the active and reactive power requests (ΔP_{req} and ΔQ_{req} respectively) are computed for each area. In particular, in case of voltage contingency the OLTC action is operated according to the procedure described in section 3.2.1.

In figure 3.5b the algorithm for the control of each regulation area is depicted. The flowchart is the same for both current and voltage regulation strategies and implements the participation of active users for the fulfillment of the power request calculated by the Network Supervisor. Since a local market logic is expected for this kind of management, a price signal [€/MWh, €/MVArh] is composed by increasing the previous value by a certain amount Δp. The buses included in the regulation area receive sequentially the message for the contribution request, starting from the pilot bus, and evaluate the power variation range due to technical constraints and comparing the offered price with the local cost. The contribution possibly coming from each bus (aggregating offers from the active users locally connected) are limited to the value ΔREQ in order to allow the participation of the other buses too. Known the availability, the actual contribution is given by the minimum value between the total range and ΔREQ.

3.5 DMS Simulation tool

This section describes the tool developed to simulate the application of the DMS logic discussed in the previous sections to a MV distribution network. The software, modeled in Matlab, offers the possibility of calculating the power flow on an electrical network for a set of operative conditions defined through suitable active and reactive power profiles for loads and generators. A screenshot of the main graphic interface of the software is shown in Figure 3.6.

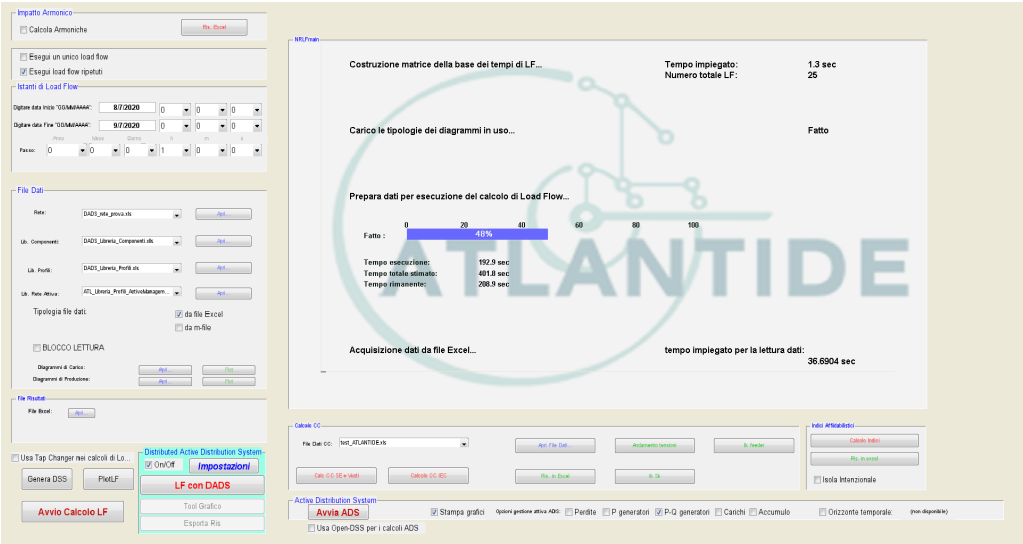

Figure 3.6: Main graphic interface of the developed software (in Italian).

The software was developed within the Italian research project ATLANTIDE [82, 83], aimed at establishing a digital archive for Italian reference distribution networks, produce

models for the network components and proposing active management systems for the users' integration in the network regulation. As a basic feature the software allows to calculate the steady state conditions of an electrical system (i.e. power flow and steady-state short circuit analysis) varying the generators' and loads' powers according to time depending power profiles. As can be seen from the main interface in Figure 3.6, the simulation time range can be set along with the time step (top-left corner), while several data-files need to be selected from the respective drop-down menu in order to define: the network layout with users' connections, the library of components used in the system, the time-varying power profiles and the active-management bids from active users.

Once the data files are loaded by the software, for each simulation instance the operation schematized in Figure 3.7 is done to update the instantaneous active and reactive power (P_i and Q_i): four coefficients are read from the data files depending respectively from the simulation year, month, day of the week and hour of the day, then the installed power (P_n and Q_n) is multiplied by those value and for the utilisation factor k_u. A similar approach is used to define the local cost for the active users participating to the network management, setting time-dependent profiles for the local cost and for the availability respect to the actual power.

The decentralised DMS discussed in the previous sections was developed as one of the tools for active management on a distribution network, along with a centralised one consisting in a central power flow optimization tool to dispatch the active and reactive power set-points to generators [84]. The two approaches are integrated in the same tool, as can be seen from the main graphic interface shown in Figure 3.6, where the centralised regulation strategy is called *Active Distribution System* and the decentralised one *Distributed Active Distribution System*.

From the main panel, the settings for the decentralised DMS can be changed in order to run simulations using the logic described in the previous section by opening a dialog window from the panel in the lower left corner of the main interface. From the settings window, which is shown in Figure 3.8, the following values can be defined:

- **Electrical Radius:** maximum value of normalized electrical distance respect to the pilot bus within an area;
- **Area voltage threshold:** maximum voltage deviation allowed for each area;
- **Power request share:** maximum contribution allowed from each bus;
- **Max line loading:** acceptable line loading limit;
- **Control step time:** time between two control actions performed by the NS.

Once the variables in Figure 3.8 are set, the decentralised DMS operation can be simulated with the logic described in the previous section. The simulation results are shown through a further graphic interface which can be seen in the screenshot in Figure

3.9, where the central graph reports the maximum and minimum values reached by the buses' voltage during the simulation: red and green bars indicate respectively voltages outside or within the objective range ($\pm 5\% V_n$ in the example) while blue bars refer to solution with the DMS action. On the right side several buttons allow to export a logfile of the simulation and to plot other important results like: voltage at each busbar during the entire simulation, tap position of the OLTC before and after the DMS action, active and reactive power contributions in each instance. These graphical interfaces are very helpful in analysing the operation of the DMS and will be used to discuss the case study results in the next section.

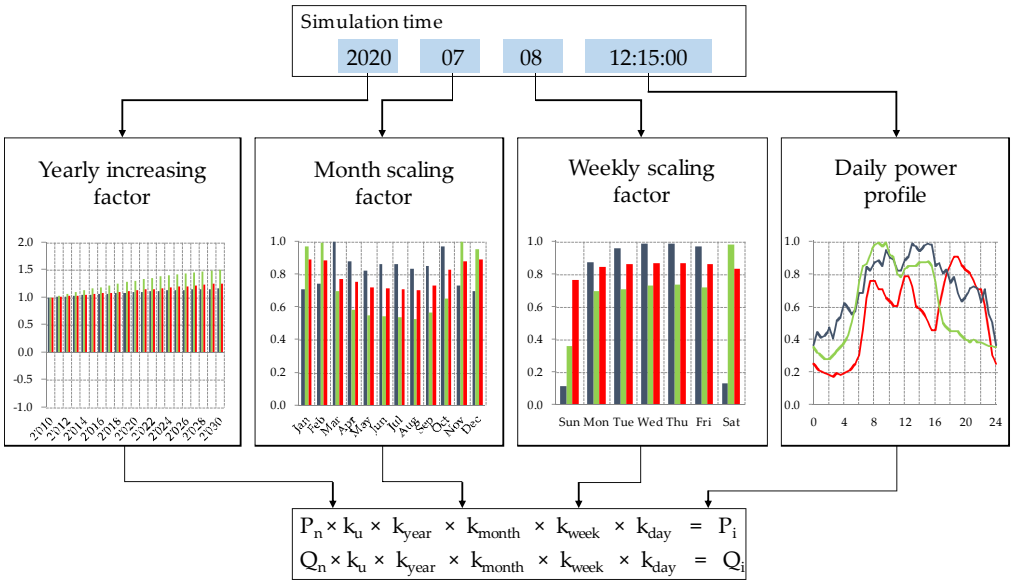

Figure 3.7: Actualization of the loads and generators power to the current simulation time through power profiles.

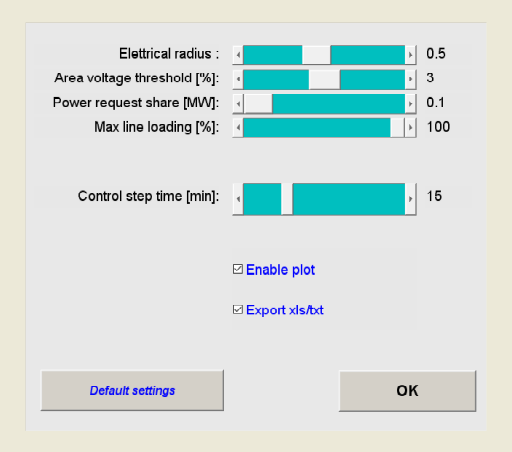

Figure 3.8: Software's graphic interface for the decentralised DMS settings.

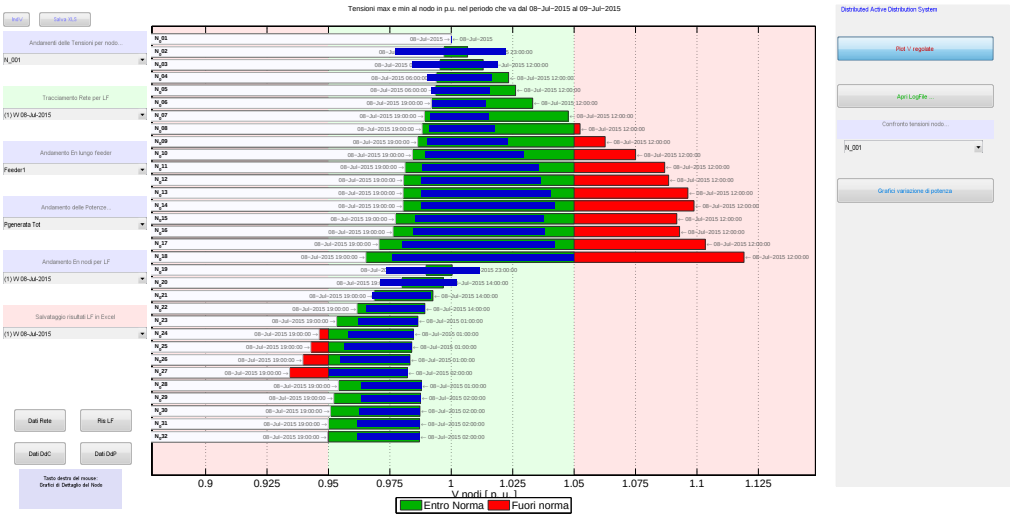

Figure 3.9: Software's graphic interface for results visualization (in Italian).

3.6 Case study applications

In this section some applications of the distributed control strategy are shown through simulations on a reference distribution system. In the following, some results regarding several scenarios are reported:

- a long-term simulation of the network's operation to assess the Hosting Capacity limits and possible improvements;
- a cooperative application of this strategy with a centralised one to investigate the possible implementation as intra-day control;
- the proposal of this procedure as a way to coordinate the distribution network to formulate an ancillary service provision offer to the Transmission System Operator (TSO).

3.6.1 Reference Distribution Network

The MV network used as test-bed for the mentioned scenarios is one of the distribution system models defined within the ATLANTIDE project [83]. In order to produce a set of grid models (i.e. one for each urbanization context: rural, industrial and urban) several indexes were used to reduce the range of real systems to fit within each category (e.g. ratio between MV and LV loads, load density, length of feeders, type of conductors), finally leading to one model for each context.

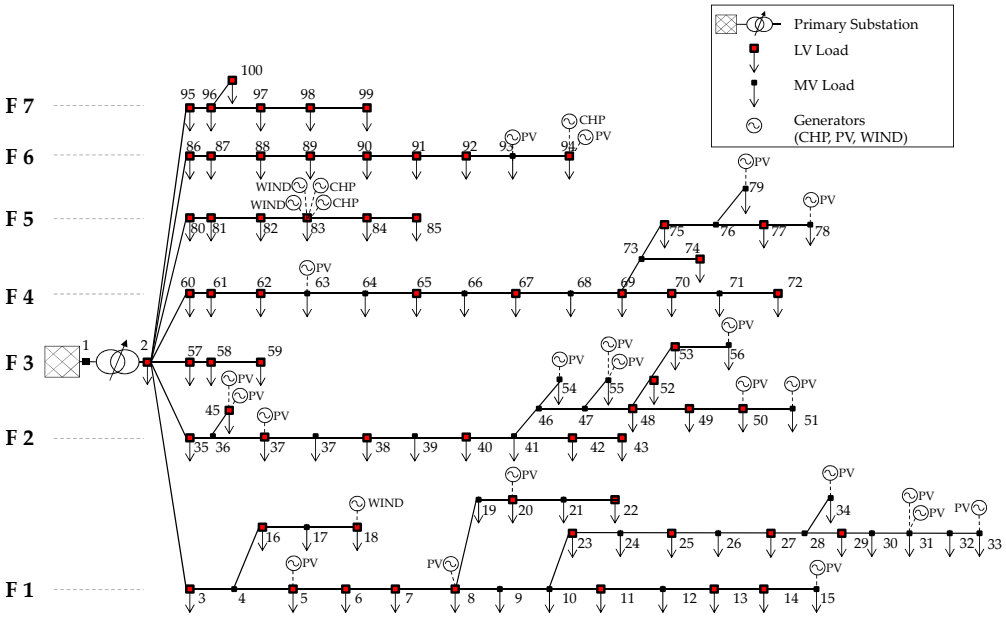

Figure 3.10: Single-line diagram of the industrial reference network.

The network adopted for the simulations has been selected as reference for the industrial context in the project and is considered a model suitable for the application of the proposed strategy since it is composed by a mix of overhead and cable lines, with significantly extended feeders and connected users with substantial installed power (both generation and loads units).

As can be seen from Figure 3.10, reporting the single-line diagram for the case study network, and from Table 3.1, recalling its main characteristics, the system consists in 7 feeders, each with different features due to the presence of various contexts within the same grid (e.g. residential areas can be recognized in feeders with a higher presence of LV loads, short feeders with high MV loads power installed clearly indicate industrial areas). The network has a radial topology departing from the HV supply obtained through a Primary Substation transformer with a 132/15 kV voltage ratio, equipped with OLTC. The total installed load power is 33 MVA, with a 38% share of LV loads, while the total generated power is 40 MVA with a 30 MVA generation plant consisting in 4 generators connected to feeder 5. The full data-set for this network model is reported in Appendix C.

Given the network layout with the mentioned loads and generators sizes, an hypothesis

about the load category shares in the feeders has been made leading to the percentages reported in Figure 3.11. The load and generation power profiles shown in Figure 3.12 have been defined to simulate the power flow trends over time according with the hypothesis on the different context for each feeder.

Table 3.1: Summary of the Industrial Network Data by feeder.

Feeder	**Extension [km]**	**S_{Load} [MVA]**	**S_{LV} [MVA]**	**% S_{LV} [%]**	**S_{Gen} [MVA]**
F 1	31.9	9.8	3.0	31	4.3
F 2	23.7	4.7	1.5	31	2.9
F 3	4.9	0.5	0.5	100	0.0
F 4	30.5	4.0	3.3	82	0.8
F 5	7.9	9.2	1.1	12	30
F 6	10.9	1.9	1.1	59	2.1
F 7	5.8	3.0	2.2	73	0.0
TOT	115.5	33.0	12.6	38	40.0

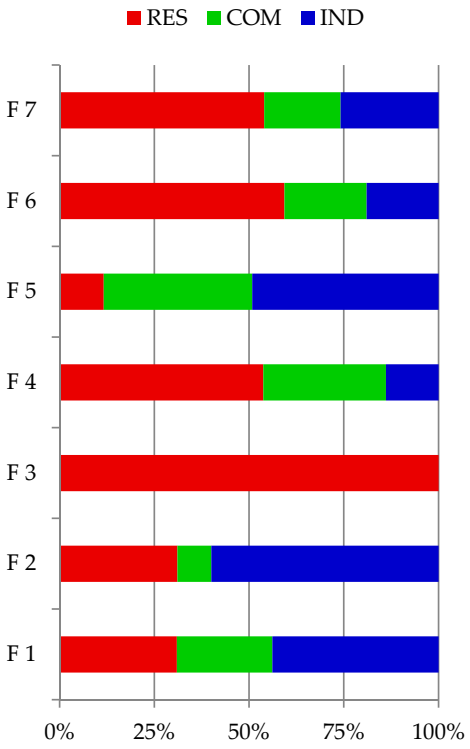

Figure 3.11: Load percentage per category and feeder.

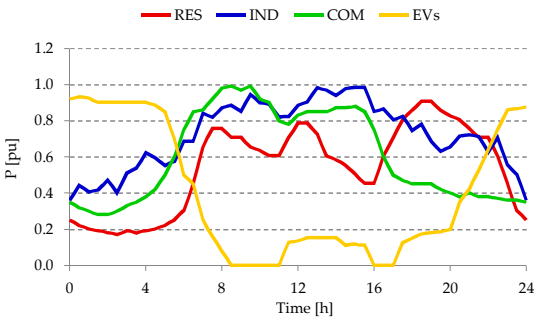

(a)

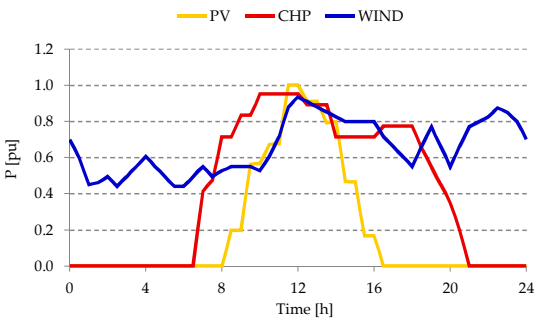

(b)

Figure 3.12: Loads (a) and generators (b) daily power profiles in pu.

Table 3.2: Long-term scenarios hypothesis.

	RECESSION	**B.A.U.**	**ROADMAP**
DG penetration	low	tendential	heavy
Load growth	negative (till 2020)	tendential	low
EVs diffusion	absent	low	heavy

3.6.2 Long-Term scenario analysis

Several long-term scenarios have been investigated to study the possible operative conditions of the distribution network under different hypothesis of the electrical system's evolution. Three scenarios have been identified in the ATLANTIDE project, depending on different assumptions on political actions to sustain the renewable energy increase and economic development:

The most stressful scenario for the distribution network operation is the one called *Roadmap*, considering the maximum GD diffusion and low load growth due to energy efficiency increase, so it is likely to result into contingencies due to reverse power flow. The evolution of load and generation peak power in each year is shown in Figure 3.13, where it could be clearly seen that the expected generation growth is faster than the load's one. For example, at 2020 the production peak is around 90 MVA compared to a maximum load power of about 60 MVA. The power coefficients used to simulate this long-term scenario are reported in Appendix C.

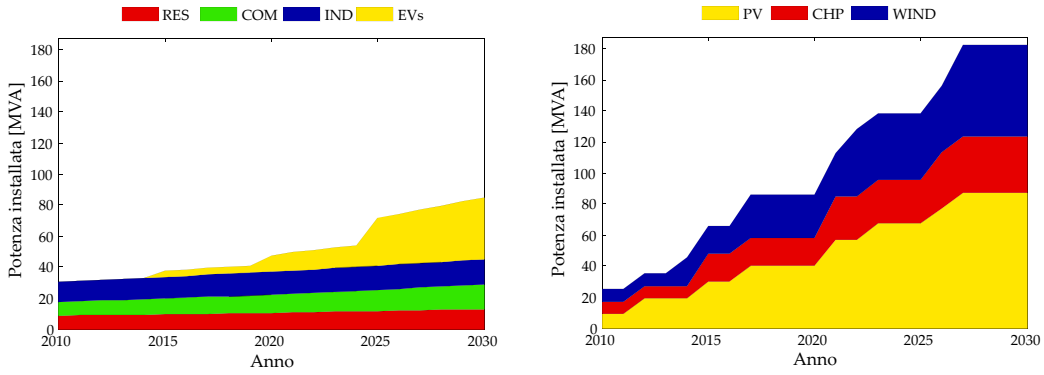

(a) (b)

Figure 3.13: Evolution trends of the peak power of loads (a) and generators (b) for the Roadmap scenario.

An analysis of the working conditions for the entire Roadmap evolutionary scenario is reported in Table 3.3. The simulation was conducted over the entire period from 2010 to 2030 to investigate the contingencies occurring in the network. The evolutionary status reports the total installed generation and load, with focus on the expected energy production over the years in which changes in the generated power were expected standing the trend in Figure 3.13b.

Regarding the voltage contingencies, results are carried out in terms of number of simu-

lated instances which lead to voltage issues in the relative year with the respective number of buses involved. From those results it can be seen that the system starts experiencing over-voltage problems from the second year of simulation as an effect of the +10MW DG increase, while from the fifth year under-voltage issues occur as well. This confirms the need of a flexible OLTC operation in order to help the voltage regulation, since it may happen that both of the contingencies are encountered at the same time.

In the rightmost section of Table 3.3 other relevant results are shown, in particular it can be seen that congestion occurrences are reported from year 5 on. Since no distribution network management is considered the generated power as for the production daily profiles shown in Figure 3.12b is not acceptable in the whole year, leading to over-current protections tripping which result into an increasing value of missed energy generation due to disconnections (i.e. E_{disc}). This value exceeds 10% of the scheduled energy by 2020 and reaches 30% by 2030.

To enable the network management through the strategy discussed in the previous sections several local costs need to be set in order to assess the economic aspect of the users participation. These costs are defined for each resource connected to the grid to differentiate the contributions in relation to a power request. Furthermore, different costs are set depending on the action performed by the DGs: Generation Curtailment (GC), Extra-Dispatching (ED) of active power and reactive power contribution. Similar options are also considered regarding the Active Demand, i.e. the responsive behaviour of loads respect to power variation requests.

Table 3.3: Operative conditions of the network under the Roadmap scenario for the 20-years evolution analysis.

Year	Evolution status				Over-voltage			Under-voltage			Other results			
	$P_{new\ DG}$ [MW]	$P_{tot\ DG}$ [MW]	$P_{tot\ Load}$ [MW]	$E_{scheduled}$ [GWh]	Number of instances	Violated instances [%]	Buses with violation [%]	Number of instances	Violated instances [%]	Buses with violation [%]	Congestions number	Average Tap	E_{disc} [GWh]	E_{disc} [%]
2010	0	33.3	40.6	45.2	0	0.0%	0.00%	0	0.0%	0.0%	0	6	0	0.0%
2012	10.164	43.5	43.91	50.4	927	0.0%	0.00%	0	0.0%	0.0%	0	6	0	0.0%
2014	10	53.5	46.07	79.2	939	0.2%	0.00%	0	0.0%	0.0%	0	6	0	0.0%
2015	30.6	84.1	46.787	106.1	25678	8.8%	0.70%	46752	16.8%	1.3%	56	6	0.3	0.2%
2017	20	104.1	49.002	139.9	65788	9.8%	1.90%	57217	19.9%	1.6%	550	6	3.3	2.4%
2021	37	141.1	54.757	172	154848	17.9%	4.40%	195925	31.6%	5.6%	9703	6	21.3	12.4%
2022	15	156.1	56.764	214.4	153617	17.5%	4.40%	212871	32.3%	6.1%	11175	6	23.8	11.1%
2023	10.5	166.6	58.593	220.7	190025	19.5%	5.40%	226585	32.8%	6.5%	14700	6	31.9	14.5%
2026	26	192.6	67.613	242.8	221679	23.3%	6.30%	524333	45.7%	15.0%	36368	5	46.2	19.0%
2027	26	218.6	70.232	291.7	236468	25.1%	6.70%	674360	47.8%	19.2%	58605	5	93.9	32.2%
2030	0	218.6	77.3	291.7	216148	21.0%	6.20%	813332	51.1%	23.2%	43367	5	83.9	28.7%

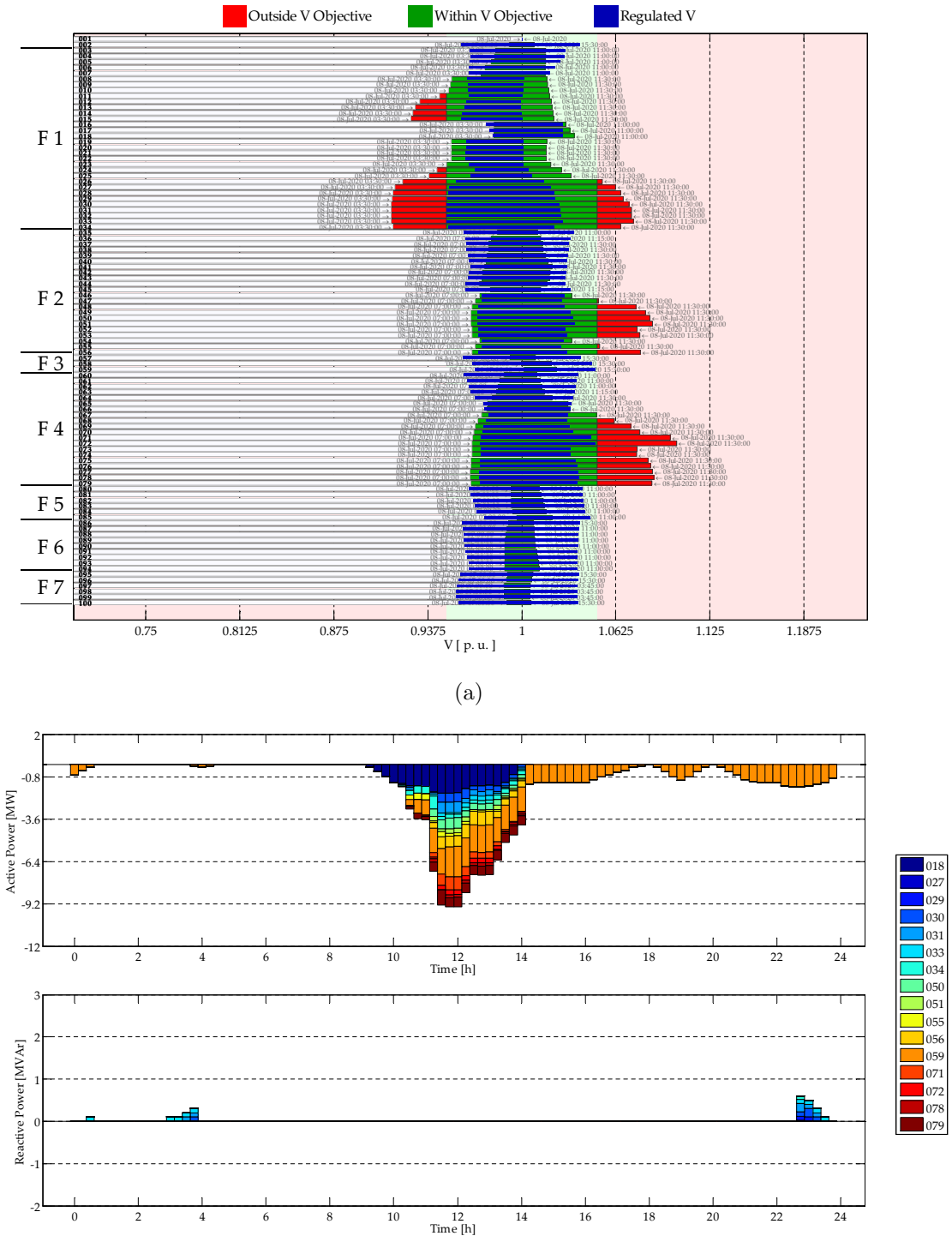

Figure 3.14: Results in terms of busbar voltage (a) and P, Q contributions (b) in the 2020 instance (i.e. first Wednesday of July, 2020).

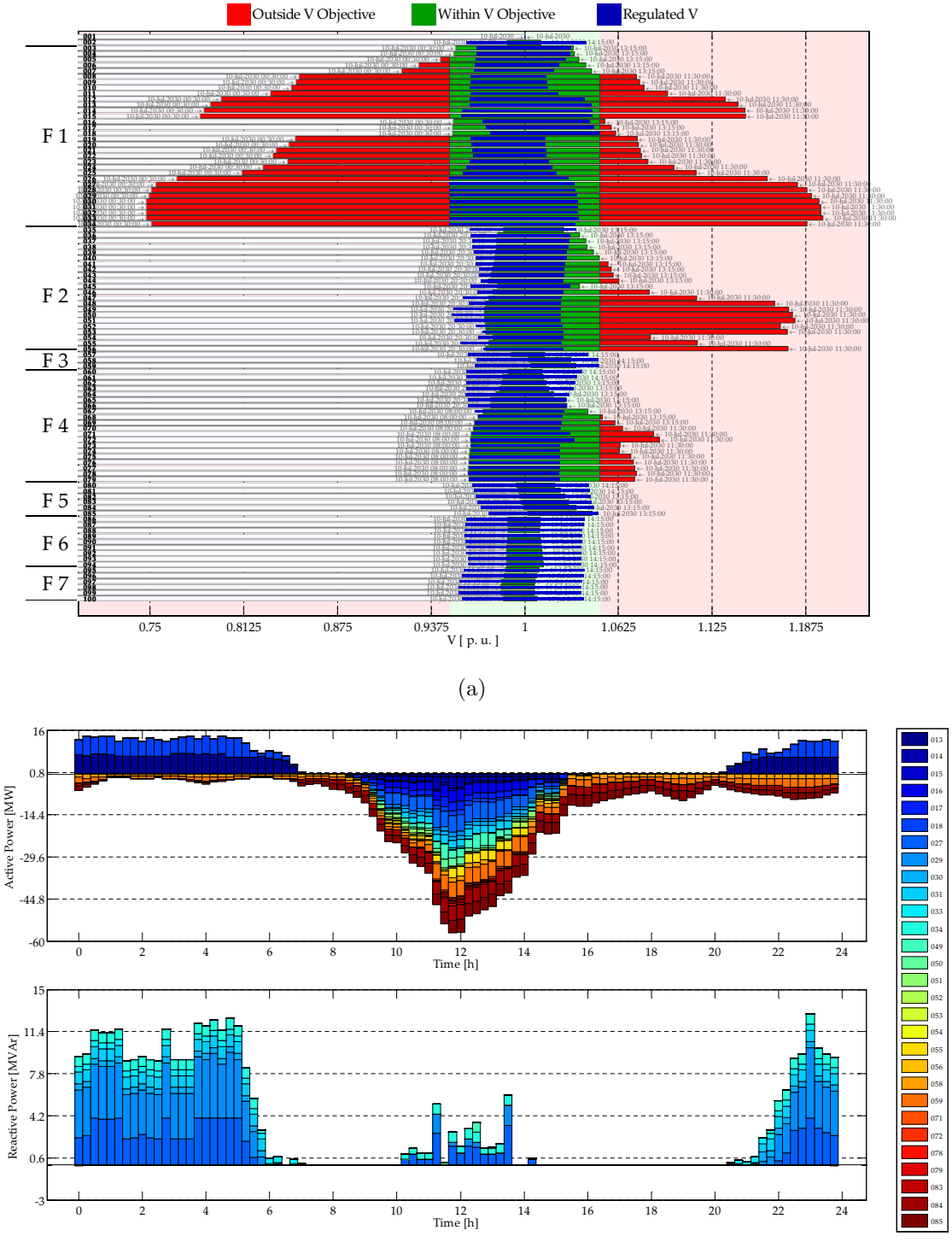

Figure 3.15: Results in terms of busbar voltage (a) and P, Q contributions (b) in the 2030 instance (i.e. first Wednesday of July, 2030).

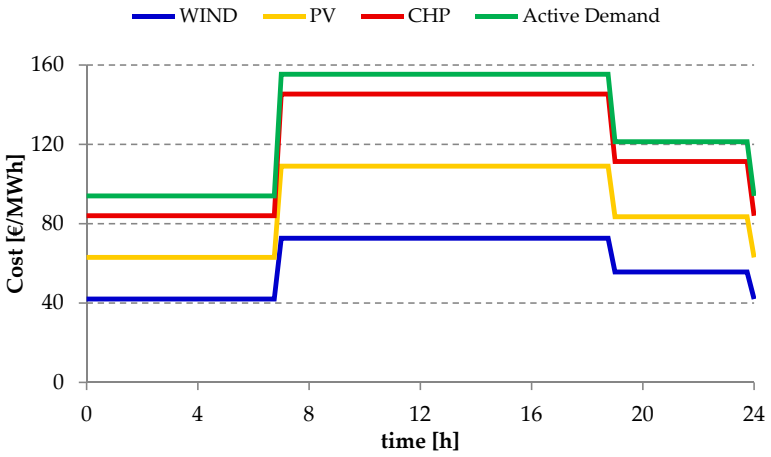

Figure 3.16: Local cost profiles for each resource in the 24-hours period.

A quantification of the cost associated to the actions taken by the users clearly depends on the energy market price, whose definition is not easy in the long term and is not the scope of this study. For this reason, a fixed price curve is considered and will provide the basis on which evaluate the local costs. In general, a criteria to differentiate the actions coming from different sources is the possibility of those units to shift the production profile over time. For renewable energy sources, without considering any storage capability, the Extra-Dispatching action (i.e. the option of producing an extra amount of active power) is not possible, while CHP plants have been assumed to have enough thermal storage capability to be available for this service. From the Generation Curtailment point of view the cost for each resource has been estimated according with the energy price: the wind plants, standing the possibility to produce during the whole day, have been assumed as the most economic, while the CHP units, having higher investment costs, are the most expensive ones. Photovoltaic generators cost has been chosen as an average value between those for the other two sources. A further cost profile has been defined to consider the possible participation by the loads, referred to as *Active Demand*, with values higher than the most expensive generation source since the objective of the analysis was to firstly exploit the generation contribution.

To test the efficiency of the proposed Distribution Management System (DMS) two instances have been considered under the Roadmap scenario: the first Wednesday of the month of July for years 2020 and 2030. The local costs shown in Figure 3.16 are coupled with availability curves setting, for each user, the percentage of injected or absorbed power available for the regulation. In this case, only CHP generators are supposed to be available for Extra-Dispatching function (extra-power production) while all the resources offer the possibility of curtailing their production. For the Active Demand it has been supposed an availability on both directions (increasing or decreasing the load), supposing some kind of

storage capability able of shifting the power profile during the 24-hours. The total injected active power is shown for the two scenarios in Figure 3.17, where it can be clearly seen that the overall production tends to follow the power profile of the PV generators, due to the strong increase of this resource over to the others assumed in the Roadmap scenario. While the simulation of the 2020 scenario highlights a P reduction mainly during the peak production period (i.e. around h. 12) due to congestion issues as a result of the reverse power flow, in the 2030 case an extra-production or Active Demand actions are evident even during the night-time.

Regarding the voltage regulation, in Figures 3.14a and 3.15a the output diagram from the code implementing the procedure is reported for both cases. Through the colour code recalled in the legend, it can be seen that over-voltage issues occur in feeders 1, 2 and 4 which are the most extended, while feeder 1 also experiences some under-voltage issues during the low-production period. The network is heavily stressed when considering the 2030 scenario, in which the scheduled active power of generators cannot be accepted because of technical constraints violations, so the DMS operation is even more evident.

Figures 3.14b and 3.15b report the active and reactive power variations from each bus involved in the DMS distributed control. From the results appears that the intervention made by the active users help pursuing a safe network operation preventing the loss of service. Particular attention should be paid to the OLTC operation, included in the DMS. in Figure 3.18 the OLTC action as *AVR* is compared with the one coordinated by the DMS, showing that in several occasions the remote voltage measures information lead to opposite actions respect to the common practice. This effect can also be seen in the diagrams in Figures 3.14a and 3.15a, where the bus 02 voltage appears to be shifting along the entire range 0.95-1.05 pu according with the control.

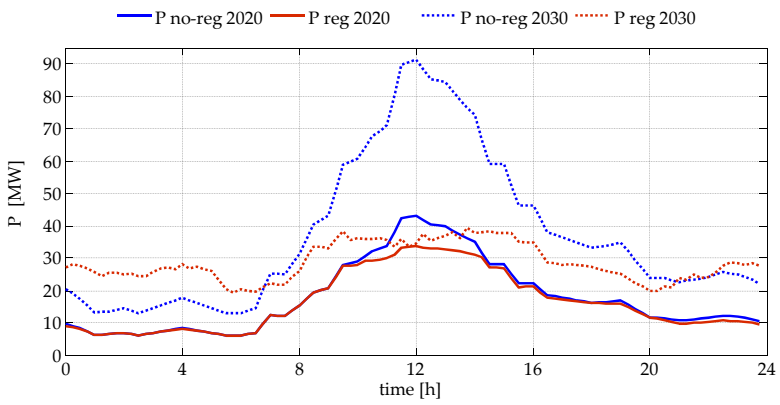

Figure 3.17: Active power production in the 24-hours period in 2020 and 2030.

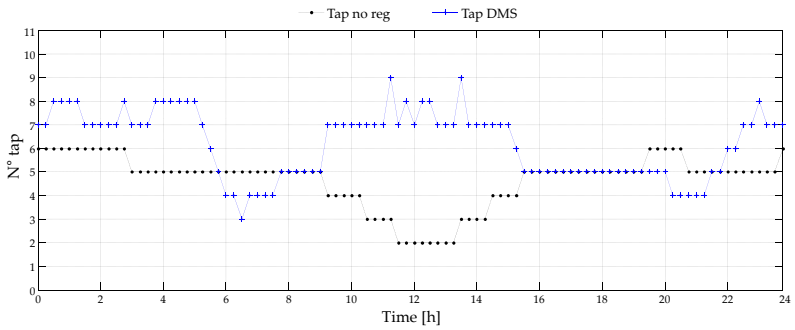

Figure 3.18: Tap position of the OLTC in Primary Substation for the 2030 scenario.

3.6.3 Cooperation with centralised energy management for intra-day operation

In this section the decentralised DMS discussed so far is used in cooperation with a centralised system aiming at optimizing the power flows in the day-ahead operation, scheduling the DERs power profiles. A centralised Distribution Management System, developed by one of the partners of project ATLANTIDE [84], calculates the DERs active and reactive power contributions by considering the relative local cost and by using it as a variable to weight their availability in the power flow optimization aimed at minimizing the cost for the network operation (i.e. minimum cost for contingencies regulation). Although differing for the approach in calculating and fulfilling the power contributions from DERs (the centralised approach dispatches the working point for DERs based on overall optimization, while the distributed approach requests contribution to an area without knowing who will actually participate), the two techniques aim at the same global result based on the same local costs.

The two DMS are then used in a "synergized" fashion adopting the centralized EMS for the generation and load forecast in the day-ahead operation and then applying the distributed DMS as the intra-day control strategy [85]. Since the main difference between the two approaches relies in the way of obtaining the power requests from DERs, the first one is intended as a planning tool, used to define the operating point for DERs to optimize the expected power flows. The decentralised DMS described in the previous sections is then employed to fix the contingencies occurring for unexpected variations respect to the scheduled values.

Adopting the reference network for the industrial context described in the previous section, the 24-hours period relative to the 2020 case is adopted to test the coordination between the two approaches for the planning and on-line operation, involving three different degrees of control as reported in Table 3.4:

- **Scenario A:** only the coordinated OLTC control described in section 3.2.1 is adopted;
- **Scenario B:** the DERs provide the active and reactive power contributions scheduled in the day-ahead operation, while the OLTC control adjusts the potential volt-

Table 3.4: Scenarios of the coordinated centralised and decentralised DMS operation.

	Coordinated OLTC	**Centralised DMS**	**Decentralised DMS**
Scenario A	✓	×	×
Scenario B	✓	✓	×
Scenario C	✓	✓	✓

age deviations;

- **Scenario C:** the power profiles scheduled in the day-ahead optimization are applied, but the distributed regulation strategy is adopted to coordinate the DER units for the intra-day distributed control.

In Figure 3.19 the total power profiles (sum of generated minus absorbed) during the 24-hours simulated period are shown for scenarios A, B and C. As can be seen in Figure 3.19a, respect to the not-regulated profile (scenario A, in black) the centralised DMS finds a solution which requires a reduction of about 10 MW at the peak production period (namely 10.9 MW at h. 11.30), consistent to the results obtained with the only application of the decentralised DMS shown in the previous section (leading to a 9.2 MW power reduction).

The results in terms of the bus voltages in some significant nodes of the network (namely the farthest bus in feeders F1, F2, F5 and F6 in Figure 3.10) are reported in Figure 3.20, where the different scenarios are compared with the not regulated situation in which the OLTC is used as an AVR based on the secondary busbar voltage with reference at 1 pu. In Scenario A the coordinated action of the OLTC (shown in Figure 3.21) leads to an improvement in the voltage deviation, but nevertheless is not able to maintain the voltage value in all feeders neither within the objective regulation band (green area between 0.95 and 1.05 pu). This is due mainly to opposite voltage trends in feeder F1 and F5 (see Figures 3.20a and 3.20c) in the first 6 hours and the last 4 due to EVs charging in feeder F1 and wind production in feeder F5, while the same situation is found during the central 6 hours (around h. 12, see Figures 3.20b and 3.20d) where the high production of PVs leads to over-voltage in feeder F2 while the loads in feeder F6 tend to lower the voltage. It should be noticed that in Scenario A, since no power contribution is given by the DERs, the line congestions can not be avoided and would eventually lead to disconnection when occurring (see the active power variations in Figure 3.19a). The voltage results for Scenario A are only shown at the scope of demonstrating the OLTC coordinated action.

In Scenario B the above discussed active power reduction is provided in order to face the line congestions especially during the first 6 hours, as a result of the EVs charging in feeder F1, and during the high PV production period around h. 12. The scheduled reactive power contributions leading to the variations shown in Figure 3.19b are calculated in the day-ahead operation to face the above discussed over- and under-voltage occurrences.

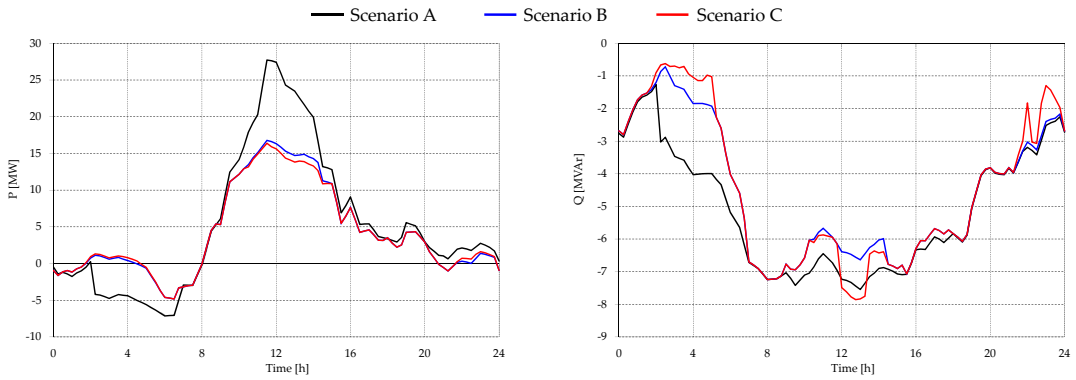

(a) (b)

Figure 3.19: Total active and reactive power profiles in Scenarios A (black), B (blue) and C (red).

Although allowing a feasible operating condition in the day-ahead operation, in the intra-day, due to perturbations in the expected power profiles, the dispatched set-points for P and Q will not result in acceptable voltage and currents and the contingencies are such as neither the coordinated OLTC action helps in containing the voltage deviation in all buses.

Scenario C considers the participation of the DGs in the intra-day operation too allowing to face the unexpected variations in the power flow. As it can be seen in Figure 5, a further small reduction in the active power is required to DERs in order to contain the branches' loading wheareas the reactive power support along with the coordinated OLTC action shown in Figure 3.21 permits a better regulation of the voltages, allowing the objective range to be respected.

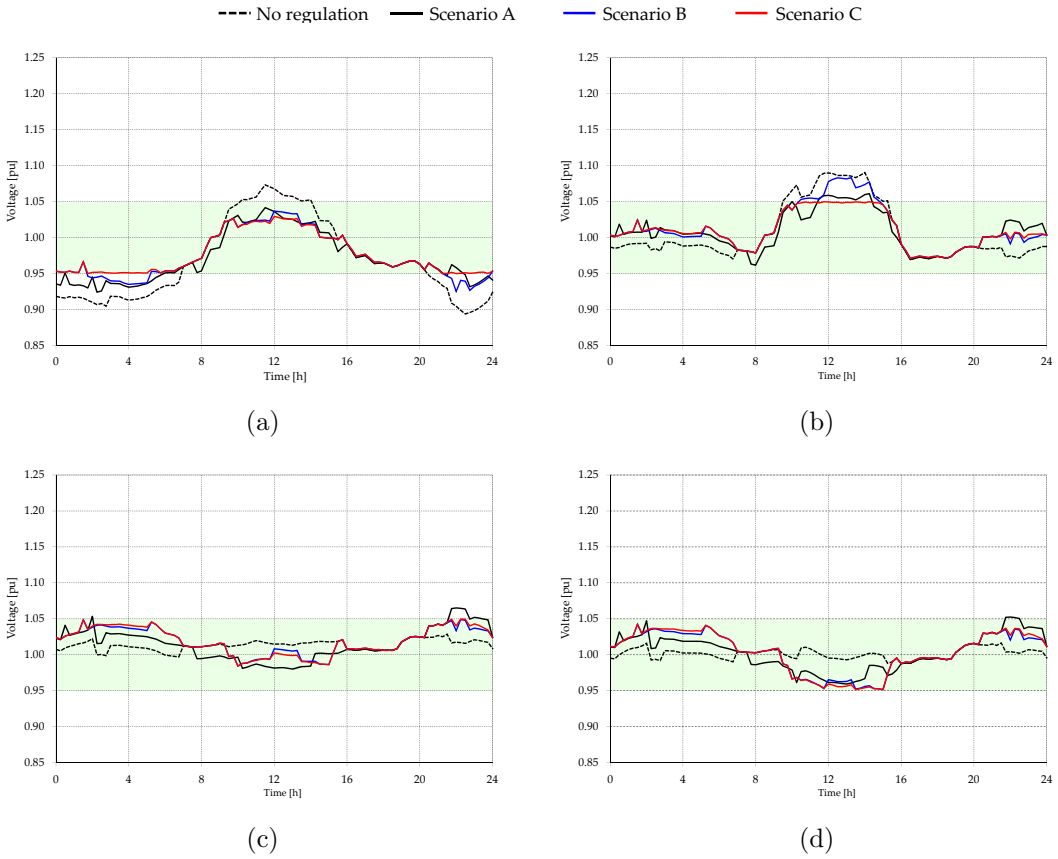

Figure 3.20: Voltage profiles on the 24-hours period for buses 33 (a), 51 (b), 85 (c) and 94 (d).

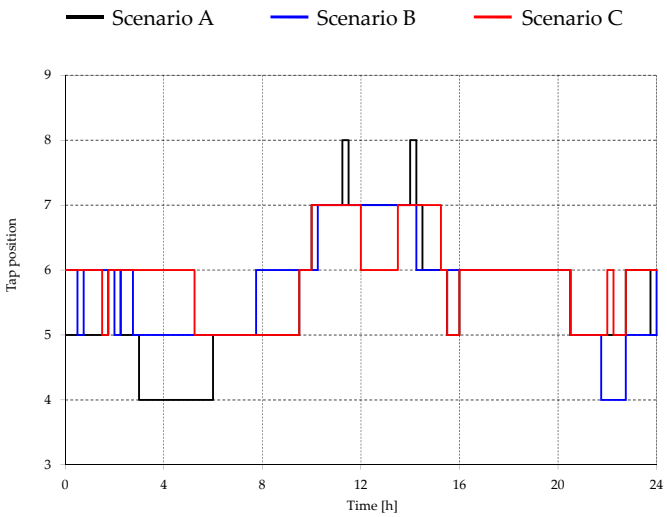

Figure 3.21: Tap position for the coordinated OLTC operation in Scenarios A (black), B (blue) and C (red).

3.6.4 Aggregation of ancillary services for energy market participation

For the third case study, the application of the DMS to a market model is proposed. The case considered in this section is one of the scenarios contained in the resolution DCO354/13 [22] of the Italian Regulatory Authority for Electricity Gas and Water Systems (AEEGSI), discussed in section 1.4.

In particular, the application reported in this section considers the market model 2, which expects the DSO to act the role of intermediary between the distribution network and the bulk grid, presenting offers on the Ancillary Services Market (ASM). In the simulations the DSO collects the DG offers through the decentralised DMS by checking the feasibility of the solution at the same time.

This model was chosen because it represents a solution which seems consistent with the distributed approach used for the regulation since it envisages the presence of a local market (ASM-D) allowing the DSO to acquire services from the users in order to make an offer to the TSO. The couple of curves for availability and cost for the participation of each active user are here considered as bids to the ASM-D, so the DSO (through the Network Supervisor) can switch the objective to the research of the maximum power exchangeable by the distribution network instead of just verifying the grid's technical constraints.

The case study has been implemented on the Reference Network described in section 3.6.1 and considering different participation availabilities for the users. Using as cost profiles those shown in Figure 3.16, the availability shares, reported in Table 3.5 are defined as percentage of the injected or absorbed instantaneous power.

Table 3.5: Active users availability to ASM-D. Reduction and increase refer to the exchanged active power towards the transmission grid.

Resource	**Participation share**	**P reduction**	**P increase**
Wind	30%	✓	×
PV	50%	✓	×
CHP	10%	✓	✓
Active Demand	20%	×	✓

The simulations conducted on the aforementioned network model considered the same 24-hours period of the previous case study (first Wednesday of July, 2020).

In this case, the ancillary services available from the active users are divided respect to the capability of increasing or reducing the active power towards the main transmission grid. Wind and Photovoltaic generators can only reduce the injected power with the respective percentages (referred to the actual production), loads can only cut their absorbed power till 20% of the actual working point while CHP units can offer services on both directions for the 10% of the actual power. For the sake of clarity in discussing the results these percentages have been kept constant throughout the entire 24-hours period while,

at each time instance, the DSO searches the maximum active power variation obtainable given those offers and after verification of the technical constraints.

In Figure 3.22 the results in terms of active power variation are reported compared to the required cost for two time instances of the 24-hours simulation (h. 11 and h. 20). Looking at the h. 11 solution (blue) it can be seen that the availability of all the generation units to the active power curtailment results in a total reduction of 10.2 MW, while the power increase service (offered by CHP and Active Demand) is quantified in 1.7 MW. At h. 20 the absence of the PV units production sensibly reduces the active power variation range to ±2.7 MW.

Each offer is evaluated taking into account the network's technical constraints, possibly reducing the active power variation available starting from the contribution at the higher cost. This effect can be seen in the h. 11 instance looking at the CHP service (the most expensive generation source at 145 €/MWh) whose variation range, according to its injected power and the percentage in Table 3.5, results in 1.05 MW. On the power reduction half-plane the accepted variation from CHP is only 0.6 MW due to congestions occurring when curtailing more than 10.2 MW. Similar observation can be drawn for the power increase service, which results limited to 1.7 MW due to congestions limiting the load reduction (costing 155 €/MWh) to 0.6 MW.

In Figure 3.23 the discussed active power variation services are reported for the entire 24-hours period. As already mentioned, standing the availability percentages reported in Table 3.5 it clearly appears that the maximum active power reduction is possible when the PV production curve reaches the highest values. The P increase service, besides having a lower range due to the limited users' availability, is sensibly reduced during the central hours when congestions are likely to occur due to the high production from DGs.

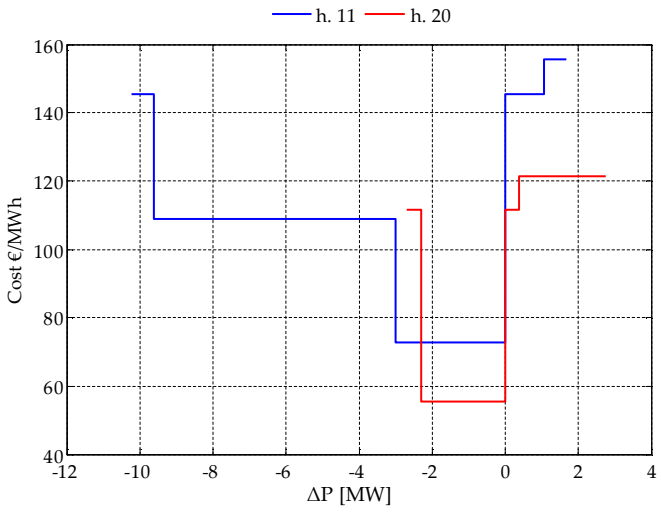

Figure 3.22: Distribution network's aggregated offer for the active power reduction or increase in two instances: h. 11 and h. 20.

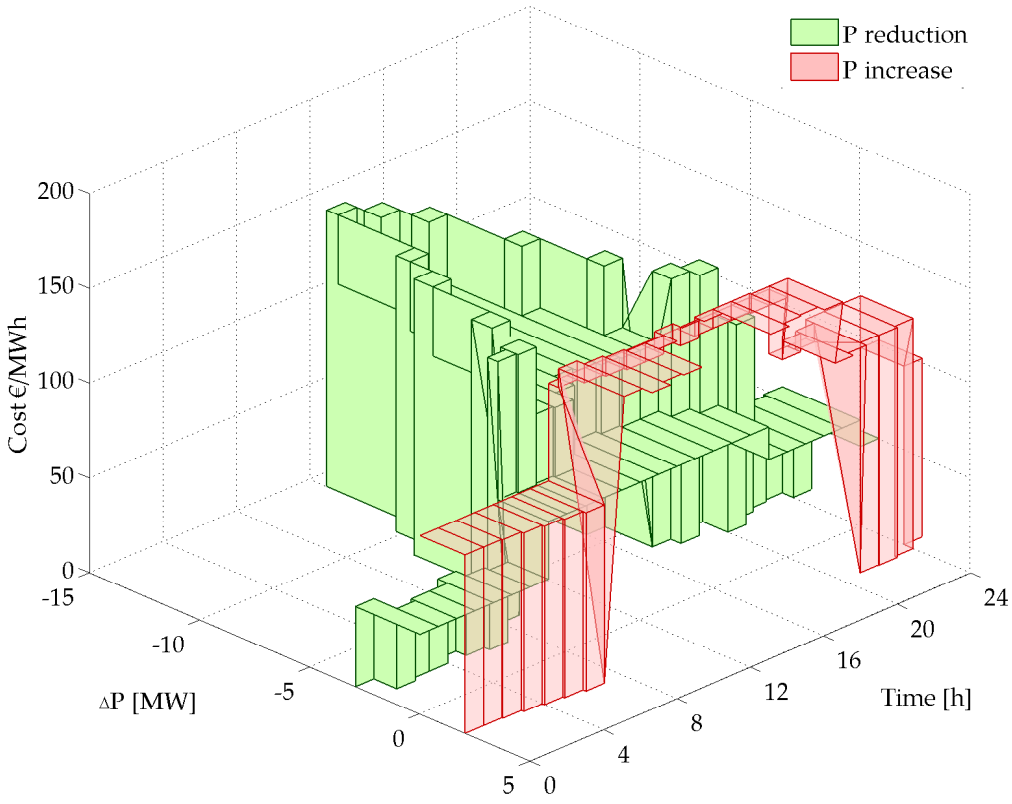

Figure 3.23: Active power reduction and increase offers trend in the distribution network for the 24-hour simulated period.

Chapter 4

Low Voltage Distribution Management System

Contents

Low voltage distribution networks are characterized by an ever growing diffusion of single- and three-phase distributed generators whose unregulated operation may deplete the power quality level. It is thus of interest to investigate the possible contribution that

such active users may provide to the system operation in a smart grid scenario. This chapter discusses a strategy for the coordination of multiple inverters connected to the same Low Voltage network, with a double objective: mitigating the voltage unbalance within the LV network and enable its participation to the provision of ancillary services for the upstream MV grid.

4.1 Strategies for inverter-interfaced users management

Standing the recent updates in the rules for the connection of distributed generators (DGs) to the network discussed in section 1.2 it clearly emerges that one of the main concerns in the modern distribution systems is the exploitation of the resources embedded in the network for grid-supporting actions. In this sense, a huge contribution may come from the participation of inverter-interfaced users in the provision of ancillary services oriented both at maintaining an acceptable level of power quality and at increasing the so-called *hosting-capacity* of the system, namely the maximum amount of power injectable by DGs without requiring grid reinforcements investments.

As the diffusion of distributed energy resources in LV networks continues growing, the number of single- and three-phase inverter-interfaced units increases, so the uncoordinated local voltage support action stated by the connection rules may not be sufficient in order to ensure an acceptable power quality level in the system. In particular, since the Volt/Var control stated by the rules is only aimed at supporting the voltage magnitude at the inverter's local bus, the absence of any coordination with the actions being performed by other units is likely to result in a voltage unbalance worsening throughout the network. An analysis of the possible effects coming from a local control of the inverter-interfaced DGs was presented [86].

Voltage unbalance issues in a distribution network lead to higher losses and heating effects on the appliances in particular for induction motors, electronic converters and speed drives [87]. Furthermore, given the asymmetry in the LV branches geometry, the currents' zero-sequence component worsens the uneven voltage deviations on the phases due to currents flowing through the neutral conductor. This issue can be observed especially in systems where the neutral point is grounded at the Secondary Substation only [88]. An investigation on the voltage unbalance issues due to the DG connections in LV systems was presented in [89].

With the aim of coordinating the electronic converters interfacing the Distributed Energy Resources (DERs) to the grid facing the mentioned power quality issues, several research works were presented lately proposing control strategies acting a compensation of the voltage or current sequences [90–95]. Other works in literature deal with the cooperative control of the distributed resources to improve the energy efficiency of a micro-grid also adopting the sequence components of the measured currents [96–98].

Improving the power quality in LV networks may allow to consider market models

considering the ancillary services possibly coming from such systems [99], involving the Secondary Substations in a Distribution Management System (DMS) as proposed, for instance, in [100].

4.2 Low Voltage coordinated control

Taking into account the current standards for the connection of DGs to a Low Voltage grid, a strategy for the coordination of inverter-interfaced users is presented in the following, aiming at mitigating the voltage deviations due to unbalances in the power flow and then to improve the hosting capacity of the system while allowing the participation of small-scale generators to the network management.

The proposed strategy aims at coordinating the locally performed interventions by DGs according to the characteristic set by the standards, trying to reduce the voltage unbalance in the LV network by means of a signals communication among a central unit, called *LVNC* (Low Voltage Network Controller) and the distributed resources. In particular, the control discussed in the next sections has the objective of redistributing the active and reactive powers over the three-phases in order to compensate the voltage unbalance detected by a central unit, called Low Voltage Network Controller (LVNC). The next sections describe how the objectives for the coordinated control are calculated (initially considering only one three-phase controllable unit), then how the signals are supposed to be set for the communication to any DER connected to the LV network.

4.2.1 Problem statement and definition of the objective

In the first stage of this research, the expected scenario was the presence of a single three-phase inverter electrically close to the Point of Common Coupling *PCC* and connected through a dedicated line. With this hypothesis, the study was focused on the calculation of the phase-currents set-points required in order to mitigate the voltage unbalance seen at the PCC [101].

Since the voltage unbalance at a given bus is due to an unsymmetrical current triplet flowing through the branch upstream that bus, the proposed solution consists in the injection of a suitable current triplet downstream the controlled bus (the PCC in this case). This kind of action can be provided by three-phase inverters, which may have the possibility to unevenly modulate the current injections of each leg adjusting the power production on each phase [91,95,96,102]. A circuital example of the referred case is depicted in Figure 4.1. The picture shows a three-phase inverter which is derived from the line downstream the PCC, having as control's input the three currents flowing on the main branch, called I_m (the phases are indicated with letters from a to c and n is the neutral conductor). The objective is to suitably control the injected currents I_{inv} in order to obtain a symmetrical triplet I_r.

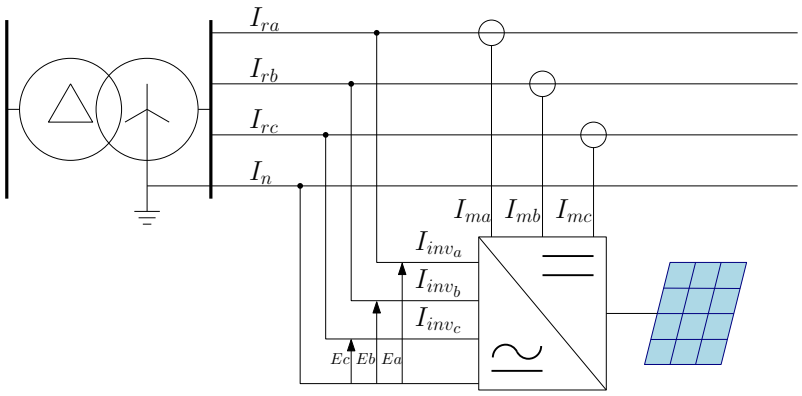

Figure 4.1: Schematic representation of a three-phase inverter controlled to compensate the asymmetric line currents.

As a working condition, it has been decided to add a further constraint consisting in maintaining the total three-phase active power, given by:

$$\sum_{k=a}^{c} P_k = \sum_{k=a}^{c} \Re\left[E_k \cdot I_{inv_k}\right] = P_{3\Phi} \tag{4.1}$$

where a, b, c are the phases, while $P_{3\Phi}$ is the total three-phase power and I_{inv} is the current injected by the inverter, including the component due to its power set-point and, in case, the one for regulation. In this way, the inverter's working point won't be influenced by the control while the user is providing a network service.

The sequence components of the current flowing in the interested branch are used as input of the control and obtained through the well known Fortescue transformation as for equation (4.2):

$$\begin{bmatrix} I_{m_0} \\ I_{m_+} \\ I_{m_-} \end{bmatrix} = \frac{1}{3} \begin{bmatrix} 1 & 1 & 1 \\ 1 & \alpha^2 & \alpha \\ 1 & \alpha & \alpha^2 \end{bmatrix} \cdot \begin{bmatrix} I_{m_a} \\ I_{m_b} \\ I_{m_c} \end{bmatrix} \tag{4.2}$$

where $\mathbf{I_{m_{0,+,-}}}$ is the measured currents triplet in the sequences frame of reference and α stands for the complex number $e^{\jmath\frac{3}{2}\pi}$ introducing the phase displacement of $+120°$. Given these values, the balancing currents triplet aiming at compensating the negative and zero sequences of the measured values is given by:

$$\begin{bmatrix} \Delta I_{B_a} \\ \Delta I_{B_b} \\ \Delta I_{B_c} \end{bmatrix} = - \begin{bmatrix} 1 & 1 & 1 \\ 1 & \alpha & \alpha^2 \\ 1 & \alpha^2 & \alpha \end{bmatrix} \cdot \begin{bmatrix} I_{m_0} \\ 0 \\ I_{m_-} \end{bmatrix} \tag{4.3}$$

The adjustment of the injected currents by the three-phase inverter in order to produce

the balancing effect would result in an active power variation $\Delta P_{3\Phi}$ quantified as:

$$\sum_{k=a}^{c} \Re\left[E_k \cdot \Delta I_{B_k}\right] = \Delta P_{3\Phi} \tag{4.4}$$

that needs to be compensated in order to satisfy the total power invariance constraint defined by equation (4.1) (E_k are the phase-neutral voltages at the inverter's connection bus). To achieve this, a corrected currents triplet ΔI_C needs to be calculated, resulting in:

$$\sum_{k=a}^{c} \Re\left[E_k \cdot \Delta I_{C_k}\right] = 0 \tag{4.5}$$

being:

$$\mathbf{\Delta I_C} = \mathbf{\Delta I_B} + \mathbf{\Delta I_P} \tag{4.6}$$

where $\mathbf{\Delta I_P}$ is a further currents triplet resulting in the required active power compensation. Observing that the active power variation $\Delta P_{3\Phi}$ given by $\mathbf{\Delta I_B}$ is compensated by the triplet $\mathbf{\Delta I_P}$, its magnitude can be calculated as:

$$|\Delta I_P| = -\frac{\Delta P_{3\Phi}}{3\langle|E|\rangle} = -\frac{\sum_{k=a}^{c} \Re\left[E_k \cdot \Delta I_{B_k}\right]}{3\langle|E|\rangle} \tag{4.7}$$

where $\langle|E|\rangle$ is the mean value of the phase voltage magnitudes. This choice was made in order to have equal $|\Delta I_P|$ magnitudes on the three phases, considering that the voltage deviation among the phases is corrected as an effect of the injection of $\mathbf{\Delta I_B}$. Finally, the $\mathbf{\Delta I_P}$ triplet is obtained as:

$$\mathbf{\Delta I_P} = |\Delta I_P| \cdot \begin{bmatrix} 1 \\ \alpha^2 \\ \alpha \end{bmatrix} \tag{4.8}$$

since it needs to be a balanced set of currents in order not to influence the balancing effect introduced by $\mathbf{\Delta I_B}$. It is worth noting that, depending on the capability of the generation system connected to the DC side of the converter, this approach can be applied straightforwardly for active power regulation while performing the balancing action. In that case, in fact, the required active power variation ΔP_{obj} will appear on the right side of equation (4.5), while in (4.7) the numerator results as $(\Delta P_{obj} - \Delta P_{3\Phi})$. A numerical example of how the current compensation technique described so far is obtained by means of a vector composition is shown in Figure 4.2, where the green currents triplet I_m represents the input and the black one I_r the result.

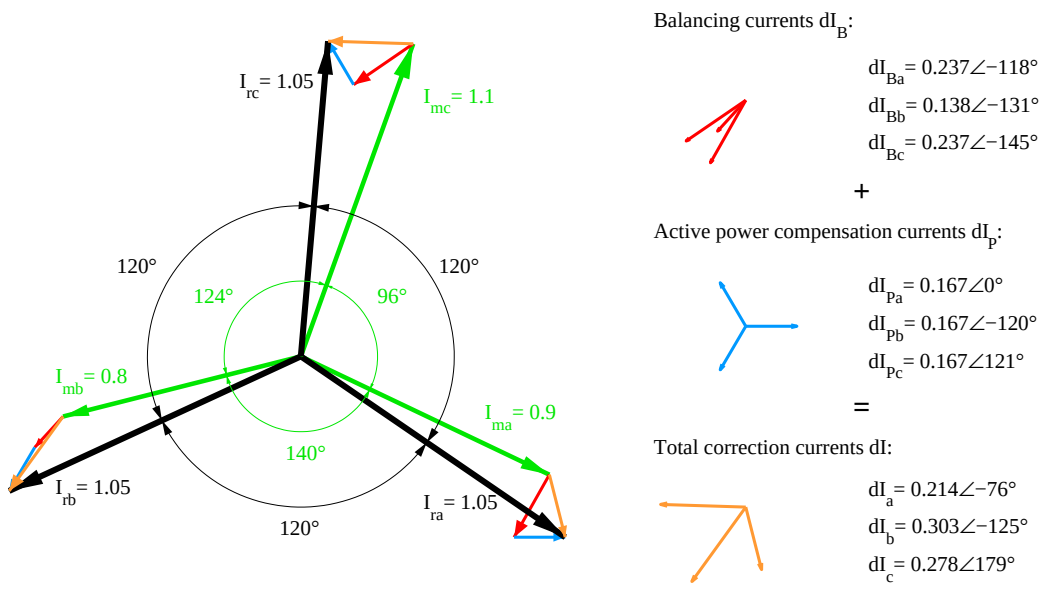

Figure 4.2: Vector composition of the current balancing technique applied to a numerical example.

4.2.2 Distributed resources participation

Under the hypothesis of a mature smart-grid scenario, as supposed in chapter 3 for the MV network regulation strategy, some sort of participation can be expected coming from the DERs as they become more responsive to signals possibly coming from the Distribution System Operator (DSO). Furthermore, the new connection rules stated by the standards cited in chapter 1 require the inverter-interfaced DGs to be able to receive and reply to remote control signals even at LV level, thus foreseeing the participation of active users to the network regulation.

In the previous section, the proposed Low Voltage unbalance correction strategy has been described as a current control suitable for locally connected three-phase inverters. This approach can be easily extended and adopted for a distributed network regulation scheme involving both single and three phase inverter-interfaced DGs . For the scope, conservative control variables such as active and reactive powers are more suited in order to better apply coordinated control strategies between remote network components [96,97, 103]. In [104], it is demonstrated that every power-like term is conservative in any given network, so the instantaneous power absorbed at the input ports of a network equals the sum of all the corresponding power terms absorbed on the whole network.

In this view, the currents vector $\mathbf{\Delta I_C}$ as defined in equation (4.6) for local phase unbalance correction can be used in combination with the corresponding voltage vectors triplet at PCC and converted into phase complex power,in order to elaborate the power control signals to be dispatched to both single and three-phase inverters connected to the network which can participate in the regulating action. Referring to a generic phase k, once the correction current terms are calculated with the approach discussed in section

4.2.1 the complex power variation is given by:

$$\Delta S_k = \Delta P_k + j\Delta Q_k = E_{PCC_k} \cdot \Delta I^*_{C_k} \tag{4.9}$$

The LV network management strategy described so far has been implemented considering two kind of actors. The first one is the central unit called Low Voltage Network Controller (LVNC in the following), placed at the network's PCC (i.e. at the secondary side of the MV/LV transformer) aiming at calculating the current variations and then the active and reactive power contributions to be required to the DERs. The second actor category is the resource interface, generally consisting in an inverter, which needs to receive the control signal (i.e. active or reactive power variation) sent by the central unit and to modify the user's working condition accordingly.

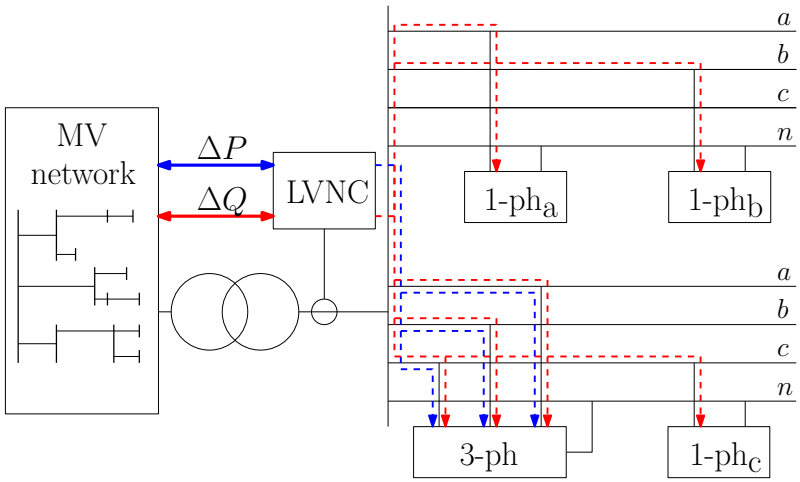

Figure 4.3: Conceptual scheme of the coordinated LV control.

A schematic representation of how the coordinated control strategy for the LV grid is supposed to work is shown in Figure 4.3. As mentioned in section 4.2.1, three-phase inverters have the interesting possibility of unevenly distributing the active power injection on the three phases, so as a working hypothesis it has been decided to forward active power variation signals only to this category of users, while single-phase connected DER only participate with a reactive power variation service. This choice was made to investigate the possible contributions of DERs as network services, but obviously an active power contribution could be considered coming from single-phase units if a local market is in place like in the MV regulation strategy discussed in chapter 3. The integration of the control with the one at upper level is depicted with bi-directional arrows, indicating that services may virtually be provided on the entire P-Q plane.

4.3 Implementation of the control strategy

In the following, the technique for the coordination of a LV network described in the previous section has been implemented for a steady-state simulation aiming at evaluating the feasibility and at investigating the possible benefits coming from this management strategy. In addition to this feasibility analysis, a further development of the control is presented to validate its application in RMS-dynamics.

4.3.1 Steady-state analysis

This section discusses the application of the control strategy proposed in the previous section in a steady-state simulation environment. This approach is particularly interesting when associated to the power-flow technique discussed in chapter 2 because it allows to include the LV coordination strategy while simulating slowly varying time-resolved power flows, for example happening during a 24-hours operation. This kind of simulations can give informations about the power quality level improvement under different operating conditions of the LV network and can help studying the support that can be expected coming from one (or more) of these systems when connected to a MV distribution grid.

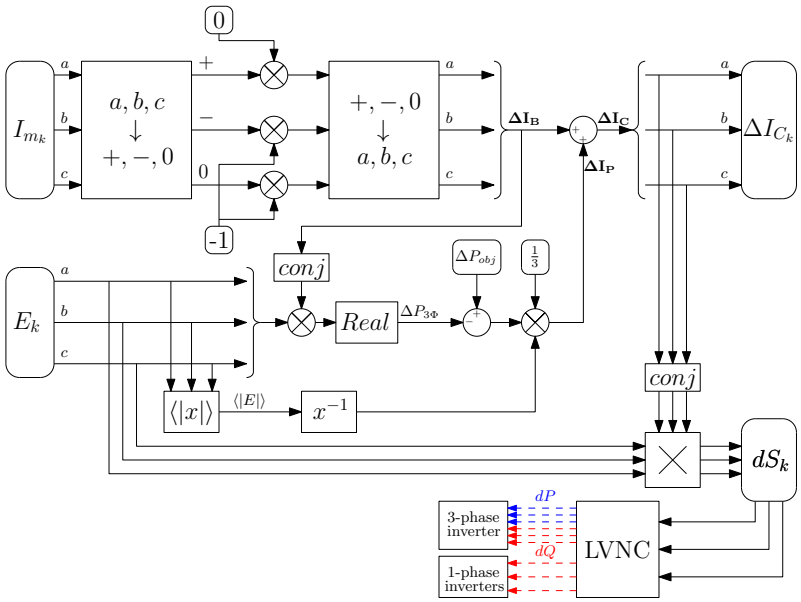

Figure 4.4: Block diagram of the LV coordination strategy implemented in steady-state.

Figure 4.4 shows a block diagram of the proposed strategy, as it is implemented in steady-state simulations. The input variables on the left side are the current triplet I_m measured at the line downstream the controlled bus k and its phase voltage triplet E. As for equation (4.3), the balancing currents $\mathbf{\Delta I_B}$ are derived from the measured ones by zeroing the positive sequence component and changing the sign of the other two. Concerning the active power invariance constraint, the block diagram shows that a term called ΔP_{obj} is added to the active power variation resulting from the injection of the balancing cur-

rents. In this way, the same scheme is applicable when a different active power objective is set, generalizing equation (4.7). On the right side of Figure 4.4, the results in terms of resulting currents $\mathbf{\Delta I_C}$ and complex power variation on the three phases are reported.

The block diagram in Figure 4.4 refers to the control that is supposed to be acted by the central unit identified as *LVNC* in Figure 4.3. The active and reactive phase power requests are forwarded to the downstream inverter-interfaced DGs in accordance to their own capability, assuming that *LVNC* receives signals from the DERs about their actual capability margins, otherwise the share of reactive (and active for three-phase inverters) power request is simply proportional to the inverter size. Under the hypothesis of not pursuing any extra active power contribution from DERs, i.e. the ΔP_{obj} term is zero as for equation (4.7), the signal sent to the single-phase units is just a reactive power request, proportional to the total requested Q_k for the $k-th$ phase in (4.9) and pictorially indicated by the red-dashed lines departing from the LVNC block in Figure 4.4. For the three-phase units, besides the reactive power requests, an active power redistribution can be requested through the dP_k signals, indicated by the blue dashed-lines.

Once the dP and dQ signals are evaluated for the three phases, each inverter in the network receives the relative request (for instance depending on its size respect to the total installed power on the same phase). The complex power variation at the inverter's connection bus is obtained adding suitable correction currents during the power flow calculation with the CCI algorithm described in section 2.4, so recalling equation (2.18) and assuming the DG to be represented by a constant power model, the total correction current becomes:

$$\Delta I_{kh(i)} = \frac{Y_{kh}}{U_{kh(i)}} \left(|U_{kh}|^2_{(i)} - |U_{kh}|^2_{(0)} \right) + \left(\frac{dP + \jmath dQ}{U_{kh(i)}} \right)^* \tag{4.10}$$

for a shunt element connected between nodes k and h (with k usually consisting in one of the phases and h in the neutral point).

4.3.2 Dynamics analysis

After the feasibility analysis, conducted through series of time-resolved steady-state simulations, the proposed control strategy was implemented in dynamics to validate its application for the management of a LV distribution network [105]. In the following, the strategy proposed in the previous sections is further developed presenting an implementation of the control for dynamics simulation. The aim of this kind of simulations is to study the application of the strategy considering the dynamic behaviour of both the central unit (*LVNC*) and the inverter controllers.

Figure 4.5 shows the block diagrams for the implementation of the control strategy in dynamics. The scheme in Figure 4.5a refers to the central unit *LVNC* which, as discussed in the previous section, acquires the current and voltage measurements at the PCC busbar. The main difference with the scheme depicted in Figure 4.4 is the presence

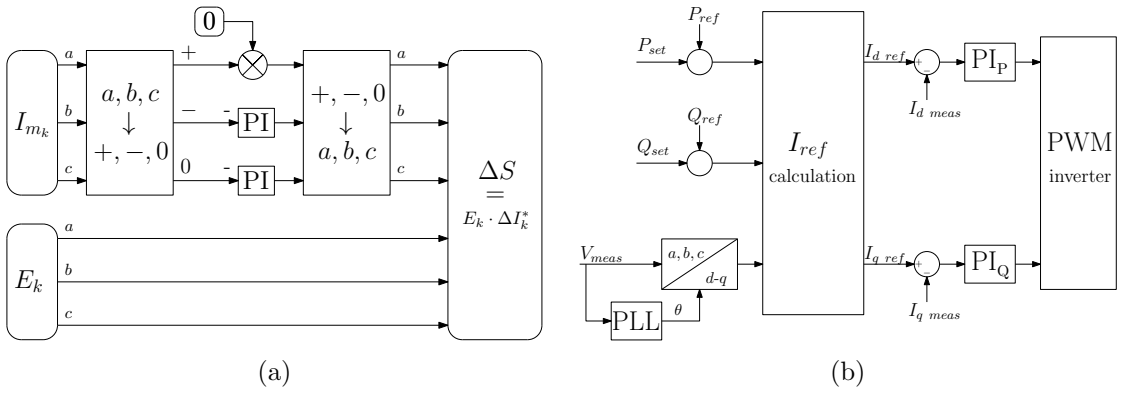

Figure 4.5: Control schemes for the implementation of the *LVNC* (a) and inverter (b) controllers in dynamics.

of the proportional-integral controllers operating the sequences compensation action. In this case, in fact, instead of calculating directly the total current variation, the sequence components of the measured currents are used as negative feedback to the controllers, dynamically adjusting the needed contribution from the DERs.

Another evident difference is the lack of the correction current to satisfy the active-power-invariance constraint, i.e. the $\mathbf{\Delta I_P}$ triplet. While in the steady-state control the positive sequence correction is added separately to take into account the active-power-invariance constraint (4.1), in dynamics this effect results from the fact that while compensating two of the sequence components, the third one (i.e. the positive sequence) varies accordingly as a result of the integral action of the controllers while reaching the new regime.

In Figure 4.5b the current-control scheme associated to the inverter units is depicted. The active and reactive power variation requests dP and dQ coming from the *LVNC* are summed with the local set-point signals P_{ref} and Q_{ref} resulting in the total power amount which needs to be obtained by changing the injected current. The new current reference values $I_{d\,ref}$ and $I_{q\,ref}$ are calculated in the d-q frame of reference in which the active and reactive power equations are written as:

$$P = V_d \cdot I_d + V_q \cdot I_q \tag{4.11}$$

$$Q = V_q \cdot I_d - V_d \cdot I_q \tag{4.12}$$

As can be seen from the scheme, a Phase-Locked-Loop (PLL) controller measures the phase θ of the voltage at the connection bus V_{meas}, allowing the transformation. Under the hypothesis that the PLL is synchronized with the phase-voltage vector, the V_q term in equations (4.11-4.12) can be neglected.

Once the new current references are set, they are compared with those injected by the inverter (i.e. I_{meas}) to create an error signal to be controlled by Proportional-Integral (PI) controllers. It is important to note that the coordination action operated by the *LVNC*

needs to have a sensibly lower dynamic than the inverter control in order to separate the effects.

4.4 Case study applications

In this section, some case studies are reported to discuss the effects of the connection of single-phase DGs to a LV network on the power quality and the benefits coming from the coordinated control discussed in the previous sections, implemented in both steady-state and dynamics. The aim of the study is to check the effects of the LV control (initially only locally-based, then coordinated) on a LV reference network under realistic working conditions. The results discussed in the following include, besides the phase voltages and the respective power contributions by DGs, the corresponding voltage unbalance factors as defined in [52].

4.4.1 Reference LV network

To validate the methodology, a realistic network model considering a typical configuration for LV systems has been chosen. The case study network considered for the following applications is a part of the Low Voltage distribution European reference network presented in the Cigré C6 Task Force report on Benchmark Systems for Network Integration of Renewable and Distributed Energy Resources [106].

The network layout is shown in Figure 4.6 and consists in the 13-buses residential sub-system of the reference network. The MV/LV transformer in Secondary Substation is a 20/0.4 kV 400 kVA transformer with short circuit voltage $vcc = 6\%(V_{1n})$ and $X/R = 6$. The neutral conductor is grounded only at the transformer's secondary busbar as is commonly done in many LV systems in Europe.

The LV lines, having the length shown in the network layout in Figure 4.6, consist in 4-wires branches with the geometry reported in Appendix D along with the respective cable types (see Figure D.2 and Table D.2). As for the common practice in LV systems the lines are composed by different cable sections for the phase and neutral conductors, based on the principle that the neutral conductor's current in a three-phase line is generally lower than the phase one. The maximum feeder's extension is 345 m (between buses R1 and R18), while the average weighted R/X ratio (i.e. the ratio divided by the actual extension of the respective line type) is about 2.6.

The load and generation data are reported in Table 4.1, where it could be seen that the network is mainly passive, since the installed load apparent power is 219 kVA (with p.f.=0,9), while the total DGs' rated power is 63 kVA. The load and generation units are unevenly connected on the three phases and the power installed on each phase is compared with the total three-phase one reporting the percent value. As shown in Figure 4.6 the network hosts 5 distributed generators interfaced by inverters, one of which (connected at bus R15) is a three-phase unit represented in red with three single-phase inverters.

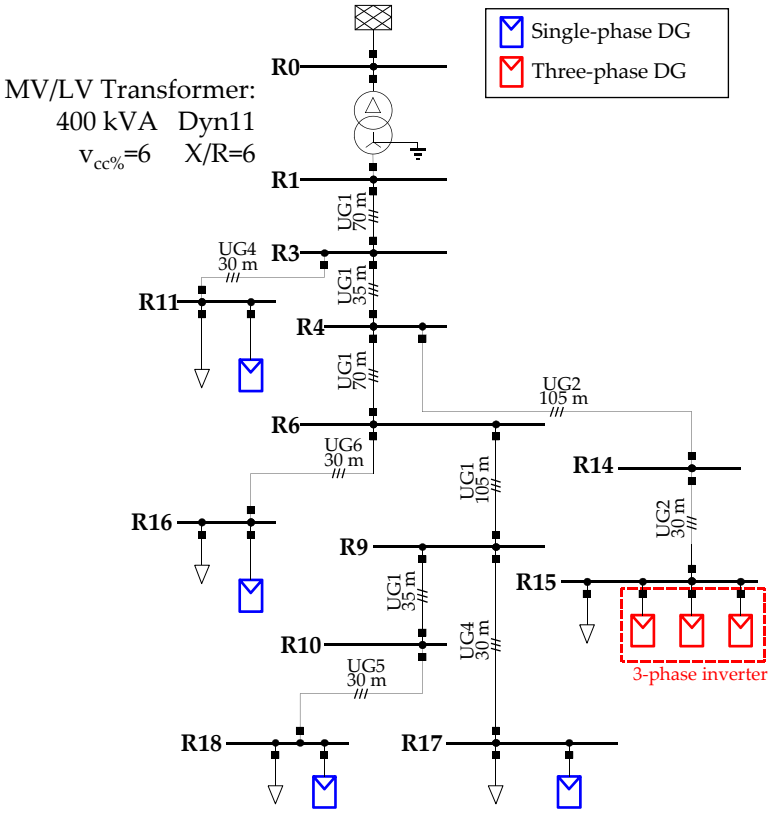

Figure 4.6: Layout of the reference European LV network.

In the following sections, applications on the reference LV network are discussed considering a 24-hours period, in which the loads' and generators' power is varied according to the daily profiles reported in Figure 4.7.

Table 4.1: Loads and Generators installed power [kVA].

Buses	**Loads**			**Generators**		
	ph a	ph b	ph c	ph a	ph b	ph c
R11	7.0	6.0	3.3	0.0	8.0	0.0
R15	20.4	30.0	30.0	10.0	10.0	10.0
R16	16.5	19.8	22.0	0.0	0.0	8.0
R17	3.6	5.0	7.0	8.0	0.0	0.0
R18	14.0	15.4	19.0	9.0	0.0	0.0
TOT	61.5 (28%)	76.2 (35%)	81.3 (37%)	27.0 (42%)	18.0 (29%)	18.0 (29%)

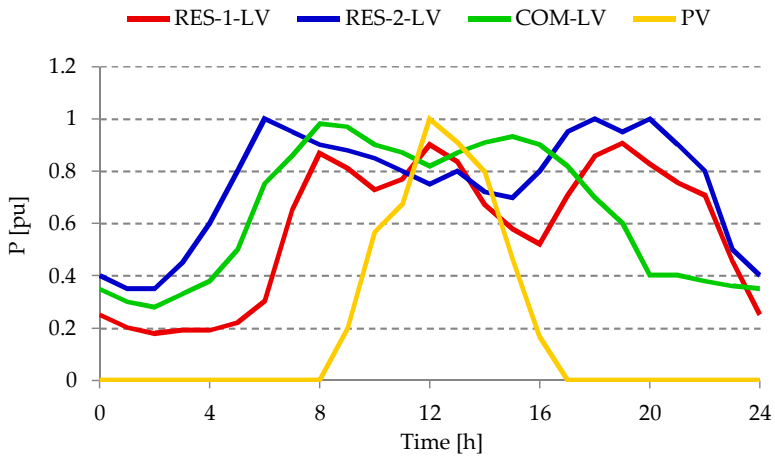

Figure 4.7: Daily power profiles for loads and generators connected to the LV network.

4.4.2 Local voltage control by Distributed Generators

This section focuses on the investigation about the effects on the buses voltage magnitudes and unbalance when applying the reactive power controls set by the recently released standards. In particular, the controls implemented in this study are those contained in the Italian standard for the connection of Distributed Generators to the Low Voltage distribution network [9], here used as application example of the general requirements set by the European Technical Specification 50549 [14].

The controls used in the following are stated by the mentioned Italian standard CEI 0-21 for inverter-intefaced generators connected to the LV system with an installed power above 6 kW. Furthermore, these local actions are not performed by default by inverters, but may be required by the DSO by setting suitable values identifying the control characteristic shown in Figure 4.8.

The grey band identifies a *Dead-Band* region, in which the reactive power control is disabled, comprised between the two lock-in voltage values V_{1l} and V_{1u} for the lower and upper sides of the voltage deviation respectively. On each side, when the busbar voltage overcomes the lock-in value, the reactive power is set according to the characteristic, reaching the value Q_{max} (or Q_{min}) in correspondence of the V_{2l} and V_{2u} values.

The mentioned maximum reactive power value (equal to the minimum one which has opposite sign), is set according to the capability area set for the control. The CEI 0-21 standard sets two kind of capability areas for LV connected generators, called *triangular* and *rectangular* on the basis of their shape on the P-Q plane. Figure 4.9 shows these two areas, indicated respectively as A and B, while a third one, called C, consists in the maximum capability available for an inverter, described by the semicircular region on the plane P-Q with radius S_n (being the inverter's rated power). Looking at areas A and B it should be noted that the reactive power limit is set using as minimum power factor the value 0.9: for the triangular area the limit vary depending on the actual injected power,

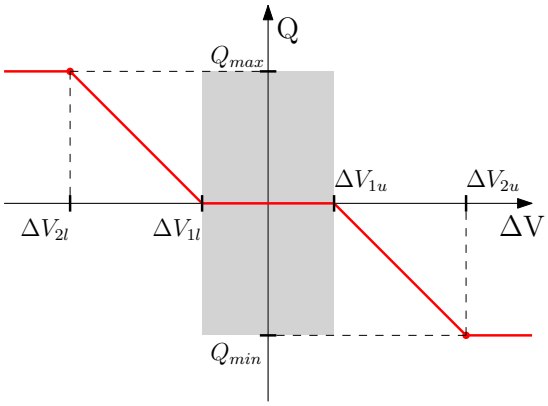

Figure 4.8: Local reactive power control characteristic $Q = f(V)$ stated by the standard CEI 0-21.

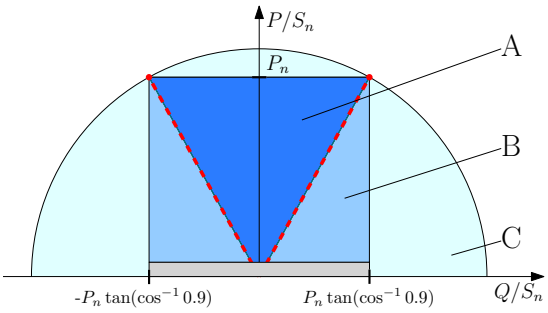

Figure 4.9: Capability areas for the Q(V) control: triangular (A), rectangular (B) and semicircular (C).

while for the rectangular one this value is kept constant. A lock-in value is set in terms of active power at $5\%P_n$ in both cases, corresponding to the minimum value stated by the standard. Area C is then considered as a best-case scenario, in which inverters give the maximum availability to the voltage support action.

In this study, a 24-hours period has been simulated applying the daily power profiles shown in the previous section, setting the control characteristic for $Q = f(V)$ control in Figure 4.8 with the following values:

- V_{1l}: -0.01 pu;
- V_{1u}: 0.01 pu;
- V_{2l}: -0.1 pu;
- V_{2u}: 0.1 pu.

Calling the not-regulated scenario *Base Case*, three local regulation scenarios are considered based on the three different capability areas in Figure 4.9:

- **Scenario A:** triangular capability area;
- **Scenario B:** rectangular capability area;
- **Scenario C:** semicircular capability area.

In Figure 4.10 the phase voltages are reported for each scenario compared to the Base Case while Figure 4.11 reports the power balance (P and Q) for the Base Case and the reactive power due to the local control (positive values indicate absorbed power). The DGs' production period is indicated by the yellow area in all graphs to highlight the possible effects coming from the local actions taken by those units while they are injecting active power. From Figure 4.11 it should be noted that, as already mentioned in the system

description in the previous section, the network is mainly passive, having consistently a positive power balance.

In Scenario A, DGs act a voltage regulation computing the reactive power according with the triangular area in Figure 4.9 using the expression:

$$Q = P \cdot \tan\left(\arccos 0.9\right) \tag{4.13}$$

depending on the instantaneous active power P. Therefore, during the off-peak hours, no regulation is provided despite the remarkable under-voltages (e.g. around h. 19), as can be seen from the power chart 4.11a.

In Scenario B the rectangular capability area in Figure 4.9 is adopted, then the reactive power limit is kept constant at $Q = P_n \cdot \tan\left(\cos^{-1} 0.9\right)$, with P_n equal to the inverter's rated power. As already mentioned, since the standard sets an active power lock-in value (minimum 5% of the rated power P_n, as chosen in this case), the control is inhibited below this threshold, with the result that the overall contribution coming in Scenario B is very similar to the one obtainable in Scenario A.

In Scenario C, instead, a semi-circular capability area of the type shown in Figure 4.9 is considered, allowing DGs to exchange with the network a reactive power depending on the actual working point according with the inverter's size S_n, even when the active power is at low or null level. The apparent rated power S_n, standing the capability areas A and B, is chosen as $S_n = P_n/0.9$ since an inverter is expected to be working at p.f. 0.9 when producing the rated active power P_n. In this situation the DGs connected to the LV network are actually performing a local ancillary service by supporting the phase-voltage magnitude even outside the production period (for instance around h. 19), exchanging reactive power with the grid without any active power production.

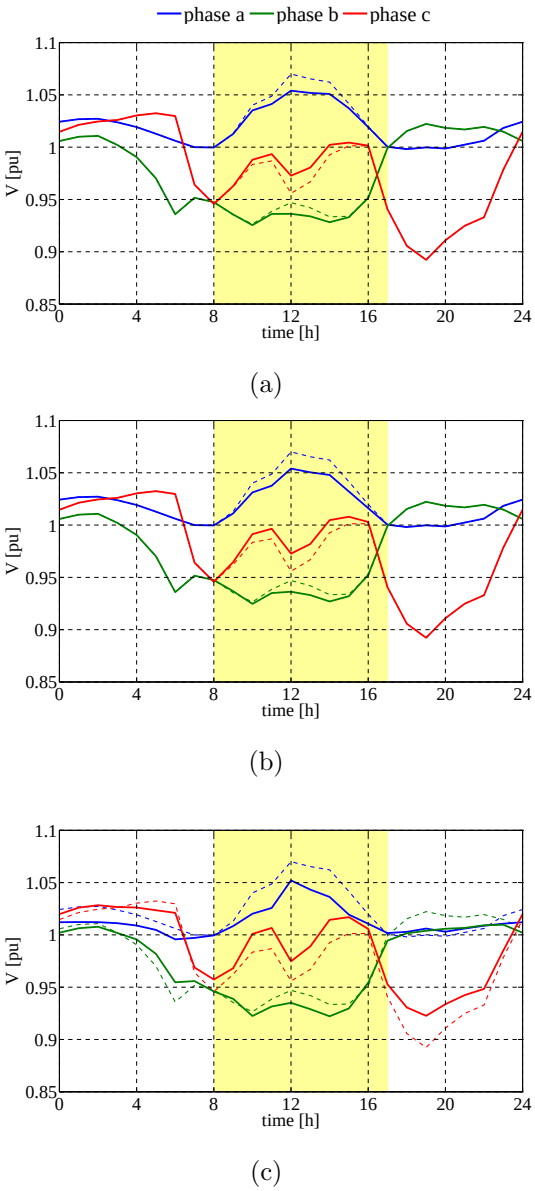

Figure 4.10: Comparison between unregulated (dashed line) and regulated (solid line) phase-neutral voltages at bus R18 during the 24-hours simulation with different capability areas: triangular (a), rectangular (b) and semicircular (c).

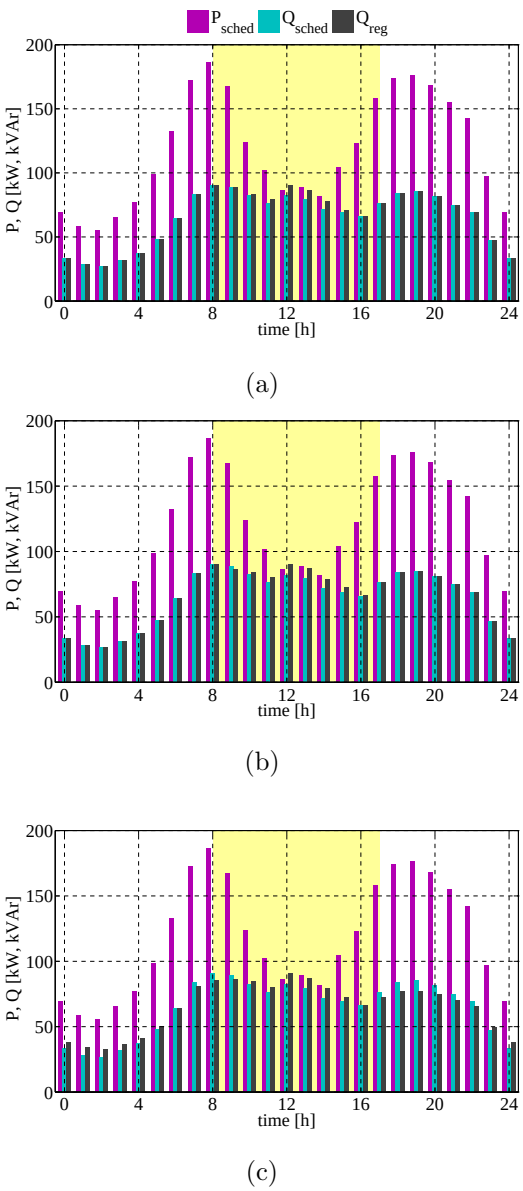

Figure 4.11: Active and reactive power scheduled values and total reactive power for local Volt/Var regulation with different capability areas: triangular (a), rectangular (b) and semicircular (c).

Figures 4.12 and 4.13 show the Voltage Unbalance Factor for the negative and zero sequences at buses R1 and R18 in the three scenarios. As could be seen in Figure 4.12b, the three scenarios lead to similar VUF values during the DGs production period, while a sensible improvement of the unbalance condition is obtainable in Scenario C in which a higher amount of reactive power is available (i.e. outside the production period). Similar comments can be made about the zero sequence (which indicates the neutral conductor's potential trend) in Figure 4.13b with the exception that during the production period the VUF_O appears to be rising due to the local Q regulation.

From the above discussed simulations, it results that the local reactive power control performed by DGs can help (under the present LV network's working conditions) containing the voltage deviations respect to the nominal value, although this type of control may possibly result in undesired shifting og the neutral point potential. In general, for a mainly passive network the local voltage control may lead to lower values of the Voltage Unbalance Factor respect to the Base Case, but not necessarily within an acceptable level since this feature is not considered as an objective of the control.

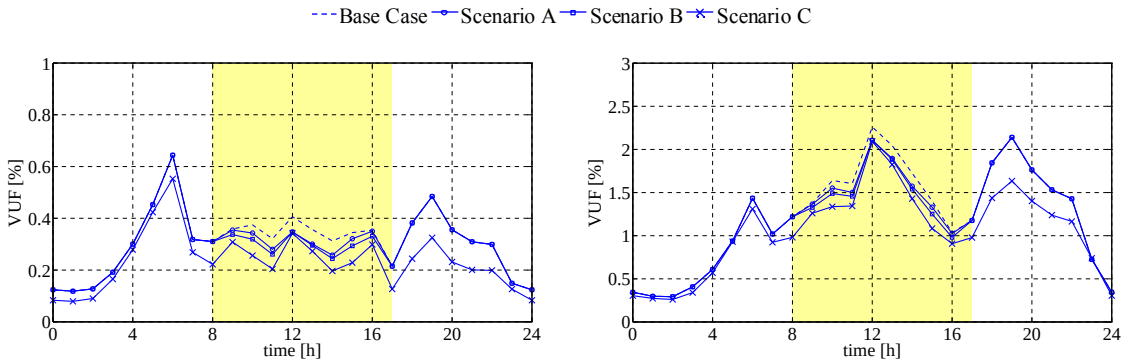

Figure 4.12: Negative sequence Voltage Unbalance Factor (VUF) at buses R1 (a) and R18 (b).

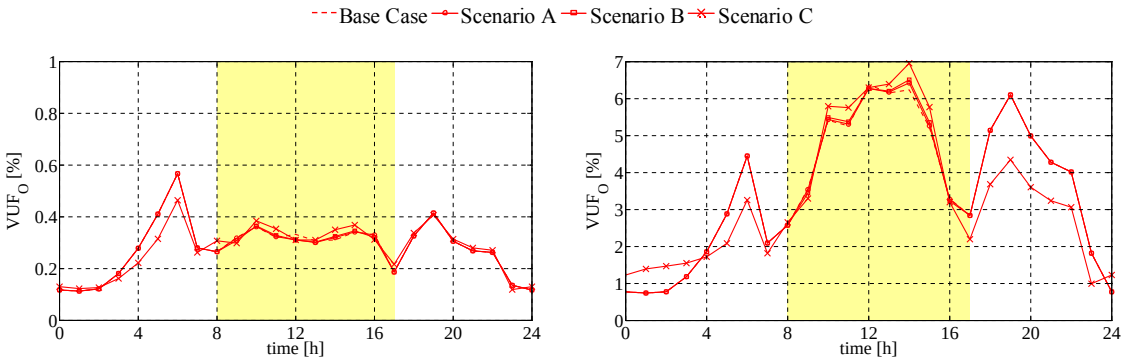

Figure 4.13: Zero sequence Voltage Unbalance Factor (VUF_O) at buses R1 (a) and R18 (b).

4.4.3 Comparison between steady-state and dynamics implementation of the LV coordinated control

In the following, the control presented in section 4.2 is applied to the LV reference network to study the effects on the voltage unbalance obtainable by the coordination of the distributed resources connected to the LV network. The control has been simulated in RMS-dynamics through the software DigSilent PowerFactory and the results are compared with those obtained in steady-state simulation.

In this study the capability limits imposed by DGs are intentionally disregarded, in order to investigate the full effects coming from the control and in particular the comparison between steady state and dynamics implementations discussed in section 4.3. In the following all the simulation results are reported for the steady state and dynamics solutions with dashed and solid lines respectively.

The Base Case has been chosen as the h. 11 time instant of Scenario C simulation shown in the previous section. Starting from this situation, two events are considered occurring sequentially:

- t=3s : the LVNC starts sending the control signals in terms of $\Delta P$and ΔQ to the DGs with the aim of balancing the currents downstream the PCC;
- t=6s: an additional reactive power production is requested by the LVNC to the inverters for the provision of an ancillary service to the upstream MV grid.

In Figure 4.15 the phase-neutral voltages are reported for each phase of buses R1, i.e. the PCC, and bus R18 at the feeder end. As shown in the previous section, the local reactive power control helps reducing the voltage deviations at the feeder end between the values 0.93 and 1.04 pu. This eventually resulted in a reduction of the unbalance for the negative and zero sequences as already seen in the previous section and also reported in Figure 4.16.

Starting from this situation, at t=3s the Low Voltage Network Controller (LVNC) is activated, so the power contributions needed in each phase to perform the voltage unbalance compensation are evaluated. The control inputs consist in the phase-voltages at the PCC, which are shown in Figure 4.15a, and the sequence components of the currents flowing in the branch downstream the PCC (i.e. line R1-R3), reported in Figure 4.14. These values are used in the control schemes depicted in Figures 4.4 and 4.5a to compute the complex power contributions reported in Figure 4.17.

In this case, since no remuneration was considered for the network services, the single-phase inverters can contribute in terms of reactive power only, whereas the three-phase unit at bus R15 is supposed to redistribute the power production of each phase in order to maintain the initial three-phase active power. This feature can be seen clearly in Figure 4.17a where the active power variation signals forwarded from the LVNC are shown. Concerning the reactive power variation reported in Figure 4.17b, the dynamics and steady

state solutions don't match perfectly probably due to the local control acted simultaneously in each DG connection bus reacting differently when including the dynamics of the LVNC control and of the inverters.

After the unbalance correction control reached the objective, at t=6s an extra reactive power production is required by the LVNC to the inverters as an ancillary service for the MV network. As shown in Figure 4.17b, this results in a step in the reactive power request by the LVNC while continuing to perform the voltage unbalance control. As a result, the currents' negative and zero sequence components are still compensated while delivering the ancillary service.

As expected, the currents unbalance correction results in a voltage balancing at PCC, while the negative sequence of the bus R18 voltage is reduced from the initial 1.5% to about 1%. The voltage zero sequence at bus R18 is also reduced, allowing to mitigate the neutral point potential shifting due to the uneven distribution of the load and generation powers.

It is worth noting that the voltage balancing effect obtained through the currents compensation is also due to the fact that by hypothesis the slack bus imposes a balanced voltage triplet. In general, the aim of the control is to limit the contribution to the voltage unbalance at PCC due to unsymmetrical power flows in the LV network.

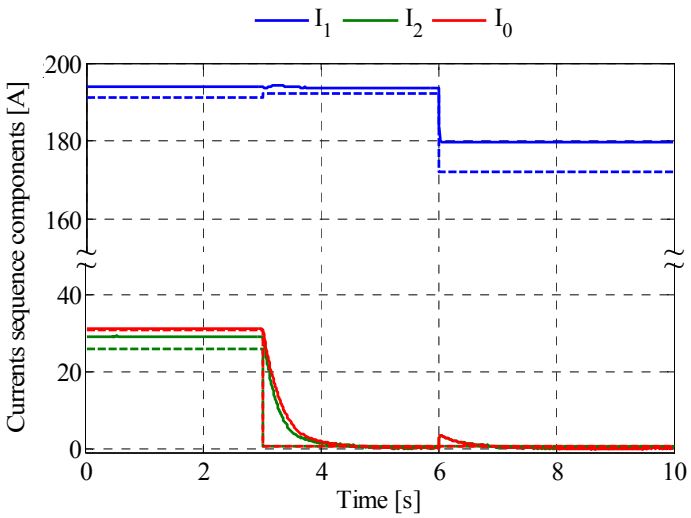

Figure 4.14: Sequence components of the measured current downstream bus R1 (PCC).

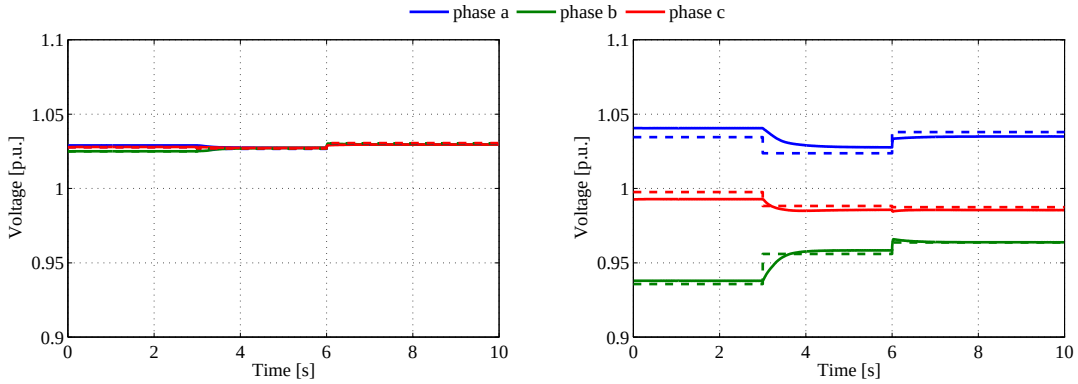

(a) (b)

Figure 4.15: Phase-neutral voltage for buses R1 (a) and R18 (b).

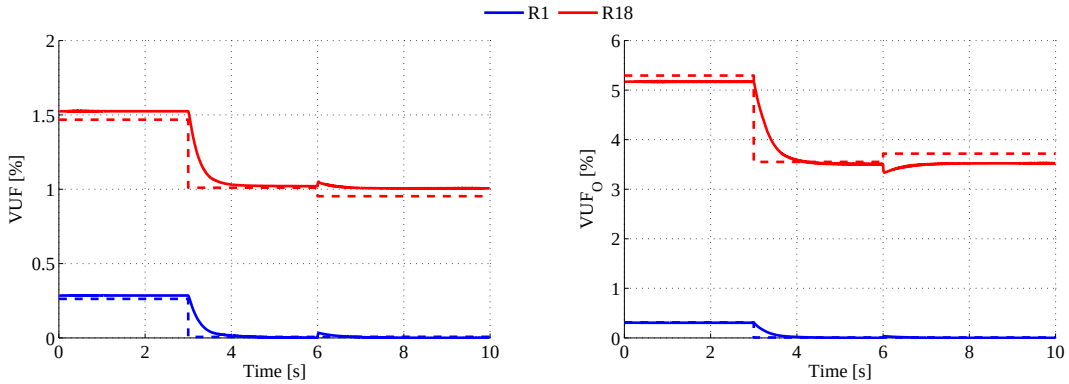

(a) (b)

Figure 4.16: VUF (a) and VUF_O (b) at buses R1 and R18.

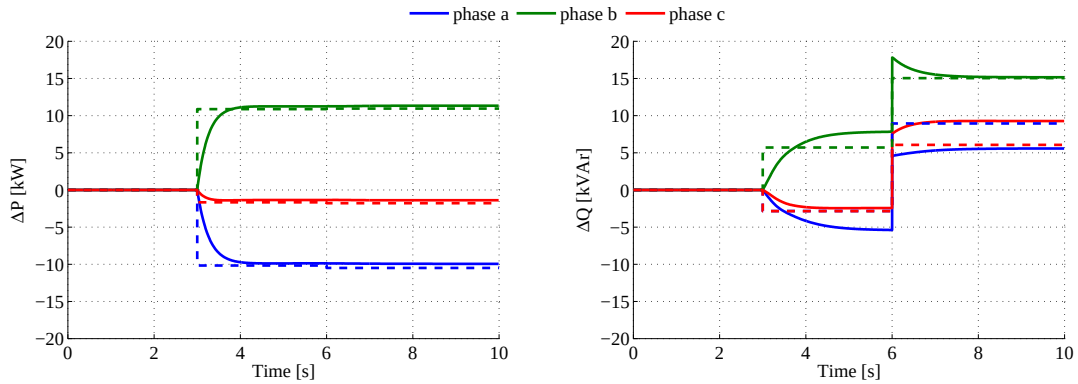

(a) (b)

Figure 4.17: Active (a) and reactive (b) power requests from LVNC.

4.4.4 LV coordinated control application for long term analysis

In the following, the LV coordinated control is applied to the case considered in section 4.4.2 to study the LV network operation in a 24-hours period. Taking as inputs the phase-neutral voltages at bus R1 and the currents flowing downstream it as for the previous case study, the LVNC elaborates the active power variation requests for the three-phase unit while setting the reactive power set-points for the local control discussed previously pursuing both the voltage magnitude and unbalance regulations.

Starting from the operation discussed in section 4.4.2 considering only the local reactive power regulation acted by DGs, the inclusion of the control discussed in the previous section allows to better exploit the presence of distributed resources in mitigating the power quality issues. These two situations are simulated in the following scenarios:

- **Scenario A:** voltage support action through local reactive power control with semi-circular capability areas as for Scenario C in section 4.4.2;
- **Scenario B:** local Volt/Var control supported by the coordination of the reactive power on the three phases aimed at reducing the voltage unbalance at PCC;
- **Scenario C:** coordinated LV regulation for voltage magnitude and unbalance control including the active power redistribution on the phases.

While Scenario A represents the solution discussed in section 4.4.2 adopting the semi-circular capability area, Scenarios B and C include the coordinated control acted by the LVNC aimed at obtaining the voltage unbalance mitigation as seen in the previous section, by performing the following features:

- reactive power coordinated contribution by all inverters, shifting the local control characteristic in Figure 4.8.
- active power redistribution on the three legs of three-phase inverters (in this case acted by the only three-phase unit connected at bus R15)

Figure 4.18 shows the phase-neutral voltage at bus R18 (i.e. the feeder-end bus) during the 24-hours period to analyse the results of the coordinated control on the LV network's working conditions. The comparison between Scenario A and B shows that even without sensibly changing the overall voltage deviation conditions at the remote buses, the coordination of the reactive power contribution locally performed by DGs affects mainly the differences among the three phases magnitudes. The balancing effect is strongly increased when considering the active power redistribution action performed by the three-phase unit in Scenario C.

The VUF and VUF_O levels are shown for bus R18 in Figure 4.19, in which a slight mitigation of the voltage's negative sequence component can be seen in Scenario B and becomes evident in Scenario C, respectively keeping the maximum VUF value below 2%

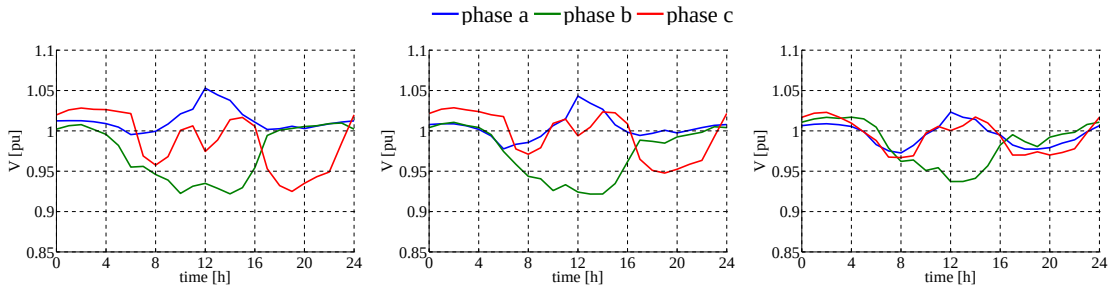

(a) Scenario A (b) Scenario B (c) Scenario C

Figure 4.18: Phase-neutral voltage at bus R18 in the three scenarios.

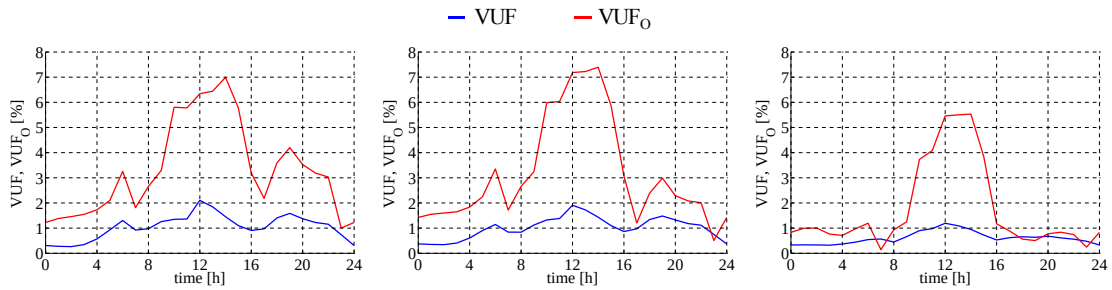

(a) Scenario A (b) Scenario B (c) Scenario C

Figure 4.19: Voltage unbalance factors for negative and zero sequence at bus R18 in the three scenarios.

and 1.5% respect to 2.2% in Scenario A. Furthermore, while it tends to increase in Scenario B, a reduction of the voltage's zero sequence can be also appreciated in Figure 4.19c as an effect of the neutral point potential reduction, although not being an objective of the control but just a consequence.

In Figure 4.20 the reactive power contributions on the phases are shown for the uncoordinated local control (Scenario A) and adopting the coordination strategy implemented by the LVNC (Scenarios B and C). In Figure 4.20b it can be seen that, differently from Scenario A, the single-phase inverters exploit their capability to exchange reactive power even when no contribution is due according to their local voltage, for instance at h. 19.

The active power redistribution on the phases is shown in Figure 4.21, in which it can be clearly seen that the three-phase active power variation (i.e. the sum of the phase values) is constantly null. In this example, in order to focus on the effects achievable by the coordinated control, it has been assumed that the three-phase inverter is able to manage the variations required to each phase (i.e. the inverter legs are oversized enough to manage the actual production and the possible variations). It should be emphasized that this kind of regulation acted by three-phase units should be possible even in off-production periods, since it doesn't involve any power injection to the grid, but just a shifting of the currents exchanged by the inverters in each phase.

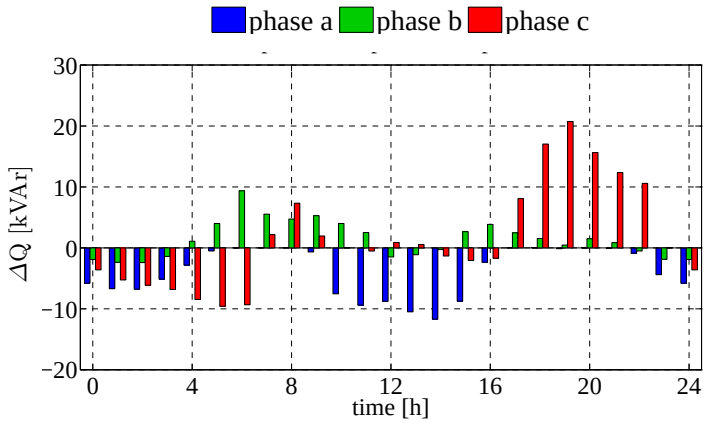

(a) Scenario A

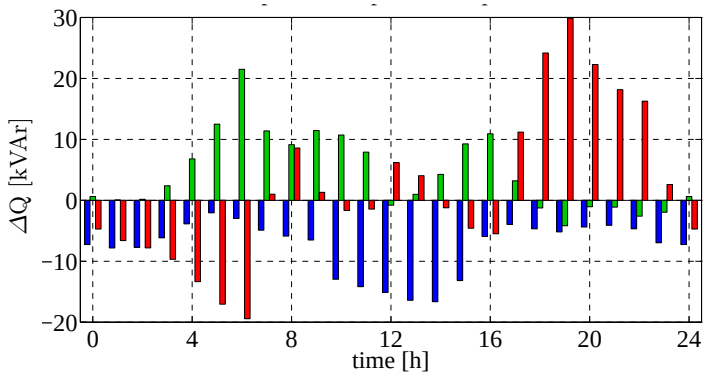

(b) Scenarios B and C

Figure 4.20: Reactive power contributions by phase in the three scenarios.

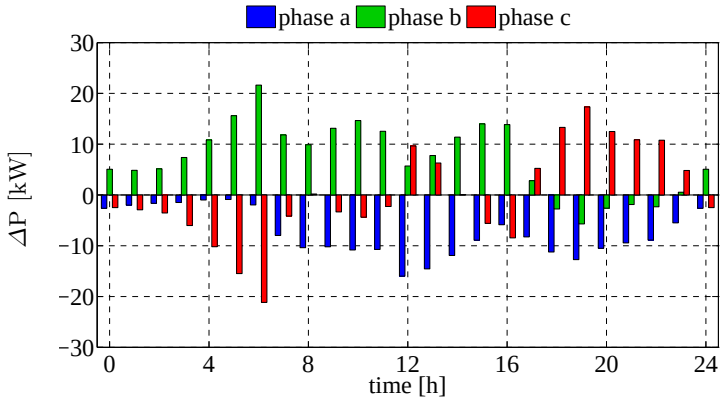

Figure 4.21: Active power redistribution on the phases in Scenario C.

Chapter 5

Distribution Management System including both MV and LV systems

Contents

As the penetration of DGs increases in LV networks, the importance of studying management strategies to involve them in the overall distribution system's regulation is getting more and more relevance. The coordination of the MV and LV subsystems through suitable controls may enable the provision of ancillary services even from the lower voltage level, leading to a more efficient exploitation of the distribution network. This chapter presents an aggregated DMS implemented combining the principles for the regulation strategies discussed respectively in chapters 3 and 4 to pursue the voltage control on both

MV and LV systems. In particular, the presented strategy aims at controlling the MV network busbars' voltage with the participation of the Secondary Substations, in which the respective controllers manage the DERs' contributions pursuing the voltage unbalance mitigation and ancillary services provision.

5.1 Coordinated management of Medium Voltage and Low Voltage networks

The problem of optimizing the operation of distribution networks is a topic that many research groups are dealing with as witnessed by the number of references which can be found, as cited in the previous chapters for instance. Despite the variety of applications presented in literature on this topic, not so many works focus on the implementation of coordinated controls to involve both the Medium Voltage and Low Voltage subsystems.

Aside from the necessity of optimizing the overall operation of a distribution network for technical and economical reasons, the coordination of MV and LV systems is starting to become a key issue in the process of moving towards the *smart-grid*.

In this context, ancillary services may be provided by LV networks (or aggregates of) under the concept of Virtual Power Plant (VPP). In [99] a market framework is proposed to face the voltage regulation problem in a distribution network hosting multiple micro-grids as an hierarchical management architecture is presented.

The same concept is applied in [107], implementing optimization models to study the provision of three ancillary services by the micro-grid agents: Volt/Var control, Active Power Losses balancing and Demand interruption.

In [100] Electrical Energy Storage (EES) systems connected at different voltage levels, i.e. MV and LV, are integrated in a coordinated voltage control scheme managing both the subsystems.

In the following a control scheme is proposed suitable for coordinating the action of both MV and LV active users. Based on the information exchange between the buses and the DMS, an adaptive area selection has been implemented according with the control discussed in chapter 3 based on a sensitivity analysis of the network. The DMS is supposed to interact also with the LV Network Controllers which coordinate the downstream inverter-interfaced DGs enabling them to participate to the MV network voltage regulation.

5.2 Aggregated DMS for MV and LV systems

In this thesis work a novel control scheme has been developed and is proposed for coordinating the action of both MV and LV active users. Based on the information exchange between the buses and the DMS, an adaptive area selection has been implemented, based on a sensitivity analysis of the network, in order to separate the network nodes into several

clusters with common power quality objectives (e.g. similar voltage conditions). MV/LV distribution transformers are equipped with LV network controllers which coordinate the downstream inverter interfaced DGs enabling them to participate to the MV network voltage regulation through appropriate signals.

Starting from the controls described in chapters 3 and 4 respectively for MV and LV regulation, an aggregated solution for a DMS controlling both the subsystems can be obtained. A possible implementation is a scheme built in a hierarchical structure, based on a Network Supervisor (located at the Primary Substation) in charge of the MV network regulation and several Low Voltage Network Controllers (located at the MV/LV distribution transformers) communicating with the downstream inverters, which implement the reactive power control based on the local voltage as stated by the connection rules.

As mentioned in section 3.2.1, the regulation strategy includes the coordination with the OLTC at the primary station transformer through the control scheme in Figure 3.3a. Based on the remote bus voltage measures, before performing the adaptive area selection procedure, the DMS elaborates and modifies the tap position for the OLTC in order to minimize the voltage deviation along the feeders, possibly containing them within an allowed band (chosen as $\pm 5\%(V_n)$), resulting in a reduction of the reactive power requests to the local inverters participating to the regulation. The complete regulation procedure, based on the area selection discussed in sections 3.2.2-3.2.3, also takes into account the MV/LV interface represented by the Low Voltage Network Controllers (LVNC) acting the voltage unbalance mitigation control as discussed in section 4.2.

The architecture of the overall DMS is depicted in Figure 5.1, highlighting the area selection for the MV grid, where the Network Supervisor can elaborate the request signals in terms of ΔP and ΔQ and drives the tap changes for the OLTC. Concurrently, each LV network is coordinated by its own LVNC unit pursuing the voltage unbalance and deviation mitigation, so allowing the Secondary Substations to participate to the provision of ancillary services to the MV grid.

To investigate the concurrent regulation effects on a distribution network, a DMS employing the aggregated architecture depicted in Figure 5.1 is proposed to pursue the voltage regulation in both MV and LV subsystems [108] and will be implemented in the simulations shown in the following section. Applying the controls described in chapters 3 and 4, the voltage regulation strategy is implemented by means of a signals communication from the Network Supervisor, placed at the Primary Substation, to the identified regulation areas. The signals, instead of being active and reactive power requests as for the cases discussed previously, consist in voltage requirements for the local Volt/Var control acted by the inverters. Referring to the general architecture of the DMS, the following steps are considered:

1. Once a voltage contingency is detected (i.e. voltage at some bus beyond the objective

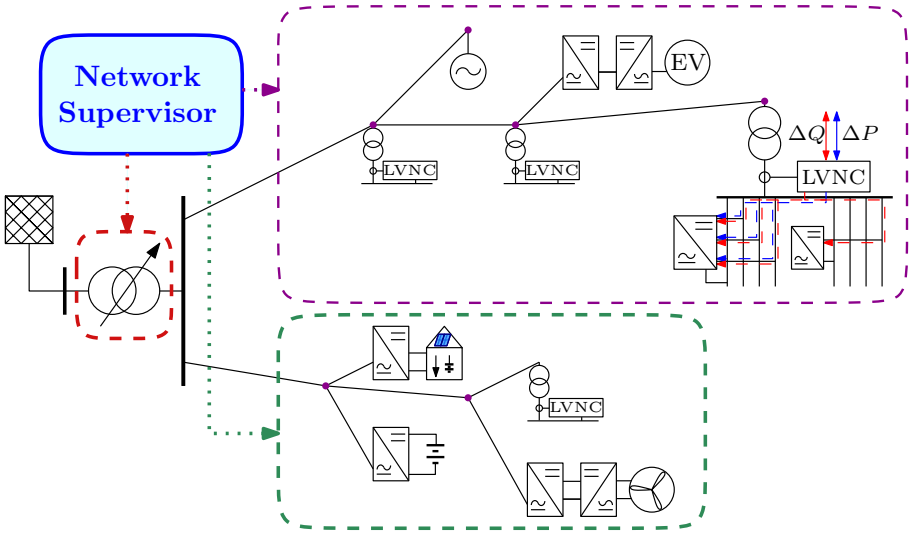

Figure 5.1: Architecture of the aggregated DMS for MV and LV coordinated management.

range) the Network Supervisor (NS) in PS evaluates the optimal tap for the OLTC and creates the regulation areas;

2. The tap position for the OLTC is changed based on the signal coming from the NS;

3. If the OLTC coordinated action doesn't result in the contingency solution, voltage set-points (V_{set}) are forwarded to the areas;

4. The Low Voltage Network Controllers (LVNC) connected to the respective area receive the voltage set-point and forward it to the inverters interfacing the DGs connected to the LV system, along with the ΔP and ΔQ signals for unbalance mitigation purpose.

5. The inverters connected to the LV network react to the signals sent by the LVNC adopting the characteristic shown in 5.2 in which:

   - the y-axis set-point is varied according with the ΔQ request for the voltage unbalance control;
   - the x-axis set-point $\Delta V_{set-point}$ is communicated to support the voltage according with the requirements set by the MV Network Supervisor.

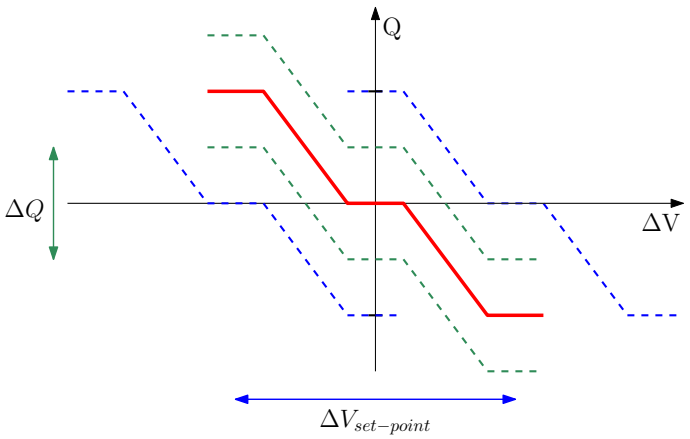

Figure 5.2: Reactive power control based on local voltage measurements and signals communication by the LVNC.

5.3 Distribution network model

The case study network considered in this section is a distribution system with 32 MV buses, distributed in 2 feeders radially departing from a primary station (PS) where a 132/20 kV, 25 MVA transformer connects the main MV busbar to the HV grid being equipped with an OLTC having $\pm 10\%\,(V_{1n})$ variation range (21 taps, $1\%\,(V_{1n})$ per tap), and a Dead-Band of $1.5\%\,(V_{1n})$. Referring to the one-line diagram of Figure 5.3, Feeder A has a total length of about 33 km, for the most part overhead lines with a total R/X ratio of 0,84. In Feeder B the line types are more mixed between overhead and cable, resulting in a R/X ratio of 1,25.

From the distribution MV network layout it can be seen that the Secondary Substations connecting Low Voltage networks are represented by two different symbols, indicating if active users are present or not in the LV subsystem. All of the LV networks connected to the main grid have been represented in this study with the layout reported in Figure 5.4 with the four-wire branches having an R/X ratio of about 4 and a maximum feeder extension of 260 m, as can be seen from the lengths reported in the scheme.

The MV 32-bus network has a total load power of 21,11 MVA and a total installed generation power of 14,03 MVA, unevenly distributed on the two feeders. Feeder A and has an installed generation power of 10,57 MVA and a total load power of 5,06 MVA whereas Feeder B hosts 3,45 MVA generation power, with a total load power of 16,05 MVA. The installed power on each phase of the LV system is reported in table 5.2 amounting at 382 kVA and 226 kVA for loads (with 0.9 p.f.) and generators (with 1 p.f.) respectively. These values are then scaled for each LV subsystem in order to obtain the total installed power at each MV-bus.

A complete data-set of the two models is contained in Appendix E.

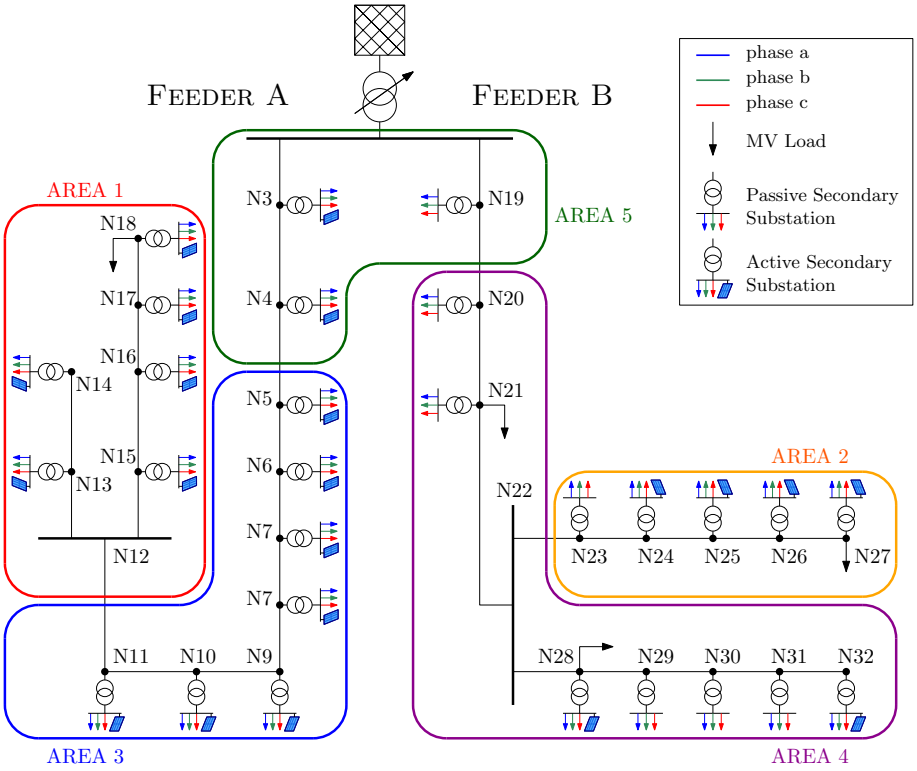

Figure 5.3: Single phase diagram of the case study MV network with voltage control areas.

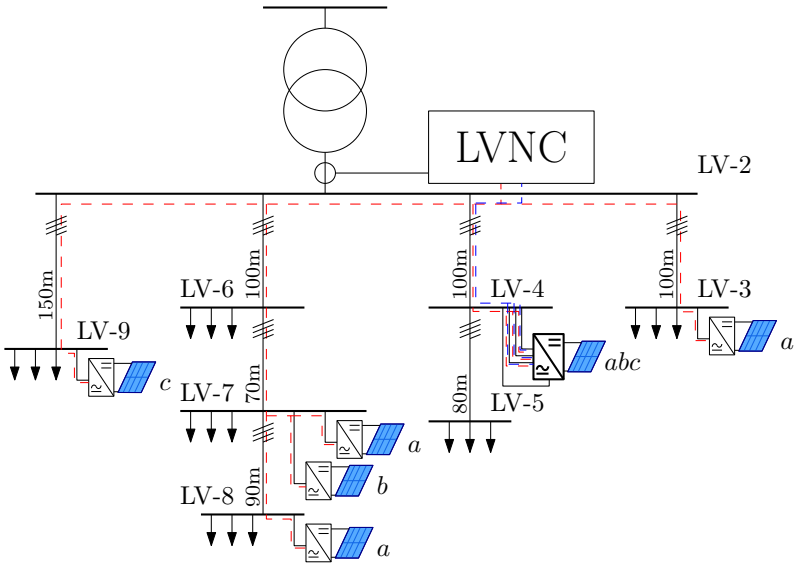

Figure 5.4: Layout of the Low Voltage networks connected to the MV system.

Table 5.1: Total load and generator installed power, as seen at the MV/LV transformers, for the Case Study Network [kVA].

Bus	**Load**			**Generation**		
	phase a	phase b	phase c	phase a	phase b	phase c
N3	124.9	159.6	145.8	296.7	326.4	332.3
N4	138.0	176.4	161.1	316.5	348.1	354.5
N5	70.7	90.4	82.5	158.4	174.2	177.4
N6	187.4	239.4	218.6	593.4	652.8	664.6
N7	40.6	51.9	47.4	118.8	130.7	133.1
N8	121.8	155.6	142.1	237.4	261.1	265.9
N9	34.1	43.6	39.8	79.2	87.1	88.7
N10	86.1	110.0	100.4	158.2	174.1	177.2
N11	34.1	43.6	39.8	118.8	130.7	133.1
N13	35.8	45.7	41.7	59.4	65.3	66.5
N14	32.5	41.6	37.9	59.4	65.3	66.5
N15	28.5	36.4	33.2	79.2	87.1	88.7
N16	150.2	192.0	175.3	395.6	435.2	443.1
N17	109.6	140.1	127.9	316.5	348.1	354.5
N18	295.5	331.3	317.0	297.0	326.7	332.6
N19	142.0	181.5	165.7	0.0	0.0	0.0
N20	169.5	216.6	197.7	0.0	0.0	0.0
N21	860.4	914.2	892.6	0.0	0.0	0.0
N23	290.3	370.9	338.6	0.0	0.0	0.0
N24	96.9	123.8	113.0	33.0	36.3	37.0
N25	129.1	165.0	150.7	49.5	54.5	55.4
N26	189.2	241.7	220.7	65.9	72.5	73.9
N27	1029.9	1130.7	1090.4	395.6	435.2	443.1
N28	1220.3	1327.8	1284.8	263.7	290.1	295.4
N29	217.7	278.2	254.0	0.0	0.0	0.0
N30	241.2	308.2	281.4	0.0	0.0	0.0
N31	241.9	309.1	282.2	0.0	0.0	0.0
N32	111.3	142.2	129.8	263.7	290.1	295.4
TOT	6429.4	7567.2	7112.0	4356.0	4791.6	4878.7

Table 5.2: Load and generation rated power per phase in the LV network [kVA].

Bus	**Load**			**Generation**		
	phase a	phase b	phase c	phase a	phase b	phase c
N3	20	15	20	20	0	0
N4	11	20	25	50	50	50
N5	15	17	20	0	0	0
N6	14	16	10	0	0	0
N7	15	20	30	16	0	0
N8	20	16	25	20	10	0
N9	15	18	20	0	0	10
TOT	110	122	150	106	60	60

5.4 Case study application

In the following, the aggregated DMS operation is studied in two scenarios, each referring to a particular working condition of the distribution network. Since the entire generated power in this network comes from photovoltaic (PV) generators, the daily peak production period is expected to be around h. 12, while it is supposed to be null during the evening and night. Contextually, the power absorbed by loads is expected to be relatively low at mid-day and high later in the day, according to the typical residential daily power profile shown in the previous chapters. With these hypothesis, the simulation scenarios identify two loading conditions characterized by different percentage of the total installed load and generation power on the MV network, listed in Table 5.1, i.e.:

- **Scenario A:** high generation (95%) and low load (40%);
- **Scenario B:** null generation combined with high load (80%).

In this study case, the aggregated DMS is applied to the network to address the voltage regulation problem enabling the exploitation of all the resources. For each area, a pilot bus is identified as the one with the worst voltage condition (under- or over-voltage), allowing the Network Supervisor to evaluate the $\Delta V_{set-point}$ value to be sent to each LVNC belonging to the identified regulation area; the latter in turn will forward the set-point to the downstream inverters which will finally perform local Volt/Var regulation.

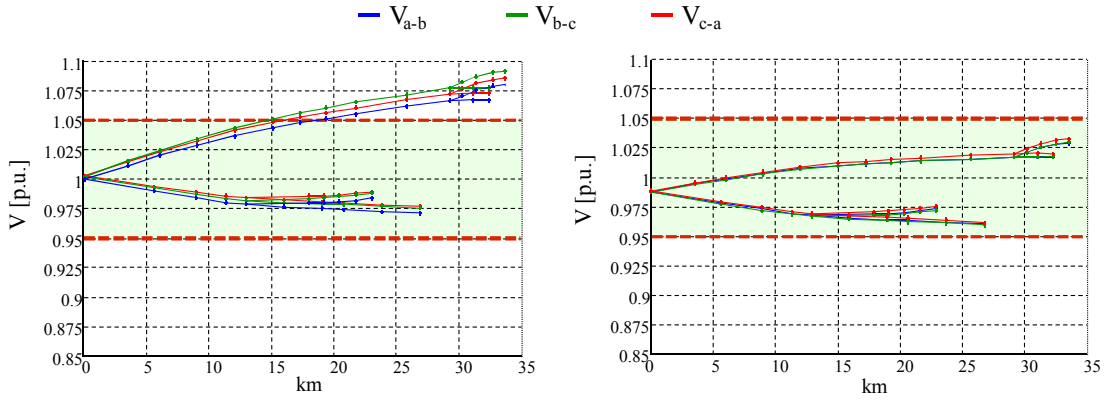

Figure 5.5: MV busbars line-line voltage in Scenario A without regulation (a) and with the aggregated DMS (b).

Figure 5.5 shows the line-line voltage profiles in the 2 MV feeders of the case study network in Scenario A, without any regulation and considering the aggregated DMS action.

As could be seen from the voltage trends in Figure 5.5a, a high power injection by the DGs connected to feeder A results in bus voltages rising above the objective level, so, even though the OLTC is operated in AVR mode keeping the MV main busbar voltage close to 1 p.u, the maximum deviation is around $+8\%(V_n)$. On the other hand, in feeder

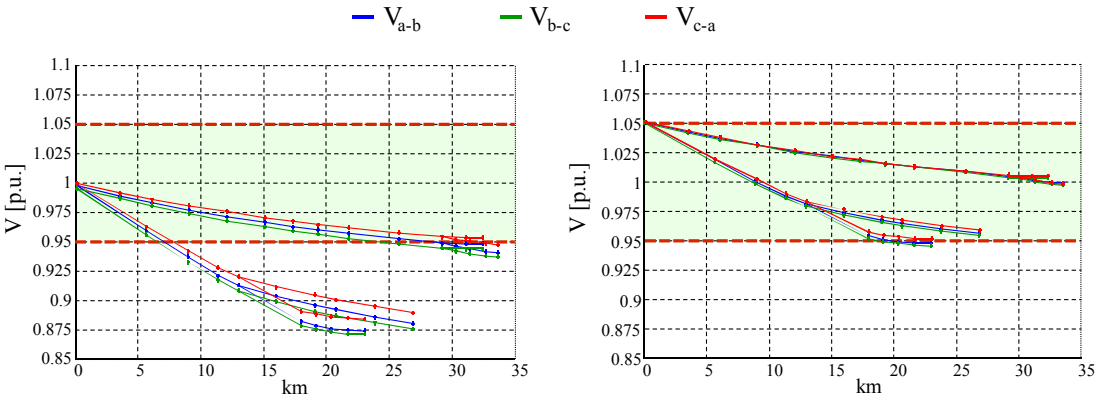

Figure 5.6: MV busbars line-line voltage in Scenario B without regulation (a) and with the aggregated DMS (b).

B, having a lower penetration of DGs, load and generation almost balance, leading to a maximum voltage deviation of around -2.5%(V_n). Under these working conditions, the DMS estimates for the OLTC a voltage reference value of 0,99 p.u., which slightly reduces the voltage deviation on feeder A without depleting feeder B bus voltages.

Subsequently, since a further voltage regulation is needed besides the coordinated OLTC action, five regulation areas are identified and pictorially represented in Figure 5.3. In Table 5.3 these areas are reported together with the corresponding pilot bus whose voltage magnitude is used for determining the requirement for the specific area. Since the set point variation is zero when the pilot bus voltage lays within the $\pm 5\%(V_n)$ objective band, from Table 5.3 it clearly appears that among the five identified regulating areas only the LVNCs belonging to Area 1 and 3 are called to participate in the MV voltage level regulation. This can be also appreciated by the reactive power exchange reported in Table 5.3, showing that only the areas involved in the MV regulation provide a sensible reactive power exchange with the network, distinguished from the other areas contribution, required for the sole voltage unbalance correction action.

In Scenario B, both feeders are characterized by a heavy load condition since in both feeders the PV plants are not producing, as in a typical condition happening during the evening hours with high residential load. As a result, the MV buses voltage drops well beyond the objective of -5%(V_n) especially in feeder B, even with the AVR operation of the OLTC in PS. In this case the DMS estimates for the OLTC a value of 1,05 p.u. as reference voltage, in order to maximize the support to the regulation, reaching the +5%(V_n) allowed deviation, so depleting the range for additional tap changes. Four regulating areas are identified by the DMS, only two of them requiring regulation. From figure 5 it may also be noted that for the line-line voltages, visibly unbalanced in the unregulated scenario, after the DMS coordinated action (areas selection and voltage set-point signals) including the LV regulation (actuating the local voltage control with the set-point received and concurrently providing the currents balancing), a sensible unbalance reduction is achieved.

Table 5.3: Aggregated DMS simulation results for the two scenarios A and B.

Scenario	**OLTC**		**Adaptive Area Coordination**				**LV Regulation**		
	V_{ref} [pu]	Tap Position	Areas	Pilot Bus	Pilot Bus Voltage [pu] OLTC AVR	OLTC Coord	ΔV_{set} [pu]	ΔQ [kVAr]	ΔLosses [%]
A	0.99	1	A1: N12, N13, N14, N15, N16, N17, N18	N18	1,087	1.073	0,033	-612.973	+15.45%
			A2: N23, N24, N25, N26, N27	N27	0,976	0.962	0	-0.131	
			A3: N5, N6, N7, N8, N9, N10, N11	N11	1,068	1.054	0,014	-228.064	
			A4: N20, N21, N22, N28, N29, N30, N31, N32	N22	0.983	0.969	0	-0.079	
			A5: N2, N3, N4, N19.	N4	1,024	1.010	0	-0.077	
B	1.05	-5	A1: N2, N19, N20, N21, N22, N23, N24, N25, N26, N27	N27	0.885	0.941	-0,019	184.115	-8.25%
			A2: N8, N9, N10, N11, N12, N13, N14, N15, N16, N17, N18	N18	0.944	0.996	0	-0.346	
			A3: N3, N4, N5, N6, N7	N7	0.968	1.019	0	-0.155	
			A4: N28, N29, N30, N31, N32	N28	0.886	0.942	-0,018	130.583	

Chapter 6

Conclusions

Due to renewable energy policies and technology improvements, distributed generators or, in general, active users penetration is continuously growing in distribution networks, in certain cases even overcoming the amount expected for 2020. In this context, by continuing relying on the *fit and forget* approach, distribution systems are likely to experience contingencies possibly leading to the loss of service if Distribution System Operators (DSO) don't operate infrastructure reinforcement investments. To face issues like voltage deviations, fault detection failure or undesired islanded operation, several standard bodies both national and international have updated their connection rules for generators, pursuing a more responsive behaviour of the distributed sources which are now required to provide some services for grid support.

Taking into account the mentioned issues and the actions that are being taken from the regulatory point of view, the importance of analysing in detail the active distribution networks in order to study those effects is becoming fundamental. Relying on simulation tools that allow a complete representation of the distribution system (including both Medium Voltage and Low Voltage levels at the same time), the consequences of the evolution trends for the Distributed Energy Resources (DER) may be suitably evaluated in order to propose innovative solutions.

Several research works in literature emphasized the fact that distribution networks' Hosting Capacity may be sensibly enhanced by integrating the active users in the network's management, exploiting the closeness between sources and loads. On this topic, two main approaches are proposed in literature differing by the fact that the DERs control is centralised or decentralised. In the first case a central unit dispatches the set-points for the DERs operation pursuing the minimization of an objective function describing a particular feature to be optimized (e.g. energy losses, voltage deviations, current flows) considering a cost associated to each action. The second approach deals with the network management considering cells within the distribution grid in which the active users are clustered to form several *agents*, each reacting on a local basis to signals coordinated by a supervisor.

This thesis is composed by three main topics, relating respectively to:

- Power system modelling with a generalized approach to represent any number of phases, even in the same system simultaneously;
- Medium Voltage (MV) network's management through a decentralised approach involving DERs to the regulation with suitable request signals forwarded to dynamically defined areas;
- Low Voltage (LV) network's management through a central unit coordinating the active users connected downstream the Secondary Substation pursuing the voltage unbalance mitigation and ancillary services provision to the upstream MV network.

6.1 Results

The first research activity line focused on the study of the power flow problem, with specific attention to multi-phase approaches. Starting from the methods proposed in literature, a multi-conductor algorithm was developed adopting an admittance matrix representation similar to the approach used for the Gauss Z_{Bus} method. In this way, a detailed modelling of the network is possible, including virtually any number of phases to be represented.

In chapter 2, the modelling approach for the network's components is discussed. Lines have been modeled following the Carson-Clem criteria, which was initially adopted in the study of electromagnetic coupling among the phases in a n-phase power line. Loads and generators or, in general, shunt elements are represented through the ZIP model, considering respectively constant-impedance, constant-current and constant-power parts. The peculiarity of the developed method is that the rated power exchanged by the shunt elements is obtained through suitable constant admittance terms added to the overall system's admittance matrix, while their actual operating set-point is changed according to the voltage dependency by varying a correction current which is injected to the respective node (i.e. the phase terminal at the connection bus). With this feature, an algorithm iterates the correction currents update in order to evaluate the actual phase-voltages at each bus.

Particular attention has been reserved to the transformer modelling, which is a challenging task when dealing with multi-phase approaches. The method proposed in section 2.3 formalizes an approach enabling the representation of basically any kind of connection among multiple buses each with any number of phases, even different from one side to another. This feature has been fully detailed given the importance of including the transformer in a multi-conductor analysis tool in order to fully represent a distribution system composed by different voltage levels.

The developed approach for multi-conductor analysis has been applied in several case studies also resulting from the cooperation with other Institutions. The first application

is the representation of a real Low Voltage distribution network in the city of Dublin involving both three-phase and single-phase branches and multiple grounding points (along the feeder and at the customers' interface), also including DGs penetration. The second application involved both a modelling effort and a control one, aiming at managing the LV network PCC's phase voltages with a Phase-Decoupled On-Load-Tap-Changer transformer. This device, supposed to vary the tap position of a MV/LV transformer's OLTC independently on the three phases to control the voltage magnitude at a certain bus of the network, has been initially represented and simulated in steady-state conditions over a 24-hours period through the model previously recalled, then validated through RMS-dynamics simulations and finally tested experimentally.

The second research activity regarded the proposal of a strategy for the Medium Voltage distribution network's regulation under the hypothesis of a fully developed smart grid with presence of a reliable communication infrastructure and smart metering. For the scope, a control procedure, discussed in chapter 3, has been developed adopting the decentralised approach to allow the inclusion of DERs in the network's management through the communication of suitable signals to areas identified clustering buses on the basis of their mutual electrical coupling and actual operative conditions. Once the network is divided into subsystems (i.e. clusters of buses) a Network Supervisor (NS) elaborates the requests in terms of active and reactive power variations to be forwarded to each group pursuing the currents and voltage regulation (i.e. to solve congestions and under- or over-voltage contingencies). The Primary Substation's OLTC is also involved in the regulation scheme, being suitably coordinated by the NS receiving remote voltage measurements thus updating the tap position to reduce the overall voltage deviations. After the optimization of the OLTC's tap position, power variation requests coupled with an offered price are sent to each cluster, in which the active users decide to participate or not based on their own convenience respect to a local cost set for each time instance.

This control strategy was firstly developed within the Italian research project ATLANTIDE, aimed at establishing a digital archive for Italian reference distribution networks, produce models for the network components and proposing active management systems for the users' integration in the network regulation. The above mentioned procedure is one of the two Active Management strategies (the other one being a centralised DMS for power flow optimization) proposed in the project and it was developed to simulate the grid's operation under different load and generation scenarios by setting power profiles enabling long-term analysis. An example of these analysis is reported in section 3.6.2 applied to one of the reference distribution networks defined in the project. This control has also been proposed as part of a cooperative centralised and decentralised Energy Management System in which an optimal scheduling of active and reactive power set-points was made by a centralised DMS while the decentralised DMS was employed to fix the contingencies occurring due to unexpected perturbations on the scheduled profiles. A further application of the decentralised DMS has been presented as a way to coordinate

the contributions coming from the DERs with the aim of evaluating the ancillary services that may be provided to the Transmission System Operator running the bulk grid regulation and the relative cost, based on the demand-offer approach on which the control is based.

The third research activity has been conducted to study the coordination of inverter-interfaced users connected to Low Voltage distribution networks. A control strategy for LV systems has been proposed in chapter 4 involving a central unit, called Low Voltage Network Supervisor (LVNC) calculating the requirements for generators connected to the distribution system pursuing two objectives: the voltage unbalance mitigation at a certain bus (usually the PCC being the LV main busbar in Secondary Substation) and the provision of ancillary services to the MV network. Standing the latest updates in the rules for the connection of Distributed Generators to LV systems, firstly an investigation about the effects of different local Volt/Var controls has been conducted. The coordinated control has been simulated along with the local Volt/Var action performed by DGs as a way to suitably configure the reactive power provision on the phases pursuing the voltage unbalance mitigation and thus reducing the magnitude deviations at the LV buses. The control has been firstly simulated in steady-state conditions (applying the algorithm developed in the first activity line) and then verified through RMS-dynamics simulations with the software DigSilent PowerFactory. The contribution by DGs has been investigated over a 24-hour time horizon separating the contributions for the different services: reactive power provision as function of the sole local voltage, reactive power provision service for voltage unbalance mitigation, fully coordinated control including active power redistribution on the phases acted by three-phase (plus neutral) inverters.

Finally, the three research activity lines converged to a common objective which was the complete representation of the distribution system, including both MV and LV stages, with the adoption of a common DMS including a Network Supervisor at Primary Substations level providing the request signals to each MV-buses cluster and several Secondary Substation feeding LV networks in which the active users are coordinated by the respective LVNC. An application proposing an aggregate DMS managing both MV and LV levels has been presented in chapter 5 for the voltage regulation in the distribution system considering the local Volt/Var control applied by the inverters, coordinated through suitable voltage set-point and reactive power variation signals to pursue both the unbalance mitigation effect on the LV system and the voltage deviation regulation on the MV side.

6.2 Perspectives for future research

Based on the results obtained from the research conducted so far and discussed in this thesis, some interesting perspectives are left for future research activity on the topic.

For instance, regarding the multi-phase representation and simulation of the network, the formalization of a generalized approach to model the transformers could allow some

further investigations on the use of particular connection options to deal with power quality issues or analysis.

From the network's management point of view, the cooperative control in MV and LV networks may be exploited to study the possible implementation of local markets for the provision of ancillary services not only from distributed generators but from active demand too. In this context, scenarios in which the active users participate to the grid management may be studied proposing suitable local costs in order to evaluate the impact that these sources may have on the ancillary services market.

With the strategies proposed in this thesis, a complete coordination of the distribution network may be considered, envisaging a *smart grid* future scenario, for instance involving the presence of electrical vehicles providing Vehicle-to-Grid (V2G) services or the connection of Energy Storage Systems (ESS) to the distribution network. In the perspective of including such storage capable units, a multi-period analysis should necessarily be considered in order to suitably exploit those resources.

6.3 List of publications

The research activity discussed in the previous chapters and recalled in section 6.1 led to several international conference publications and journal papers, as listed below.

Journal papers

[J.1] R. Caldon, M. Coppo, and R. Turri, "Distributed voltage control strategy for lv networks with inverter-interfaced generators," *Electric Power Systems Research*, vol. 107, p. 85, 2014.

[J.2] M. Coppo, P. Pelacchi, F. Pilo, G. Pisano, G. Soma, and R. Turri, "The italian smart grid pilot projects: Selection and assessment of the test beds for the regulation of smart electricity distribution," *Electric Power Systems Research*, vol. 120, pp. 136–149, 2015.

[J.3] K. Sunderland, M. Coppo, M. Conlon, and R. Turri, "A correction current injection method for power flow analysis of unbalanced multiple-grounded 4-wire distribution networks," *Electric Power Systems Research*, vol. 132, pp. 30–38, 2016.

[J.4] J. Hu, M. Marinelli, M. Coppo, A. Zecchino, and H. W. Bindner, "Coordinated voltage control of a decoupled three-phase on-load tap changer transformer and photovoltaic inverters for managing unbalanced networks," *Electric Power Systems Research*, vol. 131, pp. 264–274, 2 2016.

Peer reviewed conference papers

[C.1] A. Bracale, R. Caldon, G. Celli, M. Coppo, D. D. Canto, R. Langella, G. Petretto, F. Pilo, G. Pisano, D. Proto, S. Scalari, and R. Turri, "Analysis of the italian distribution system evolution through reference networks," in *Innovative Smart Grid Technologies (ISGT Europe), 2012 3rd IEEE PES International Conference and Exhibition on*, 2012, pp. 1–8.

[C.2] A. Bracale, R. Caldon, M. Coppo, D. Dal Canto, R. Langella, G. Petretto, F. Pilo, G. Pisano, D. Proto, S. Ruggeri, S. Scalari, and R. Turri, "Active management of distribution networks with the atlantide models," in *Power Generation, Transmission, Distribution and Energy Conversion (MEDPOWER 2012), 8th Mediterranean Conference on*, Oct 2012, pp. 1–7.

[C.3] R. Caldon, M. Coppo, M. Tessari, and R. Turri, "Use of single-phase inverter-interfaced dgs for power quality improvement in lv networks," in *Proceedings of the Universities Power Engineering Conference*, 2012, pp. 1–5.

[C.4] R. Caldon, M. Coppo, and R. Turri, "Voltage unbalance compensation in lv networks with inverter interfaced distributed energy resources," in *Energy Conference and Exhibition (ENERGYCON), 2012 IEEE International*, 2012, pp. 527–532.

[C.5] R. Caldon, M. Coppo and R. Turri, "A network voltage control strategy for lv inverter interfaced users," in *Power Generation, Transmission, Distribution and Energy Conversion (MEDPOWER 2012), 8th Mediterranean Conference on*, 2012, pp. 527–532.

[C.6] R. Caldon, M. Coppo, R. Sgarbossa, and R. Turri, "A simplified algorithm for oltc control in active distribution mv networks," in *AEIT Annual Conference, 2013*. IEEE, 2013, pp. 1–6.

[C.7] R. Caldon, M. Coppo, A. Raciti, R. Sgarbossa, and R. Turri, "Modeling the control of islanded networks supplied by inverters: The case of mv and lv systems," in *AEIT Annual Conference, 2013*. IEEE, 2013, pp. 1–5.

[C.8] K. Sunderland, M. Coppo, M. F. Conlon, and R. Turri, "Application of a correction current injection power flow algorithm to an unbalanced 4-wire distribution network incorporating tn-c-s earthing," in *Power Engineering Conference (UPEC), 2013 48th International Universities'*, 2013, pp. 1–6.

[C.9] R. Caldon, M. Coppo, R. Sgarbossa, L. Sgarbossa, and R. Turri, "Risk of unintentional islanding in lv distribution networks with inverter-based dgs," in *Power Engineering Conference (UPEC), 2013 48th International Universities'*. IEEE, 2013, pp. 1–6.

[C.10] R. Caldon, M. Coppo, A. Raciti, and R. Turri, "Dynamic control of inverter-connected generators for intentionally islanded mv distribution networks," in *Power Engineering Conference (UPEC), 2013 48th International Universities'*. IEEE, 2013, pp. 1–6.

[C.11] F. Pilo, G. Pisano, S. Ruggeri, S. Scalari, D. D. Canto, G. Petretto, A. Testa, R. Langella, L. Feola, R. Caldon, R. Turri, and M. Coppo, "Applications of dms in the atlantide project: Models and tools," in *Electricity Distribution (CIRED 2013), 22nd International Conference and Exhibition on*, 2013, pp. 1–5.

[C.12] R. Caldon, M. Coppo, D. Dal Canto, G. Gigliucci, L. Feola, R. Langella, F. Pilo, G. Petretto, G. Pisano, S. Ruggeri, A. Testa, and R. Turri, "Application of atlantide models to harmonic penetration studies," in *2013 4th IEEE/PES Innovative Smart Grid Technologies Europe, ISGT Europe 2013*, 2013.

[C.13] R. Caldon, M. Coppo, and R. Turri, "Coordinated voltage control in mv and lv distribution networks with inverter-interfaced users," in *2013 IEEE Grenoble Conference PowerTech, POWERTECH 2013*, 2013, pp. 1–5.

[C.14] M. Coppo, R. Turri, M. Marinelli, and X. Han, "Voltage management in unbalanced low voltage networks using a decoupled phase-tap-changer transformer," in *Power Engineering Conference (UPEC), 2014 49th International Universities*, 2014, pp. 1–6.

[C.15] F. Amadei, A. Cerretti, M. Coppo, P. Mattavelli, R. Sgarbossa, and R. Turri, "Temporary islanding operations of mv/lv active distribution networks under fault conditions," in *Power Engineering Conference (UPEC), 2014 49th International Universities*. IEEE, 2014, pp. 1–6.

[C.16] R. Caldon, M. Coppo and R. Turri, "Distributed active network management strategy including dg and storage systems," in *AEIT Annual Conference 2014*. IEEE, 2014, pp. 1–6.

[C.17] F. Pilo, M. Coppo, G. Pisano, G. Soma, and R. Turri, "Cooperative centralised and decentralised energy management systems for active networks," in *Electricity Distribution (CIRED 2015), 23nd International Conference and Exhibition on*, 2015.

[C.18] R. Caldon, M. Coppo, A. Raciti, and R. Turri, "Exploiting inverter-interfaced dg for voltage unbalance mitigation and ancillary services in distribution systems," in *1st International Forum on Research and Technologies for Society and Industry (RTSI)*. IEEE, 2015.

[C.19] A. Zecchino, M. Marinelli, M. Coppo, J. Hu, and R. Turri, "Voltage and reactive power control in an unbalanced active low voltage grid using a decoupled phase on-load-tap-changer transformer and photovoltaic inverters," in *Power Engineering Conference (UPEC), 2015 50th International Universities'*. IEEE, 2015.

Appendix A

Dublin city LV network

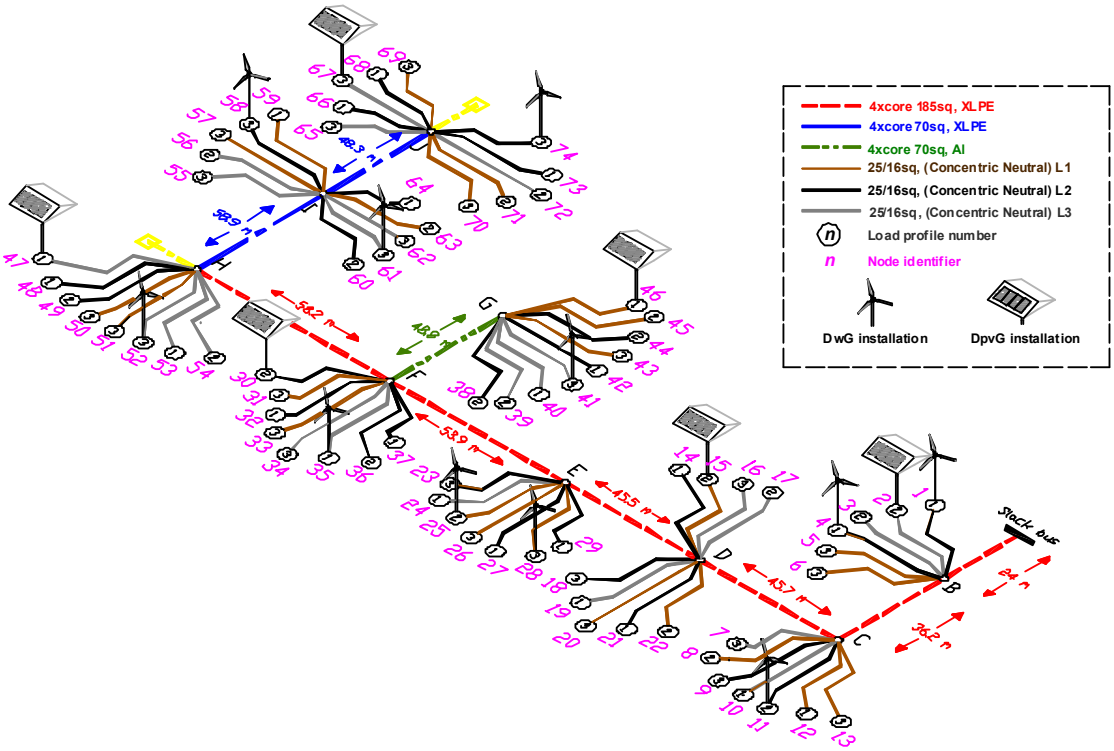

Figure A.1: Layout of the Dublin LV network.

Table A.1: Cables data in the Dublin LV network.

Wire Type	Section [mm²]	d [mm]	GMR [mm]	Rc [ohm]	g [S]	Imax [A]
1	185	15.730	6.125	0.212	0	330
2	70	10.250	3.991	0.569	0	240
3	70	9.860	3.839	0.507	0	260
4	25	5.580	2.173	1.180	0	140
5	16	4.880	1.900	1.120	0	140

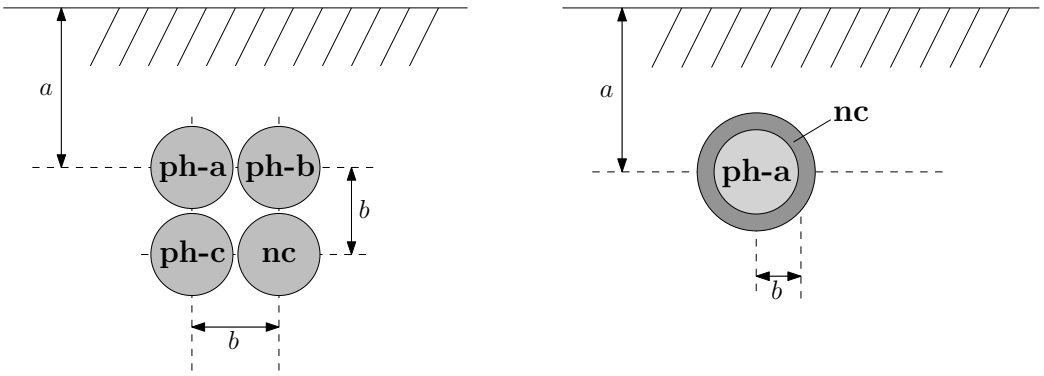

(a) (b)

Figure A.2: Cable disposition for three-phase (a) and Concentric-Neutral single-phase (b) lines in the Dublin LV network.

Table A.2: Line configurations in the Dublin LV network.

Configuration	phase n.	phase cable type	neutral cable type	a [cm]	b [cm]
185mm^2 XLPE	3	1	1	100	1.655
70mm^2 XLPE	3	2	2	100	1.070
70mm^2 NAKBA	3	3	3	100	1.070
25/16mm^2 C-N	1	4	5	100	0.280

Table A.3: Lines data in the Dublin LV network.

From-Bus	To-Bus	Line Type	Length [km]
A	B	2	0.024
B	C	2	0.0362
C	D	2	0.0457
D	E	2	0.0455
E	F	2	0.0589
F	G	3	0.0488
F	H	2	0.0582
H	I	1	0.0589
I	J	1	0.0483
B	1	4	0.0127
B	2	4	0.0581
B	3	4	0.0394
B	4	4	0.0556
B	5	4	0.0445
B	6	4	0.0091
C	7	4	0.02
C	8	4	0.0259
C	9	4	0.0397
C	10	4	0.0203
C	11	4	0.0248
C	12	4	0.0344
C	13	4	0.0399
D	14	4	0.0225
D	15	4	0.0221
D	16	4	0.0212
D	17	4	0.0348
D	18	4	0.0252
D	19	4	0.0371
D	20	4	0.0406
D	21	4	0.0343
D	22	4	0.0376
E	23	4	0.0362
E	24	4	0.0231
E	25	4	0.0349
E	26	4	0.0392
E	27	4	0.0208
E	28	4	0.0231
E	29	4	0.0238
F	30	4	0.0357
F	31	4	0.0345
F	32	4	0.0374
F	33	4	0.0229
F	34	4	0.0201
F	35	4	0.0258
F	36	4	0.023
F	37	4	0.0393
G	38	4	0.0221
G	39	4	0.0396
G	40	4	0.0557
G	41	4	0.0396
G	42	4	0.0245
G	43	4	0.0214
G	44	4	0.0265
G	45	4	0.0374
G	46	4	0.0354
H	47	4	0.0199
H	48	4	0.0226
H	49	4	0.0214
H	50	4	0.0366
H	51	4	0.0287
H	52	4	0.0397
H	53	4	0.0357
H	54	4	0.0453
I	55	4	0.0295
I	56	4	0.0312
I	57	4	0.0348
I	58	4	0.0285
I	59	4	0.0272
I	60	4	0.0348
I	61	4	0.0254
I	62	4	0.0298
I	63	4	0.038
I	64	4	0.0304
J	65	4	0.0226
J	66	4	0.0377
J	67	4	0.0473
J	68	4	0.0354
J	69	4	0.0414
J	70	4	0.0431
J	71	4	0.0344
J	72	4	0.0205
J	73	4	0.0212
J	74	4	0.0243

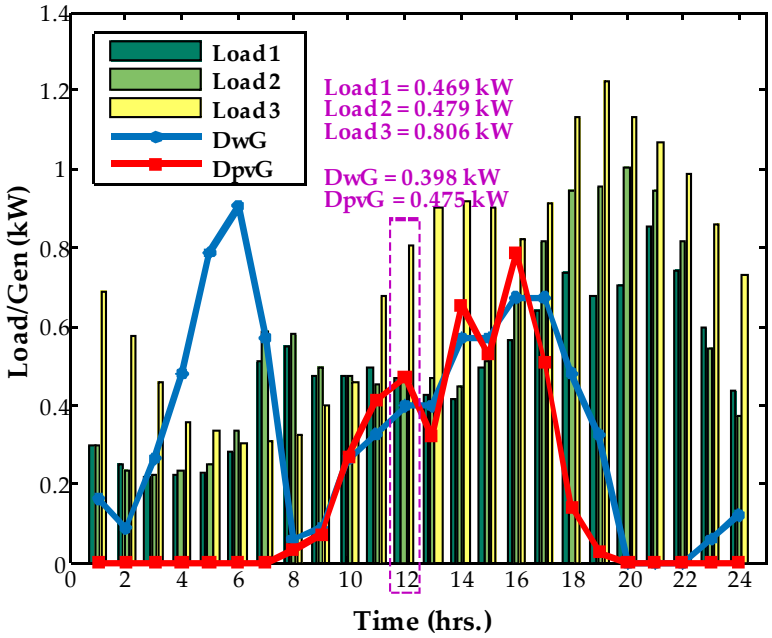

Figure A.3: Daily power profiles for load and generation in the Dublin LV network. Values for the h.12 time instance are highlighted.

Appendix B

Danish LV network

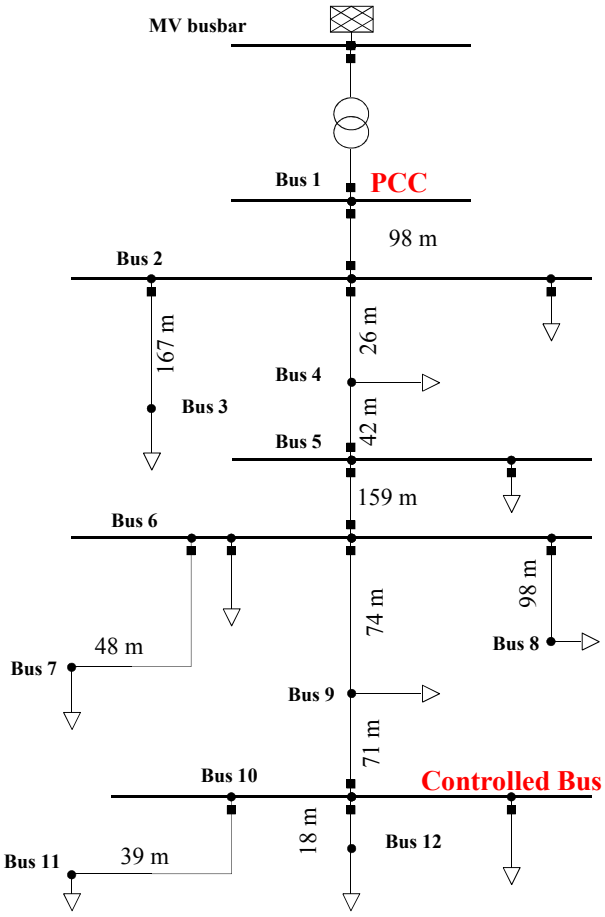

Figure B.1: Layout of the Danish LV network.

Table B.1: Transformer's data in the Danish LV network.

V_{1n} [kV]	V_{2n} [kV]	S_n [kVA]	v_{cc} [%]	p_{cc} [%]
10	0.4	300	4	0.5

Table B.2: OLTC data in the Danish LV network.

Operation	ΔV_{step} [pu]	DB [pu]	$step_{max}$	$step_{min}$
Discrete	0.0250	±0.0200	+2	-2
Continuous	0.0010	±0.0025	+50	-50

Table B.3: Line types' data in the Danish LV network.

Type	Material	Section [mm^2]	r [Ω/km]	x [Ω/km]	c [μF/km]
1	Al	240	0.127	0.077	0.730
2	Al	150	0.207	0.077	0.580
3	Al	150	0.207	0.053	0.580
4	Al	95	0.321	0.054	0.480

Table B.4: Lines data in the Danish LV network.

From-N	To-N	Line Type	Length [km]
Bus 1	Bus 2	3	98
Bus 2	Bus 3	2	167
Bus 2	Bus 4	2	26
Bus 4	Bus 5	1	42
Bus 5	Bus 6	1	159
Bus 6	Bus 7	4	98
Bus 6	Bus 8	4	20
Bus 6	Bus 9	2	74
Bus 9	Bus 10	2	71
Bus 10	Bus 11	2	39
Bus 10	Bus 12	2	18

Table B.5: Load peak power per phase (p.f.=0.9) [kW]

Bus	phase a	phase b	phase c
Bus 2	3.0	3.0	6.3
Bus 3	5.6	2.0	5.1
Bus 4	2.0	5.1	2.0
Bus 5	2.0	2.9	2.3
Bus 6	2.0	6.3	2.0
Bus 7	2.0	5.3	2.0
Bus 8	5.6	2.8	2.0
Bus 9	3.0	2.1	2.0
Bus 10	6.2	2.7	2.0
Bus 11	4.4	5.7	5.3
Bus 12	2.5	2.0	4.6

Appendix C

Reference Italian MV distribution network (industrial context)

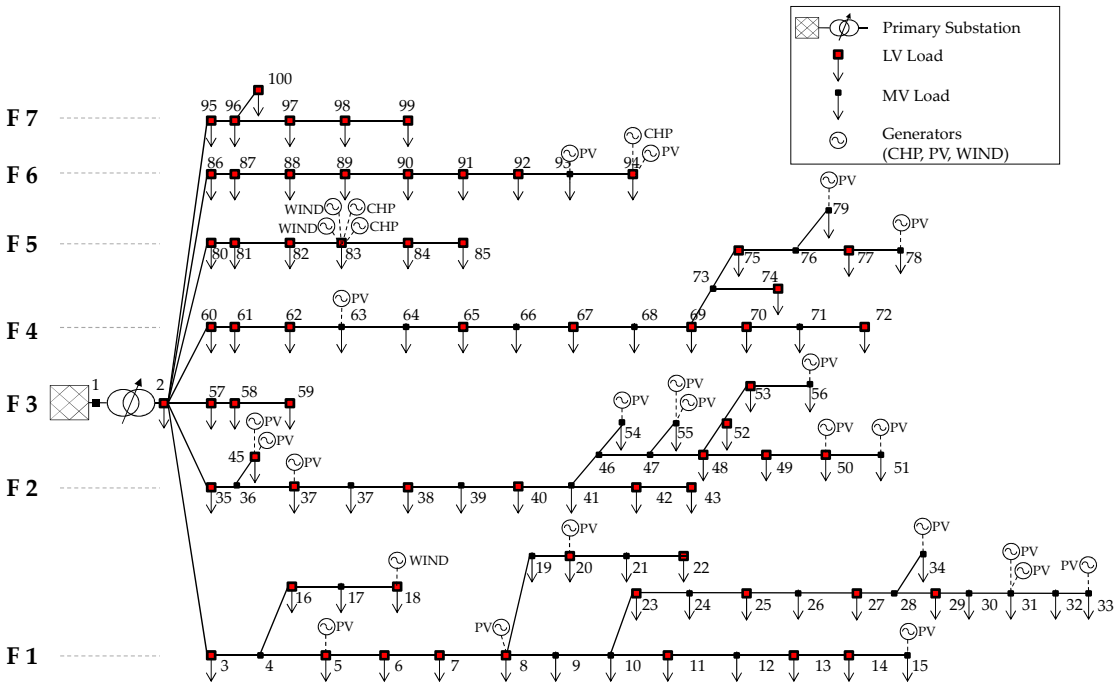

Figure C.1: Single-line diagram of the clustered industrial reference network.

Table C.1: Transformer's data for the MV reference network.

V_{1n} [kV]	V_{2n} [kV]	S_n [MVA]	v_{cc} [%]	p_{cc} [%]	dU [%]	DB [%]	Tap range
127.0	16.2	25	11.11	0.43	1.67	1.5	± 10

Table C.2: Line types' data in the MV reference network.

Type	V_n [kV]	r [Ω/km]	l [mH/km]	c [nF/km]	I_{max} [A]
OC AL 150mm^2-340	15	0.134	0.456	282.942	340.00
OC AL 35mm^2-140	15	0.859	0.456	169.765	140.00
OH AL 20mm^2-100	15	1.211	1.262	8.758	100.00
OH CU 16mm^2-105	15	1.117	1.335	7.879	105.00
OH CU 20mm^2-120	15	0.870	1.321	7.860	120.00
OH CU 25mm^2-140	15	0.733	1.288	7.948	140.00
OH CU 45mm^2-218	15	0.399	1.236	8.882	217.50
OH CU 63mm^2-270	15	0.285	1.194	8.960	270.00
OH CW 25mm^2-93	15	1.901	1.301	8.017	93.00
OH LA 35mm^2-140	15	0.931	1.234	9.138	140.00
UC AL 120mm^2-260	15	0.225	0.716	396.119	260.00
UC AL 150mm^2-240	15	0.207	0.274	360.016	240.00
UC AL 150mm^2-280	15	0.214	0.409	420.371	280.00
UC AL 185mm^2-330	15	0.164	0.367	449.979	330.00
UC AL 240mm^2-360	15	0.126	0.334	499.994	360.00
UC AL 70mm^2-180	15	0.450	0.477	320.668	180.00
UC AL 95mm^2-190	15	0.323	0.284	299.751	190.00
UC CU 25mm^2-128	15	0.929	0.682	215.575	127.79
UC CU 40mm^2-154	15	0.450	0.295	239.669	154.00

Table C.3: Lines data in the MV reference network.

From-Bus	To-Bus	Line Type	Length [km]
N 002	N 003	UC AL 185 330	1.74
N 002	N 035	UC AL 185 330	2.518
N 002	N 057	UC AL 185 330	0.35
N 002	N 060	UC AL 240 360	1.49
N 002	N 080	UC AL 185 330	2.07
N 002	N 080	UC AL 185 330	2.07
N 002	N 086	UC AL 185 330	1.66
N 002	N 095	UC AL 150 240	0.917
N 003	N 004	OC AL 150 340	0.08
N 004	N 005	OC AL 150 340	0.511
N 004	N 016	OH CU 45 218	1.011
N 005	N 006	UC AL 185 330	0.762
N 006	N 007	UC AL 185 330	0.6
N 007	N 008	UC AL 185 330	3.72
N 008	N 009	UC AL 185 330	0.22
N 008	N 019	UC AL 240 360	0.426
N 009	N 010	UC AL 185 330	0.32
N 010	N 011	OH CU 16 105	0.59
N 010	N 023	UC AL 185 330	0.39
N 011	N 012	OH CU 16 105	1.49
N 012	N 013	OH CU 16 105	0.32
N 013	N 014	OH CU 16 105	0.37
N 014	N 015	OH CU 16 105	0.28
N 016	N 017	UC AL 120 260	0.468
N 017	N 018	UC AL 120 260	0.477
N 019	N 020	UC AL 240 360	0.742
N 020	N 021	UC AL 95 190	0.506
N 021	N 022	OH CU 16 105	0.19
N 022	N 032	OH CU 16 105	0.45
N 023	N 024	OH LA 35 140	0.559
N 024	N 025	OH CU 16 105	0.35
N 025	N 026	OH CW 25 93	0.643
N 026	N 027	OH CU 25 140	1.202
N 027	N 028	OH LA 35 140	0.2
N 028	N 029	OH CU 25 140	0.12
N 028	N 034	UC CU 25 128	0.03
N 029	N 030	OH CU 45 218	0.54
N 030	N 031	OH CU 45 218	0.2
N 031	N 032	OH CU 45 218	0.233
N 032	N 033	OH CU 25 140	1.342
N 035	N 036	OH CU 45 218	0.884
N 036	N 037	OH CU 45 218	0.37
N 036	N 045	OH CU 25 140	0.232
N 037	N 038	UC AL 185 330	0.148
N 038	N 039	UC AL 185 330	0.755
N 039	N 040	UC AL 185 330	0.57
N 040	N 041	UC AL 185 330	0.985
N 041	N 042	UC AL 70 180	1.13
N 041	N 046	UC AL 70 180	0.936
N 042	N 043	OH AL 20 100	2.098
N 043	N 044	OH CU 16 105	1.465
N 046	N 047	OH AL 20 100	0.824
N 046	N 054	UC AL 185 330	0.375
N 047	N 048	OH AL 20 100	1.675
N 047	N 055	OH CU 16 105	0.115
N 048	N 049	OH CU 16 105	0.542
N 048	N 052	UC AL 120 260	0.533
N 049	N 050	UC AL 70 180	0.53
N 050	N 051	UC AL 70 180	0.39
N 052	N 012	OH CU 16 105	0.865
N 052	N 053	OH LA 35 140	0.785
N 053	N 056	UC AL 70 180	0.23
N 057	N 058	OH CU 16 105	0.55
N 058	N 059	UC AL 95 190	0.435
N 060	N 061	OH CU 63 270	1.262
N 061	N 062	UC AL 185 330	0.811
N 062	N 063	OH CU 63 270	0.808
N 063	N 064	UC AL 185 330	1.417
N 064	N 065	OH CU 16 105	0.65
N 065	N 066	UC AL 185 330	0.4
N 066	N 067	OH CU 16 105	0.88
N 067	N 068	OH CU 16 105	0.59
N 068	N 069	OH CU 16 105	0.53
N 069	N 070	OH CU 20 120	0.45
N 069	N 073	OH CU 16 105	1.06
N 070	N 071	OH CU 20 120	1.41
N 071	N 072	OH CU 25 140	0.6
N 073	N 074	OH CU 16 105	0.34
N 073	N 075	OH CU 16 105	1.25
N 075	N 076	OH LA 35 140	0.36
N 076	N 077	OH LA 35 140	0.4
N 076	N 079	OC AL 35 140	0.356
N 077	N 078	OH CU 25 140	0.433
N 080	N 081	UC AL 185 330	0.79
N 080	N 081	UC AL 185 330	0.79
N 081	N 082	UC AL 185 330	0.568
N 081	N 082	UC AL 185 330	0.568
N 082	N 083	UC AL 185 330	0.51
N 082	N 083	UC AL 185 330	0.51
N 083	N 084	UC AL 120 260	0.35
N 083	N 091	UC AL 120 260	0.526
N 084	N 085	UC AL 150 240	1.577
N 084	N 099	UC CU 40 154	0.135
N 086	N 087	UC AL 185 330	2.241
N 087	N 088	UC AL 150 240	1.177
N 088	N 089	UC AL 150 280	1.253
N 089	N 090	UC AL 150 280	0.766
N 090	N 091	UC AL 120 260	0.902
N 091	N 092	OH LA 35 140	0.182
N 092	N 093	OH CU 25 140	0.531
N 093	N 094	OC AL 35 140	0.321
N 095	N 096	UC AL 150 240	0.77
N 096	N 097	UC AL 150 280	1.462
N 096	N 100	UC CU 40 154	0.121
N 097	N 098	UC AL 120 260	0.37
N 098	N 099	UC AL 150 240	1.16

Table C.4: Installed load power and respective type in the MV reference network (appearance: *=before 2020; **=after 2020).

Bus	P [MW]	Q [MVAr]	ku	Type
2	0.027	0.013	0.8	RES
3	0.014	0.004	0.8	RES
5	0.298	0.145	1.0	IND
5	0.135	0.065	0.8	RES
6	0.014	0.006	0.8	RES
7	0.451	0.218	1.0	COM
7	0.135	0.065	0.8	RES
8	0.130	0.063	0.8	RES
8	1.901	0.921	1.0	IND
9	0.314	0.152	1.0	COM
10	0.565	0.274	1.0	COM
11	0.302	0.146	0.8	RES
12	0.035	0.017	1.0	COM
13	0.286	0.138	0.8	RES
13	0.104	0.047	1.0	IND
13*	1.300	0.000	1.0	Evs
14	0.243	0.117	0.8	RES
15	0.020	0.010	1.0	COM
15*	1.300	0.000	1.0	Evs
16	0.086	0.042	0.8	RES
17	0.124	0.060	1.0	IND
18	0.630	0.305	1.0	IND
18	0.054	0.009	0.8	RES
19	0.160	0.074	1.0	IND
19	0.473	0.229	1.0	COM
20	0.216	0.105	0.8	RES
20	0.224	0.108	1.0	IND
20	0.013	0.006	1.0	COM
20	0.124	0.057	1.0	IND
20**	2.000	0.000	1.0	Evs
21	0.166	0.080	1.0	IND
21**	2.000	0.000	1.0	Evs
22	0.135	0.064	0.8	RES
22**	2.000	0.000	1.0	Evs
23	0.135	0.065	0.8	RES
24	0.054	0.026	1.0	COM
24	0.042	0.020	1.0	COM
25	0.216	0.105	0.8	RES
26	0.068	0.033	1.0	COM
26	0.136	0.066	1.0	IND
26*	1.000	0.000	1.0	Evs
27	0.149	0.072	0.8	RES
27*	1.300	0.000	1.0	Evs
29	0.135	0.064	0.8	RES
29*	1.000	0.000	1.0	Evs
30	0.056	0.026	1.0	COM
30*	1.000	0.000	1.0	Evs
31	0.016	0.008	1.0	COM
32	0.351	0.152	0.8	RES
33	0.012	0.006	1.0	COM
34	0.098	0.048	1.0	COM
35	0.072	0.035	1.0	COM
35	0.135	0.065	0.8	RES
37	0.149	0.072	0.8	RES
37	0.245	0.119	1.0	IND
38	0.224	0.108	1.0	IND
39	0.240	0.112	1.0	IND
39	0.135	0.065	0.8	RES
39	0.067	0.026	1.0	COM
40	0.200	0.097	1.0	IND
41	0.054	0.026	0.8	RES
42	0.066	0.031	1.0	COM
43	0.186	0.085	0.8	RES
44	0.394	0.191	0.8	RES
44	0.060	0.029	1.0	COM
44	0.060	0.028	1.0	COM
45	0.280	0.136	1.0	IND
45	0.004	0.002	1.0	COM
45	0.135	0.065	0.8	RES
45	0.176	0.065	1.0	IND
48	0.057	0.027	0.8	RES
49	0.321	0.155	1.0	IND
49	0.027	0.013	0.8	RES
50	0.005	0.002	1.0	COM
50	0.014	0.007	0.8	RES
51	0.008	0.004	1.0	COM
52	0.014	0.007	0.8	RES
53	0.011	0.005	0.8	RES
54	0.395	0.191	1.0	IND
55	0.035	0.017	1.0	COM
55	0.451	0.218	1.0	IND
56	0.002	0.001	1.0	COM
57	0.043	0.019	0.8	RES
58	0.244	0.110	0.8	RES
59	0.143	0.064	0.8	RES
60	0.135	0.065	0.8	RES
61	0.243	0.115	0.8	RES
62	0.162	0.078	0.8	RES
63	0.005	0.002	1.0	COM
64	0.672	0.314	1.0	COM
65	0.641	0.294	0.8	RES
66	0.124	0.006	1.0	IND
67	0.054	0.026	0.8	RES
68	0.124	0.060	1.0	IND
69	0.135	0.065	0.8	RES
70	0.303	0.122	0.8	RES
71	0.058	0.028	1.0	COM
72	0.106	0.051	1.0	IND
72	0.206	0.099	0.8	RES
74	0.433	0.203	1.0	COM
75	0.041	0.019	0.8	RES
77	0.027	0.013	0.8	RES
78	0.157	0.076	1.0	IND
79	0.001	0.001	1.0	COM
80	0.135	0.065	0.8	RES
81	0.127	0.061	0.8	RES
81	0.140	0.068	1.0	IND
82	0.075	0.036	1.0	COM
82	0.189	0.092	0.8	RES
83	0.086	0.042	0.8	RES
83	3.150	1.526	1.0	IND
83	3.150	1.526	1.0	COM
84	0.203	0.098	0.8	RES
85	0.235	0.050	0.8	RES
85	0.567	0.275	1.0	IND
85	0.190	0.087	1.0	IND
86	0.086	0.042	0.8	RES
87	0.173	0.084	0.8	RES
88	0.068	0.033	0.8	RES
88	0.280	0.136	1.0	COM
89	0.273	0.132	0.8	RES
89	0.320	0.155	1.0	IND
90	0.068	0.033	0.8	RES
91	0.014	0.004	0.8	RES
92	0.135	0.065	0.8	RES
93	0.005	0.002	1.0	COM
94	0.189	0.072	0.8	RES
94	0.002	0.001	0.8	RES
94	0.080	0.039	1.0	COM
95	0.086	0.042	0.8	RES
96	0.221	0.336	0.8	RES
97	0.572	0.277	0.8	RES
98	0.567	0.275	1.0	COM
99	0.410	0.199	0.8	RES
100	0.608	0.294	1.0	IND
100	0.086	0.042	0.8	RES
100	0.120	0.058	1.0	IND

Table C.5: Installed DGs power and respective type in the MV reference network (appearance: *=before 2020; **=after 2020).

Bus	P [MW]	Q [MVAr]	Type
18	0.7	0	WIND
83	5	0	WIND
83	2.5	0	WIND
83	5	0	CHP
83	2.5	0	CHP
94	0.5	0	CHP
59	10	0	WIND
18	10	0	CHP
85	10	0	WIND
13	5	0	CHP
54	5	0	CHP
58	7	0	WIND
84	8	0	WIND
85	8	0	CHP
84	8	0	WIND
57	8	0	WIND
5	0.385	0	PV
8	1.048	0	PV
15	0.155	0	PV
20	0.340	0	PV
31	0.330	0	PV
31	0.330	0	PV
33	0.935	0	PV
34	0.098	0	PV
37	0.120	0	PV
45	0.220	0	PV
45	0.380	0	PV
50	0.700	0	PV
51	0.266	0	PV
54	0.318	0	PV
55	0.450	0	PV
55	0.110	0	PV
56	0.300	0	PV
63	0.550	0	PV
78	0.049	0	PV
79	0.190	0	PV
93	0.550	0	PV
94	1.000	0	PV
54	0.318	0	PV
15	1.300	0	PV
18	2.100	0	PV
18	0.160	0	PV
30	1.260	0	PV
31	1.730	0	PV
34	0.260	0	PV
55	1.166	0	PV
55	1.200	0	PV
56	0.988	0	PV
71	3.000	0	PV
72	3.000	0	PV
72	2.000	0	PV
78	1.600	0	PV
79	1.000	0	PV
31	5.000	0	PV
51	5.000	0	PV
29	3.000	0	PV
27	4.000	0	PV
14	5.000	0	PV
13	2.000	0	PV
17	3.000	0	PV
49	3.500	0	PV
53	3.000	0	PV
52	2.000	0	PV
44	2.000	0	PV
16	1.000	0	PV
17	3.000	0	PV
18	2.000	0	PV
20	2.500	0	PV
21	1.500	0	PV
22	3.000	0	PV
29	3.000	0	PV
30	3.000	0	PV
31	1.000	0	PV

Table C.6: Daily power coefficients for loads and generators [pu].

Time	RES	IND	COM	Evs	PV	CHP	WIND
00:00	0.252	0.361	0.350	0.920	0.000	0.000	0.700
00:15	0.237	0.402	0.335	0.925	0.000	0.000	0.650
00:30	0.222	0.442	0.320	0.930	0.000	0.000	0.600
00:45	0.212	0.425	0.310	0.928	0.000	0.000	0.525
01:00	0.202	0.407	0.300	0.925	0.000	0.000	0.450
01:15	0.197	0.413	0.290	0.913	0.000	0.000	0.456
01:30	0.192	0.418	0.280	0.900	0.000	0.000	0.462
01:45	0.187	0.445	0.280	0.900	0.000	0.000	0.479
02:00	0.181	0.472	0.280	0.900	0.000	0.000	0.495
02:15	0.176	0.437	0.290	0.900	0.000	0.000	0.468
02:30	0.171	0.401	0.300	0.900	0.000	0.000	0.440
02:45	0.181	0.456	0.315	0.900	0.000	0.000	0.468
03:00	0.192	0.511	0.330	0.900	0.000	0.000	0.495
03:15	0.187	0.524	0.340	0.900	0.000	0.000	0.523
03:30	0.181	0.537	0.350	0.900	0.000	0.000	0.550
03:45	0.187	0.580	0.365	0.900	0.000	0.000	0.578
04:00	0.192	0.623	0.380	0.900	0.000	0.000	0.605
04:15	0.197	0.609	0.400	0.894	0.000	0.000	0.578
04:30	0.202	0.595	0.420	0.887	0.000	0.000	0.550
04:45	0.212	0.573	0.460	0.869	0.000	0.000	0.523
05:00	0.222	0.551	0.500	0.850	0.000	0.000	0.495
05:15	0.237	0.564	0.550	0.775	0.000	0.000	0.468
05:30	0.252	0.576	0.600	0.700	0.000	0.000	0.440
05:45	0.277	0.631	0.675	0.600	0.000	0.000	0.440
06:00	0.302	0.686	0.750	0.500	0.000	0.000	0.440
06:15	0.378	0.686	0.800	0.475	0.000	0.000	0.468
06:30	0.454	0.685	0.850	0.450	0.000	0.000	0.495
06:45	0.554	0.764	0.855	0.350	0.000	0.208	0.523
07:00	0.655	0.842	0.860	0.250	0.000	0.416	0.550
07:15	0.706	0.830	0.890	0.205	0.000	0.446	0.523
07:30	0.756	0.818	0.920	0.160	0.000	0.475	0.495
07:45	0.756	0.845	0.950	0.120	0.000	0.594	0.512
08:00	0.756	0.871	0.980	0.080	0.000	0.713	0.528
08:15	0.731	0.878	0.985	0.040	0.099	0.713	0.539
08:30	0.706	0.884	0.990	0.000	0.197	0.713	0.550
08:45	0.706	0.868	0.980	0.000	0.197	0.772	0.550
09:00	0.706	0.851	0.970	0.000	0.197	0.832	0.550
09:15	0.680	0.898	0.980	0.000	0.380	0.832	0.550
09:30	0.655	0.945	0.990	0.000	0.563	0.832	0.550
09:45	0.645	0.922	0.955	0.000	0.564	0.891	0.539
10:00	0.635	0.899	0.920	0.000	0.565	0.950	0.528
10:15	0.620	0.895	0.910	0.000	0.619	0.950	0.567
10:30	0.605	0.890	0.900	0.000	0.673	0.950	0.605
10:45	0.605	0.855	0.850	0.000	0.674	0.950	0.660
11:00	0.605	0.819	0.800	0.000	0.675	0.950	0.715
11:15	0.655	0.821	0.790	0.064	0.837	0.950	0.798
11:30	0.706	0.823	0.780	0.127	0.999	0.950	0.880

11:45	0.746	0.855	0.805	0.131	0.999	0.950	0.908
12:00	0.786	0.886	0.830	0.135	0.999	0.950	0.935
12:15	0.786	0.895	0.840	0.144	0.954	0.921	0.921
12:30	0.786	0.904	0.850	0.152	0.908	0.891	0.908
12:45	0.756	0.944	0.850	0.153	0.909	0.891	0.894
13:00	0.726	0.984	0.850	0.153	0.909	0.891	0.880
13:15	0.665	0.976	0.850	0.153	0.851	0.891	0.866
13:30	0.605	0.968	0.850	0.153	0.793	0.891	0.853
13:45	0.595	0.954	0.860	0.153	0.795	0.802	0.839
14:00	0.585	0.940	0.870	0.153	0.797	0.713	0.825
14:15	0.570	0.959	0.870	0.133	0.632	0.713	0.811
14:30	0.554	0.977	0.870	0.113	0.466	0.713	0.798
14:45	0.529	0.981	0.875	0.115	0.465	0.713	0.798
15:00	0.504	0.984	0.880	0.116	0.463	0.713	0.798
15:15	0.479	0.983	0.865	0.113	0.314	0.713	0.798
15:30	0.454	0.982	0.850	0.111	0.165	0.713	0.798
15:45	0.454	0.917	0.800	0.055	0.166	0.713	0.798
16:00	0.454	0.851	0.750	0.000	0.167	0.713	0.798
16:15	0.529	0.858	0.675	0.000	0.084	0.743	0.756
16:30	0.605	0.865	0.600	0.000	0.000	0.772	0.715
16:45	0.655	0.835	0.550	0.000	0.000	0.772	0.688
17:00	0.706	0.805	0.500	0.000	0.000	0.772	0.660
17:15	0.756	0.815	0.485	0.063	0.000	0.772	0.633
17:30	0.806	0.824	0.470	0.125	0.000	0.772	0.605
17:45	0.832	0.785	0.460	0.138	0.000	0.772	0.578
18:00	0.857	0.745	0.450	0.150	0.000	0.772	0.550
18:15	0.882	0.764	0.450	0.163	0.000	0.713	0.605
18:30	0.907	0.782	0.450	0.175	0.000	0.653	0.660
18:45	0.907	0.733	0.450	0.178	0.000	0.602	0.715
19:00	0.907	0.684	0.450	0.180	0.000	0.550	0.770
19:15	0.882	0.657	0.435	0.183	0.000	0.500	0.715
19:30	0.857	0.630	0.420	0.185	0.000	0.450	0.660
19:45	0.842	0.643	0.410	0.193	0.000	0.400	0.605
20:00	0.827	0.655	0.400	0.200	0.000	0.350	0.550
20:15	0.817	0.685	0.390	0.275	0.000	0.275	0.605
20:30	0.806	0.714	0.380	0.350	0.000	0.200	0.660
20:45	0.781	0.718	0.390	0.387	0.000	0.100	0.715
21:00	0.756	0.721	0.400	0.424	0.000	0.000	0.770
21:15	0.731	0.717	0.390	0.475	0.000	0.000	0.784
21:30	0.706	0.712	0.380	0.526	0.000	0.000	0.798
21:45	0.706	0.670	0.380	0.583	0.000	0.000	0.811
22:00	0.706	0.628	0.380	0.640	0.000	0.000	0.825
22:15	0.655	0.668	0.375	0.695	0.000	0.000	0.850
22:30	0.605	0.707	0.370	0.750	0.000	0.000	0.875
22:45	0.529	0.632	0.365	0.805	0.000	0.000	0.863
23:00	0.454	0.556	0.360	0.860	0.000	0.000	0.850
23:15	0.378	0.529	0.360	0.863	0.000	0.000	0.825
23:30	0.302	0.501	0.360	0.866	0.000	0.000	0.800
23:45	0.277	0.431	0.355	0.871	0.000	0.000	0.750
24.00	0.252	0.361	0.350	0.876	0.000	0.000	0.700

Table C.7: Week power coefficients for loads and generators [pu].

Day	RES	IND	COM	Evs	PV	CHP	WIND
Mon	0.846	0.870	0.693	0.840	0.636	0.800	0.636
Tue	0.859	0.956	0.706	0.856	0.610	0.800	0.610
Wed	0.864	0.989	0.731	0.878	0.631	0.800	0.631
Thu	0.864	0.989	0.734	0.857	0.685	0.800	0.685
Fri	0.862	0.972	0.719	0.801	0.716	0.800	0.716
Sat	0.833	0.128	0.978	0.352	0.707	0.000	0.707
Sun	0.762	0.111	0.361	0.301	0.637	0.000	0.637

Table C.8: Month power coefficients for loads and generators [pu].

Month	RES	IND	COM	Evs	PV	CHP	WIND
Gen	0.633	0.559	0.968	0.701	0.124	0.814	0.762
Feb	0.629	0.589	0.993	0.702	0.359	0.775	0.725
Mar	0.548	0.792	0.695	0.695	0.495	0.752	0.704
Apr	0.539	0.696	0.585	0.683	0.484	0.711	0.666
May	0.513	0.651	0.547	0.682	0.670	0.874	0.818
Jun	0.508	0.680	0.546	0.562	1.000	0.814	0.762
Jul	0.504	0.683	0.540	0.547	0.717	0.771	0.722
Aug	0.501	0.661	0.525	0.500	0.629	0.799	0.747
Sep	0.520	0.675	0.565	0.711	0.607	0.722	0.675
Oct	0.588	0.768	0.650	0.705	0.354	0.870	0.814
Nov	0.627	0.579	1.000	0.703	0.119	0.808	0.756
Dec	0.633	0.553	0.952	0.682	0.123	0.778	0.728

Table C.9: Year growth coefficients for loads [pu] (generators are supposed to be installed at fixed years for the long term analysis).

Month	RES	IND	COM	Evs
2010	1.000	1.000	1.000	1.000
2011	1.020	1.010	1.030	1.109
2012	1.040	1.020	1.061	1.198
2013	1.061	1.030	1.093	1.267
2014	1.082	1.041	1.126	1.288
2015	1.104	1.051	1.159	1.299
2016	1.126	1.062	1.194	1.315
2017	1.149	1.072	1.230	1.387
2018	1.172	1.083	1.267	1.408
2019	1.195	1.094	1.305	1.450
2020	1.219	1.105	1.344	1.500
2021	1.243	1.116	1.384	1.670
2022	1.268	1.127	1.426	1.789
2023	1.294	1.138	1.469	1.890
2024	1.319	1.149	1.513	1.960
2025	1.346	1.161	1.558	2.400
2026	1.373	1.173	1.605	2.509
2027	1.400	1.184	1.653	2.678
2028	1.428	1.196	1.702	2.803
2029	1.457	1.208	1.754	2.957
2030	1.486	1.220	1.806	3.1

Appendix D

Benchmark European LV network

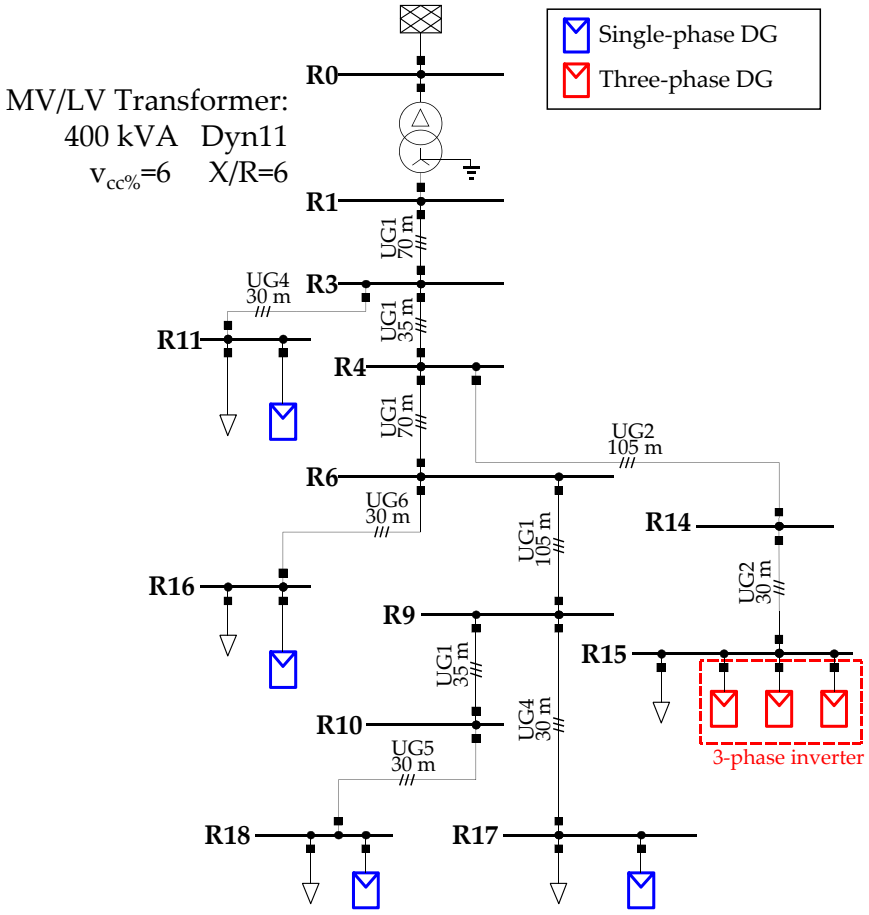

Figure D.1: Layout of the Benchmark European LV network.

Table D.1: Transformer's data for the European LV reference network.

V_{1n} [kV]	V_{2n} [kV]	S_n [MVA]	v_{cc} [%]	p_{cc} [%]	dU [%]	DB [%]	Tap range
20	0.4	0.4	6	1	-	-	-

Table D.2: Cables data in the European LV reference network.

Conductor	**Section [mm²]**	**R_{dc} [mm]**	**d_c [mm]**	**GMR [mm]**
1	240	0.162	17.500	6.710
2	150	0.265	13.800	5.310
3	120	0.325	12.400	4.750
4	70	0.568	9.440	3.680
5	35	1.110	6.680	2.600
6	25	1.540	5.640	2.200
7	16	1.150	5.100	1.986

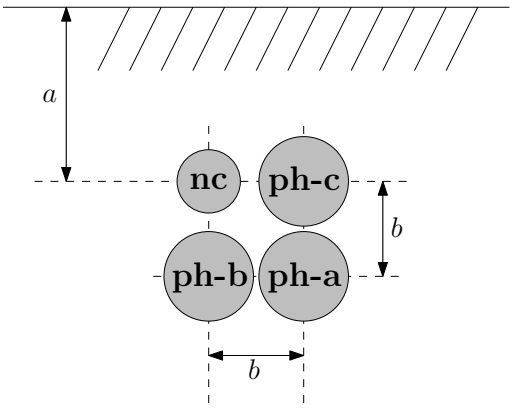

Figure D.2: Disposition of the four wires composing the three-phase lines in the European LV reference network.

Table D.3: LV network's branches composition and length in the European LV reference network.

Bus	**Bus**	**Conductor type**		***a***	***b***	**Length**
From	**To**	**phase**	**neutral**	[cm]	[cm]	[m]
R1	R3	1	2	100	5.2	70
R3	R4	1	2	100	5.2	35
R4	R6	1	2	100	5.2	70
R6	R9	1	2	100	5.2	105
R9	R10	1	2	100	5.2	35
R3	R11	6	7	100	2.4	30
R4	R14	2	3	100	4.2	105
R14	R15	2	3	100	4.2	30
R6	R16	4	5	100	3.2	30
R9	R17	6	7	100	2.4	30
R10	R18	5	7	100	2.6	30

Table D.4: Loads and Generators installed power in the European LV reference network [kVA].

Buses	**Loads**			**Generators**		
	ph a	ph b	ph c	ph a	ph b	ph c
R11	7.0	6.0	3.3	0.0	8.0	0.0
R15	20.4	30.0	30.0	10.0	10.0	10.0
R16	16.5	19.8	22.0	0.0	0.0	8.0
R17	3.6	5.0	7.0	8.0	0.0	0.0
R18	14.0	15.4	19.0	9.0	0.0	0.0
TOT	61.5	76.2	81.3	27.0	18.0	18.0
	(28%)	(35%)	(37%)	(42%)	(29%)	(29%)

Appendix E

MV and LV distribution network

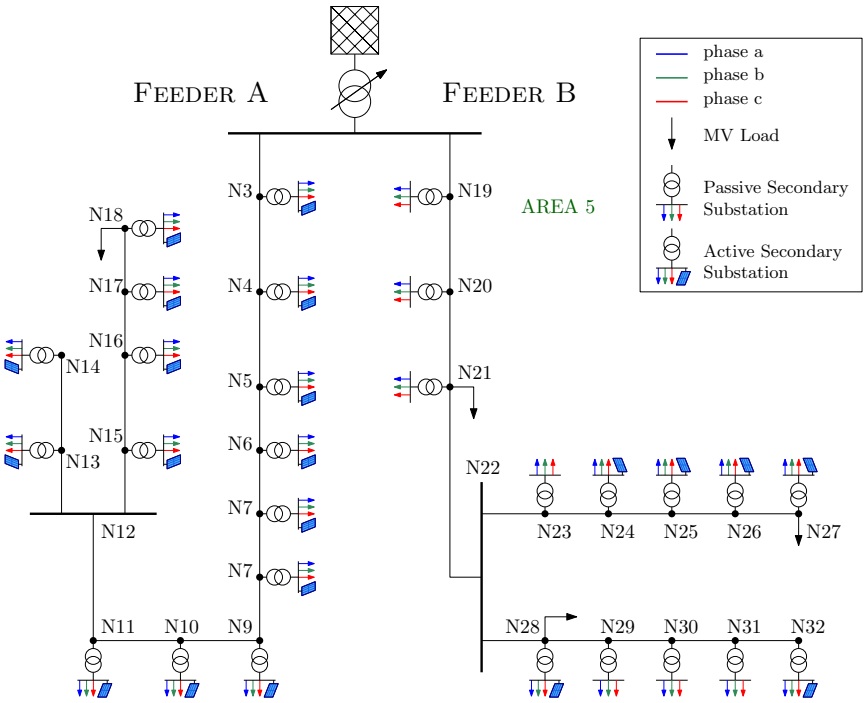

Figure E.1: Single phase diagram of the case study MV network with voltage control areas.

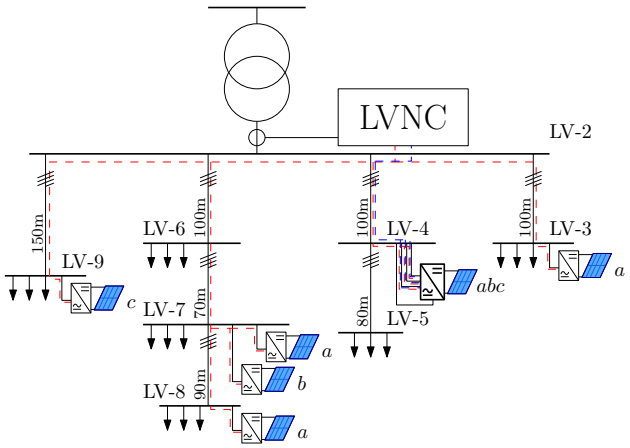

Figure E.2: Layout of the Low Voltage networks connected to the MV system.

Table E.1: Transformer's data for the MV and LV networks.

V_{1n} [kV]	V_{2n} [kV]	S_n [MVA]	v_{cc} [%]	p_{cc} [%]	dU [%]	DB [%]	Tap range
132	20	40	13	1	0.5	1.5	± 10
20	0.4	0.6	6	1	-	-	-

Table E.2: Line types' data for the MV 32-bus network.

Type	V_n [kV]	r [Ω/km]	x [Ω/km]	c [μF/km]	I_{max} [A]
MV type 1	20	0.200	0.314	0.007	360
MV type 2	20	0.300	0.361	0.009	300
MV type 3	20	0.300	0.360	0.015	240

Table E.3: Cable data for the LV 9-bus network.

Conductor	Section [mm^2]	R_{dc} [mm]	d_c [mm]	GMR [mm]
CU-50 mm^2	50	0.368	9.2	3.581

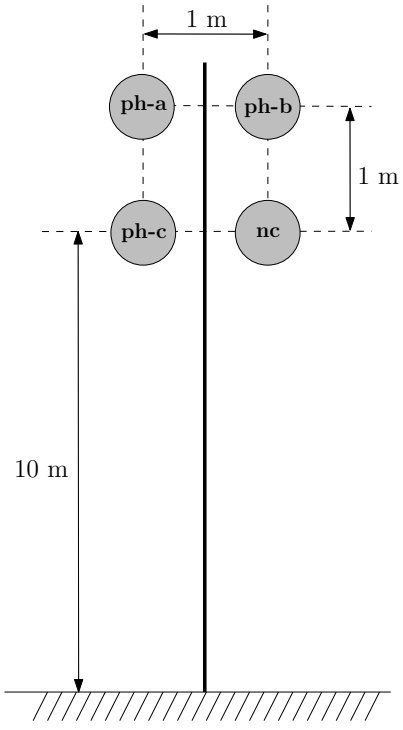

Figure E.3: Disposition of the four wires composing the three-phase lines in the LV 9-bus model.

Table E.4: 32-bus MV network's lines data.

From-Bus	To-Bus	Line Type	Length [km]
N2	N3	MV type 1	3.500
N3	N4	MV type 1	2.500
N4	N5	MV type 1	3.000
N5	N6	MV type 1	3.000
N6	N7	MV type 1	3.000
N7	N8	MV type 1	2.252
N8	N9	MV type 1	2.000
N9	N10	MV type 1	2.400
N10	N11	MV type 1	4.000
N11	N12	MV type 1	3.500
N12	N13	MV type 2	1.870
N13	N14	MV type 2	1.280
N12	N15	MV type 3	1.000
N15	N16	MV type 3	1.100
N16	N17	MV type 3	1.300
N17	N18	MV type 3	1.000
N2	N19	MV type 1	3.600
N19	N20	MV type 1	3.304
N20	N21	MV type 1	2.400
N21	N22	MV type 1	1.600
N22	N23	MV type 2	3.000
N23	N24	MV type 2	3.080
N24	N25	MV type 2	1.650
N25	N26	MV type 2	3.080
N26	N27	MV type 2	3.080
N22	N28	MV type 3	5.000
N28	N29	MV type 3	1.200
N29	N30	MV type 3	1.200
N30	N31	MV type 3	1.300
N31	N32	MV type 3	1.350

Table E.5: 9-bus LV network's lines data.

From-Bus	To-Bus	Line Type	Length [km]
LV-2	LV-3	LV type	0.100
LV-2	LV-4	LV type	0.100
LV-4	LV-5	LV type	0.080
LV-2	LV-6	LV type	0.100
LV-6	LV-7	LV type	0.070
LV-7	LV-8	LV type	0.080
LV-2	LV-9	LV type	0.150

Table E.6: Total load and generator installed power, as seen at the MV/LV transformers on the MV 32-bus network [kVA].

Bus	**Load**			**Generation**		
	phase a	phase b	phase c	phase a	phase b	phase c
N3	124.9	159.6	145.8	296.7	326.4	332.3
N4	138.0	176.4	161.1	316.5	348.1	354.5
N5	70.7	90.4	82.5	158.4	174.2	177.4
N6	187.4	239.4	218.6	593.4	652.8	664.6
N7	40.6	51.9	47.4	118.8	130.7	133.1
N8	121.8	155.6	142.1	237.4	261.1	265.9
N9	34.1	43.6	39.8	79.2	87.1	88.7
N10	86.1	110.0	100.4	158.2	174.1	177.2
N11	34.1	43.6	39.8	118.8	130.7	133.1
N13	35.8	45.7	41.7	59.4	65.3	66.5
N14	32.5	41.6	37.9	59.4	65.3	66.5
N15	28.5	36.4	33.2	79.2	87.1	88.7
N16	150.2	192.0	175.3	395.6	435.2	443.1
N17	109.6	140.1	127.9	316.5	348.1	354.5
N18	295.5	331.3	317.0	297.0	326.7	332.6
N19	142.0	181.5	165.7	0.0	0.0	0.0
N20	169.5	216.6	197.7	0.0	0.0	0.0
N21	860.4	914.2	892.6	0.0	0.0	0.0
N23	290.3	370.9	338.6	0.0	0.0	0.0
N24	96.9	123.8	113.0	33.0	36.3	37.0
N25	129.1	165.0	150.7	49.5	54.5	55.4
N26	189.2	241.7	220.7	65.9	72.5	73.9
N27	1029.9	1130.7	1090.4	395.6	435.2	443.1
N28	1220.3	1327.8	1284.8	263.7	290.1	295.4
N29	217.7	278.2	254.0	0.0	0.0	0.0
N30	241.2	308.2	281.4	0.0	0.0	0.0
N31	241.9	309.1	282.2	0.0	0.0	0.0
N32	111.3	142.2	129.8	263.7	290.1	295.4
TOT	6429.4	7567.2	7112.0	4356.0	4791.6	4878.7

Table E.7: Load and generation rated power per phase in the LV 9-bus network [kVA].

Bus	**Load**			**Generation**		
	phase a	phase b	phase c	phase a	phase b	phase c
LV-3	20	15	20	20	0	0
LV-4	11	20	25	50	50	50
LV-5	15	17	20	0	0	0
LV-6	14	16	10	0	0	0
LV-7	15	20	30	16	0	0
LV-8	20	16	25	20	10	0
LV-9	15	18	20	0	0	10
TOT	110	122	150	106	60	60

Bibliography

[1] IEA-PVPS, "Trends 2015 in photovoltaic applications - survey report of selected iea countries between 1992 and 2014," *Report IEA-PVPS T1-27*, 2015.

[2] Gestore Serivizi Energetici (GSE), "Statistical report on solar photovoltaic," 2014, in Italian. [Online]. Available: http://www.gse.it/it/Statistiche/RapportiStatistici/Pagine/default.aspx

[3] T. Stetz, M. Rekinger, and I. Theologitis, "Transition from uni directional to bi directional distribution grids," *IEA PVPS Task 14 Task Report*, November 2014. [Online]. Available: http://www.iea-pvps.org/

[4] CEI Comitato Elettrotecnico Italiano, "Technical standard-CEI 0-21; Variante V1, Reference technical rules for the connection of active and passive users to the LV electrical utilities," December 2014, (in Italian).

[5] C. F. Covrig, M. Ardelean, J. Vasiljevska, A. Mengolini, G. Fulli, E. Amoiralis, M. S. Jiménez, and C. Filiou, "Smart grid projects outlook 2014," *JRC Science and Policy Reports*, 2014.

[6] Solar Power Europe, "Global market outlook for solar power / 2015 - 2019." [Online]. Available: http://www.solarpowereurope.org/

[7] Y. Yang, P. Enjeti, F. Blaabjerg, and H. Wang, "Wide-scale adoption of photovoltaic energy: Grid code modifications are explored in the distribution grid," *Industry Applications Magazine, IEEE*, vol. 21, no. 5, pp. 21–31, 2015.

[8] J. P. Lopes, N. Hatziargyriou, J. Mutale, P. Djapic, and N. Jenkins, "Integrating distributed generation into electric power systems: A review of drivers, challenges and opportunities," *Electric power systems research*, vol. 77, no. 9, pp. 1189–1203, 2007.

[9] CEI Comitato Elettrotecnico Italiano, "Technical standard-CEI 0-21, Reference technical rules for the connection of active and passive users to the LV electrical Utilities," September 2014, (in Italian).

[10] CEI Comitato Elettrotecnico Italiano, "Technical standard-CEI 0-16, Reference technical rules for the connection of active and passive consumers to the HV and MV electrical networks of distribution Company," September 2014, (in Italian).

[11] VDE, "VDE-AR-N 4105: Power generation systems connected to the low-voltage distribution network. Technical minimum requirements for the connection to and parallel operation with low-voltage distribution networks." August 2011.

[12] BDEW, "Technical guideline: Generating plants connected to the medium-voltage network. guideline for generating plants' connection to and parallel operation with the medium-voltage network," June 2008.

[13] CENELEC, "EN 50438 Requirements for micro-generating plants to be connected in parallel with public low-voltage distribution networks," December 2013.

[14] CENELEC, "CLC/TS 50549-1 Requirements for the connection of a generating plant to a distribution system - Part 1: Connection to a LV distribution system and above 16 A," January 2015.

[15] CENELEC, "CLC/TS 50549-2 Requirements for the connection of a generating plant to a distribution system - Part 2: Connection to a MV distribution system," January 2015.

[16] VDE-FNN, "The 50.2 Hz problem - Conclusion of the study on the 50.2 Hz shutdown of PV systems in the low voltage distribution network." [Online]. Available: https://www.vde.com/en/fnn/pages/50-2-hz-study.aspx

[17] R. Bründlinger, T. Strasser, G. Lauss, A. Hoke, S. Chakraborty, G. Martin, B. Kroposki, J. Johnson, and E. de Jong, "Lab tests: Verifying that smart grid power converters are truly smart," *Power and Energy Magazine, IEEE*, vol. 13, no. 2, pp. 30–42, March 2015.

[18] A. A. Bayod-Rújula, "Future development of the electricity systems with distributed generation," *Energy*, vol. 34, no. 3, pp. 377–383, 2009.

[19] Department of Energy & Climate Change, OFGEM, "Smart grid vision and routemap," 2014. [Online]. Available: https://www.ofgem.gov.uk/electricity/distribution-networks/forums-seminars-and-working-groups/decc-and-ofgem-smart-grid-forum

[20] Liz Sidebotham, Northern Powergrid, "Customer-led network revolution, project closedown report," 2015. [Online]. Available: http://www.smarternetworks.org/

[21] Scottish Power Energy Networks, "ARC - Accelerating Renewable Connections Full Submission," 2013. [Online]. Available: http://www.smarternetworks.org/

[22] Italian Authority for Electricity Gas and Water (AEEGSI in Italian), "Pubblico dibattito per la riforma delle modalità di approvvigionamento delle risorse per il servizio di dispacciamento, con particolare riferimento agli impianti di generazione distribuita e agli impianti alimentati dalle fonti rinnovabili non programmabili," August 2013, (in Italian). [Online]. Available: http://www.autorita.energia.it/it/docs/dc/13/354-13.jsp

[23] J. A. Martinez and J. Mahseredjian, "Load flow calculations in distribution systems with distributed resources. a review," in *IEEE Power and Energy Society General Meeting*, 2011, pp. 1–8.

[24] R. Berg, E. S. Hawkins, and W. W. Pleines, "Mechanized calculation of unbalanced load flow on radial distribution circuits," *Power Apparatus and Systems, IEEE Transactions on*, vol. PAS-86, no. 4, pp. 415–421, 1967.

[25] D. Shirmohammadi, H. W. Hong, A. Semlyen, and G. X. Luo, "A compensation-based power flow method for weakly meshed distribution and transmission networks," *Power Systems, IEEE Transactions on*, vol. 3, no. 2, pp. 753–762, 1988.

[26] C. S. Cheng and D. Shirmohammadi, "Three-phase power flow method for real-time distribution system analysis," *IEEE Transactions on Power Systems*, vol. 10, no. 2, pp. 671–679, 1995.

[27] R. M. Ciric, A. P. Feltrin, and L. F. Ochoa, "Power flow in four-wire distribution networks-general approach," *Power Systems, IEEE Transactions on*, vol. 18, no. 4, pp. 1283–1290, 2003.

[28] A. Ulinuha, M. Masoum, and S. Islam, "Unbalance power flow calculation for a radial distribution system using forward-backward propagation algorithm," in *Power Engineering Conference, 2007. AUPEC 2007. Australasian Universities.* IEEE, 2007, pp. 1–6.

[29] J. Subrahmanyam, "Load flow solution of unbalanced radial distribution systems," *Department of Elecrical and Electronics Engg, BRECW, Hyderabad, AP, India-500*, vol. 59, 2009.

[30] S. Mishra, "A simple algorithm for unbalanced radial distribution system load flow," in *TENCON 2008 - 2008 IEEE Region 10 Conference*, 2008, pp. 1–6.

[31] M. E. Baran and F. F. Wu, "Optimal sizing of capacitors placed on a radial distribution system," *Power Delivery, IEEE Transactions on*, vol. 4, no. 1, pp. 735–743, 1989.

[32] D. R. R. Penido, L. R. Araujo, J. L. R. Pereira, P. A. N. Garcia, and S. Carneiro, "Four wire newton-raphson power flow based on the current injection method," in

Power Systems Conference and Exposition, 2004. IEEE PES, 2004, pp. 239–242 vol.1.

[33] D. R. R. Penido, L. R. de Araujo, S. C. Jr., J. L. R. Pereira, and P. A. N. Garcia, "Three-phase power flow based on four-conductor current injection method for unbalanced distribution networks," *IEEE Transactions on Power Systems*, vol. 23, no. 2, pp. 494–503, 2008.

[34] T. H. Chen, M.-S. Chen, K. J. Hwang, P. Kotas, and E. A. Chebli, "Distribution system power flow analysis-a rigid approach," *Power Delivery, IEEE Transactions on*, vol. 6, no. 3, pp. 1146–1152, 1991.

[35] T.-H. Chen and N.-C. Yang, "Loop frame of reference based three-phase power flow for unbalanced radial distribution systems," *Electric Power Systems Research*, vol. 80, no. 7, pp. 799–806, 7 2010.

[36] J. C. M. V. Jr., W. Freitas, and A. Morelato, "Phase-decoupled method for three-phase power-flow analysis of unbalanced distribution systems," *Generation, Transmission and Distribution, IEE Proceedings-*, vol. 151, no. 5, pp. 568–574, 2004.

[37] R. C. Dugan and T. E. McDermott, "An open source platform for collaborating on smart grid research," in *Power and Energy Society General Meeting, 2011 IEEE*, 2011, pp. 1–7.

[38] K. P. Schneider, D. Chassin, Y. Chen, and J. C. Fuller, "Distribution power flow for smart grid technologies," in *Power Systems Conference and Exposition, 2009. PSCE '09. IEEE/PES*, 2009, pp. 1–7.

[39] R. Benato, A. Paolucci, and R. Turri, "Power flow solution by a complex admittance matrix method," *European Transactions On Electrical Power*, vol. 11, no. 3, pp. 181–188, 2001.

[40] K. Sunderland, M. Coppo, M. F. Conlon, and R. Turri, "Application of a correction current injection power flow algorithm to an unbalanced 4-wire distribution network incorporating tn-c-s earthing," in *Power Engineering Conference (UPEC), 2013 48th International Universities'*, 2013, pp. 1–6.

[41] K. Sunderland, M. Coppo, M. Conlon, and R. Turri, "A correction current injection method for power flow analysis of unbalanced multiple-grounded 4-wire distribution networks," *Electric Power Systems Research*, vol. 132, pp. 30–38, 2016.

[42] M. Albano, R. Turri, S. Dessanti, A. Haddad, H. Griffiths, and B. Howat, "Computation of the electromagnetic coupling of parallel untransposed power lines," in *Universities Power Engineering Conference, 2006. UPEC '06. Proceedings of the 41st International*, vol. 1, 2006, pp. 303–307.

[43] P. Arboleya, C. Gonzalez-Moran, and M. Coto, "Unbalanced power flow in distribution systems with embedded transformers using the complex theory in stationary reference frame," *Power Systems, IEEE Transactions on*, vol. 29, no. 3, pp. 1012–1022, 2014.

[44] M. Abdel-Akher, K. M. Nor, and A. H. A. Rashid, "Improved three-phase power-flow methods using sequence components," *IEEE Transactions on Power Systems*, vol. 20, no. 3, pp. 1389–1397, 2005.

[45] T. H. Chen and J. D. Chang, "Open wye-open delta and open delta-open delta transformer models for rigorous distribution system analysis," *IEE Proceedings C Generation, Transmission and Distribution*, vol. 139, no. 3, pp. 227–234, 1992.

[46] R. M. del Vecchio, "Multiterminal three phase transformer model with balanced or unbalanced loading," *IEEE Transactions on Power Delivery*, vol. 23, no. 3, pp. 1439–1447, 2008.

[47] S. S. Moorthy and D. Hoadley, "A new phase-coordinate transformer model for ybus analysis," *IEEE Transactions on Power Systems*, vol. 17, no. 4, pp. 951–956, 2002.

[48] R. C. Dugan and S. Santoso, "An example of 3-phase transformer modeling for distribution system analysis," *Proceedings of the IEEE Power Engineering Society Transmission and Distribution Conference*, vol. 3, pp. 1028–1032, 2003.

[49] T. H. Chen and H. Y. Kuo, "Network modelling of traction substation transformers for studying unbalance effects," *IEE Proceedings- Generation, Transmission and Distribution*, vol. 142, no. 2, pp. 103–108, 1995.

[50] Esb networks distribution code. [Online]. Available: http://www.esb.ie/esbnetworks/en/downloads/Distribution-Code.pdf

[51] R. M. D. Service. Standard load profiles. [Online]. Available: http://www.rmdservice.com/guidance/standard_load_profiles.htm

[52] M. H. J. Bollen, "Definitions of voltage unbalance," *IEEE Power Engineering Review*, vol. 22, no. 11, pp. 49–50, 2002.

[53] P. Pillay and M. Manyage, "Definitions of voltage unbalance," *IEEE Power Engineering Review*, pp. 50–51, 2001.

[54] M. Coppo, R. Turri, M. Marinelli, and X. Han, "Voltage management in unbalanced low voltage networks using a decoupled phase-tap-changer transformer," in *Power Engineering Conference (UPEC), 2014 49th International Universities*, 2014, pp. 1–6.

[55] Siemens AG. Fitformer® reg. [Online]. Available: http://www.energy.siemens.com/hq/en/power-transmission/transformers/distribution-transformers/distribution/fit-former-reg.htm

[56] M. Stifter, B. Bletterie, H. Brunner, D. Burnier, H. Sawsan, F. Andren, R. Schwalbe, A. Abart, R. Nenning, F. Herb, and R. Pointner, "Dg demonet validation: Voltage control from simulation to field test," in *Innovative Smart Grid Technologies (ISGT Europe), 2011 2nd IEEE PES International Conference and Exhibition on*, 2011, pp. 1–8.

[57] W. Khamphanchai, M. Kuzlu, and M. Pipattanasomporn, "A smart distribution transformer management with multi-agent technologies," in *Innovative Smart Grid Technologies (ISGT), 2013 IEEE PES*, Feb 2013, pp. 1–6.

[58] T. Vandoorn, J. D. M. De Kooning, B. Meersman, J. Guerrero, and L. Vandevelde, "Voltage-based control of a smart transformer in a microgrid," *IEEE Transactions on Industrial Electronics*, vol. 60, no. 4, pp. 1291–1305, 2013.

[59] I. Roasto, E. Romero-Cadaval, J. Martins, and T. Jalakas, "Active power electronic transformer as a power conditioner for nonlinear loads," in *Compatibility and Power Electronics (CPE), 2013 8th International Conference on*, 2013, pp. 63–68.

[60] X. Han, S. You, F. Thordarson, D. V. Tackie, S. M. Ostberg, O. M. Pedersen, H. W. Bindner, and N. C. Nordentoft, "Real-time measurements and their effects on state estimation of distribution power system," in *Innovative Smart Grid Technologies Europe (ISGT EUROPE), 2013 4th IEEE/PES*, 2013, pp. 1–5.

[61] A. Zecchino, M. Marinelli, M. Coppo, J. Hu, and R. Turri, "Voltage and reactive power control in an unbalanced active low voltage grid using a decoupled phase on-load-tap-changer transformer and photovoltaic inverters," in *Power Engineering Conference (UPEC), 2015 50th International Universities'*. IEEE, 2015, pp. 1–6.

[62] J. Hu, M. Marinelli, M. Coppo, A. Zecchino, and H. W. Bindner, "Coordinated voltage control of a decoupled three-phase on-load tap changer transformer and photovoltaic inverters for managing unbalanced networks," *Electric Power Systems Research*, vol. 131, pp. 264–274, 2 2016.

[63] Syslab-powerlabdk. [Online]. Available: http://www.powerlab.dk/facilities/syslab.aspx

[64] E. Haesen, A. D. Alarcon-Rodriguez, J. Driesen, R. Belmans, and G. Ault, "Opportunities for active der management in deferral of distribution system reinforcements," in *Power Systems Conference and Exposition, 2009. PSCE '09. IEEE/PES*, 2009, pp. 1–8.

[65] A. Kulmala, S. Repo, and P. Jarventausta, "Coordinated voltage control in distribution networks including several distributed energy resources," *Smart Grid, IEEE Transactions on*, vol. PP, no. 99, pp. 1–11, 2014.

[66] F. Pilo, G. Pisano, and G. G. Soma, "Optimal coordination of energy resources with a two-stage online active management," *Industrial Electronics, IEEE Transactions on*, vol. 58, no. 10, pp. 4526–4537, 2011.

[67] F. Silvestro, A. Baitch, F. Pilo, B. B. Jensen, M. Fan, G. Pisano, P. Georgilakis, N. Hatziargyriou, and G. Petretto, "Demand side integration aspects in active distribution planning," in *Electricity Distribution (CIRED 2013), 22nd International Conference and Exhibition on*, 2013, pp. 1–4.

[68] F. Pilo, G. Pisano, S. Ruggeri, S. Scalari, D. D. Canto, G. Petretto, A. Testa, R. Langella, L. Feola, R. Caldon, R. Turri, and M. Coppo, "Applications of dms in the atlantide project: Models and tools," in *Electricity Distribution (CIRED 2013), 22nd International Conference and Exhibition on*, 2013, pp. 1–5.

[69] G. Celli, F. Pilo, G. Pisano, and G. G. Soma, "Optimal operation of active distribution networks with distributed energy storage," in *Energy Conference and Exhibition (ENERGYCON), 2012 IEEE International*, 2012, pp. 557–562.

[70] G. Carpinelli, G. Celli, S. Mocci, F. Mottola, F. Pilo, and D. Proto, "Optimal integration of distributed energy storage devices in smart grids," *IEEE Transactions on Smart Grid*, vol. 4, no. 2, pp. 985–995, 2013.

[71] S. D. J. McArthur, E. M. Davidson, V. M. Catterson, A. L. Dimeas, N. D. Hatziargyriou, F. Ponci, and T. Funabashi, "Multi-agent systems for power engineering applications—part i: Concepts, approaches, and technical challenges," *Power Systems, IEEE Transactions on*, vol. 22, no. 4, pp. 1743–1752, 2007.

[72] M. E. Baran and I. M. El-Markabi, "A multiagent-based dispatching scheme for distributed generators for voltage support on distribution feeders," *Power Systems, IEEE Transactions on*, vol. 22, no. 1, pp. 52–59, 2007.

[73] P. H. Nguyen, J. M. A. Myrzik, and W. L. Kling, "Coordination of voltage regulation in active networks," *Transmission and Distribution Conference and Exposition*, pp. 1–6, 2008.

[74] A. D. Dominguez-Garcia and C. N. Hadjicostis, "Distributed algorithms for control of demand response and distributed energy resources," in *Decision and Control and European Control Conference (CDC-ECC), 2011 50th IEEE Conference on*, 2011, pp. 27–32.

[75] A. D. Dominguez-Garcia and C. N. Hadjicostis, "Coordination and control of distributed energy resources for provision of ancillary services," in *Smart Grid Communications (SmartGridComm), 2010 First IEEE International Conference on*, 2010, pp. 537–542.

[76] A. D. Dominguez-Garcia, S. T. Cady, and C. N. Hadjicostis, "Decentralized optimal dispatch of distributed energy resources," in *Decision and Control (CDC), 2012 IEEE 51st Annual Conference on*, 2012, pp. 3688–3693.

[77] G. Zhabelova and V. Vyatkin, "Multiagent smart grid automation architecture based on iec 61850/61499 intelligent logical nodes," *IEEE Transactions on Industrial Electronics*, vol. 59, no. 5, pp. 2351–2362, 2012.

[78] A. Tanenbaum, *Reti di calcolatori.* Pearson Education Italia, 2003. Italian Book.

[79] A. Kumar, S. C. Srivastava, and S. N. Singh, "A zonal congestion management approach using ac transmission congestion distribution factors," *IEEE Transactions on Power Systems*, vol. 19, no. 1, pp. 554–562, 2004.

[80] S. Satsangi, A. Saini, and A. Saraswat, "Clustering based voltage control areas for localized reactive power management in deregulated power system," *Int.J.of Electrical and Computer Engineering (IJECE)*, vol. 6, no. 1, pp. 21–27, 2010.

[81] J. Zhong, E. Nobile, A. Bose, and K. Bhattacharya, "Localized reactive power markets using the concept of voltage control areas," in *Power Engineering Society General Meeting, 2006. IEEE*, 2006, p. 1 pp., iD: 1.

[82] F. Pilo, G. Pisano, S. Scalari, D. D. Canto, A. Testa, R. Langella, R. Caldon, and R. Turri, "Atlantide — digital archive of the italian electric distribution reference networks," in *Integration of Renewables into the Distribution Grid, CIRED 2012 Workshop*, 2012, pp. 1–4.

[83] A. Bracale, R. Caldon, G. Celli, M. Coppo, D. D. Canto, R. Langella, G. Petretto, F. Pilo, G. Pisano, D. Proto, S. Scalari, and R. Turri, "Analysis of the italian distribution system evolution through reference networks," in *Innovative Smart Grid Technologies (ISGT Europe), 2012 3rd IEEE PES International Conference and Exhibition on*, 2012, pp. 1–8.

[84] F. Pilo, G. Pisano, S. Ruggeri, S. Scalari, D. D. Canto, G. Petretto, A. Testa, R. Langella, L. Feola, R. Caldon, R. Turri, and M. Coppo, "Applications of dms in the atlantide project: Models and tools," in *Electricity Distribution (CIRED 2013), 22nd International Conference and Exhibition on*, 2013, pp. 1–5.

[85] F. Pilo, M. Coppo, G. Pisano, G. Soma, and R. Turri, "Cooperative centralised and decentralised energy management systems for active networks," in *Electricity Distribution (CIRED 2015), 23nd International Conference and Exhibition on*, 2015.

[86] E. Demirok, D. Sera, P. Rodriguez, and R. Teodorescu, "Enhanced local grid voltage support method for high penetration of distributed generators," in *IECON 2011 - 37th Annual Conference on IEEE Industrial Electronics Society*, 2011, pp. 2481–2485, iD: 2.

[87] W. H. Kersting and W. H. Phillips, "Phase frame analysis of the effects of voltage unbalance on induction machines," *IEEE Transactions on Industry Applications*, vol. 33, no. 2, pp. 415–420, 1997.

[88] L. Sainz, J. Pedra, and J. J. Mesas, "Study of neutral conductor current in three-phase networks with single-phase converters," *IEEE Transactions on Power Delivery*, vol. 21, no. 3, pp. 1466–1476, 2006.

[89] E. Zraik and S. Y. Park, "Influence of voltage unbalance due to single phase distributed generators in the power distribution systems," in *North American Power Symposium (NAPS), 2013*, 2013, pp. 1–6, iD: 5.

[90] F. Wang, J. L. Duarte, and M. A. M. Hendrix, "Reconfiguring grid interfacing converters for power quality improvement," in *Proceedings 2008 - 4th IEEE BeNeLux Young Researchers Symposium in Electrical Power Engineering*, 2008.

[91] S. Seguí-Chilet, F. J. G. Sales, S. Orts, G. Garcerá, E. Figueres, M. Alcañiz, and R. Masot, "Approach to unbalance power active compensation under linear load unbalances and fundamental voltage asymmetries," *International journal of electrical power and energy systems*, vol. 29, no. 7, pp. 526–539, 2007.

[92] A. Chidurala, T. K. Saha, and N. Mithulananthan, "Power quality enhancement in unbalanced distribution network using solar-dstatcom," in *Power Engineering Conference (AUPEC), 2013 Australasian Universities*, 2013, pp. 1–6, iD: 3.

[93] K. H. Chua, Y. Lim, P. Taylor, S. Morris, and J. Wong, "Energy storage system for mitigating voltage unbalance on low-voltage networks with photovoltaic systems," *IEEE Transactions on Power Delivery*, vol. 27, no. 4, pp. 1783–1790, 2012.

[94] B. Meersman, B. Renders, L. Degroote, T. Vandoorn, and L. Vandevelde, "Control design of grid-connected three-phase inverters for voltage unbalance correction," in *Universities Power Engineering Conference (UPEC), 2009 Proceedings of the 44th International*, 2009, pp. 1–5.

[95] W. Sinsukthavorn, E. Ortjohann, A. Mohd, N. Hamsic, and D. Morton, "Control strategy for three-/four-wire-inverter-based distributed generation," *Industrial Electronics, IEEE Transactions on*, vol. 59, no. 10, pp. 3890–3899, 2012.

[96] P. Tenti, D. Trombetti, E. Tedeschi, and P. Mattavelli, "Compensation of load unbalance, reactive power and harmonic distortion by cooperative operation of distributed

compensators," in *Power Electronics and Applications, 2009. EPE '09. 13th European Conference on*, 2009, pp. 1–10.

[97] P. Tenti, A. Costabeber, and P. Mattavelli, "Improving power quality and distribution efficiency in micro-grids by cooperative control of switching power interfaces," in *Power Electronics Conference (IPEC), 2010 International*, 2010, pp. 472–479.

[98] L. S. Czarnecki and P. M. Haley, "Unbalanced power in four-wire systems and its reactive compensation," *Power Delivery, IEEE Transactions on*, vol. 30, no. 1, pp. 53–63, 2015.

[99] A. G. Madureira and J. A. P. Lopes, "Ancillary services market framework for voltage control in distribution networks with microgrids," *Electric Power Systems Research*, vol. 86, pp. 1–7, 2012.

[100] P. Wang, D. H. Liang, J. Yi, P. F. Lyons, P. J. Davison, and P. C. Taylor, "Integrating electrical energy storage into coordinated voltage control schemes for distribution networks," *Smart Grid, IEEE Transactions on*, vol. 5, no. 2, pp. 1018–1032, 2014.

[101] R. Caldon, M. Coppo, and R. Turri, "Voltage unbalance compensation in lv networks with inverter interfaced distributed energy resources," in *Energy Conference and Exhibition (ENERGYCON), 2012 IEEE International*, 2012, pp. 527–532.

[102] S. P. Oe, E. Christopher, M. Sumner, S. Pholboon, M. Johnson, and S. A. Norman, "Microgrid unbalance compensator - mitigating the negative effects of unbalanced microgrid operation," in *Innovative Smart Grid Technologies Europe (ISGT EUROPE), 2013 4th IEEE/PES*, 2013, pp. 1–5.

[103] A. Costabeber, P. Tenti, and P. Mattavelli, "Distributed cooperative control of low-voltage residential microgrids," in *Power Electronics for Distributed Generation Systems (PEDG), 2012 3rd IEEE International Symposium on*, 2012, pp. 457–463.

[104] P. Tenti, P. Mattavelli, and E. Tedeschi, "Compensation techniques based on reactive power conservation," *Electrical Power Quality and Utilisation, Journal*, vol. 13, pp. 17–24, 2007.

[105] R. Caldon, M. Coppo, A. Raciti, and R. Turri, "Exploiting inverter-interfaced dg for voltage unbalance mitigation and ancillary services in distribution systems," in *1st International Forum on Research and Technologies for Society and Industry (RTSI)*. IEEE, 2015.

[106] Task Force C6.04.02, "Benchmark systems for network intergration of renewable and distributed energy resources," Cigré, Tech. Rep., 2011.

[107] M. H. Gomes and J. T. Saraiva, "Allocation of reactive power support, active loss balancing and demand interruption ancillary services in microgrids," *Electric Power Systems Research*, vol. 80, no. 10, pp. 1267–1276, 10 2010.

[108] R. Caldon, M. Coppo, and R. Turri, "Coordinated voltage control in mv and lv distribution networks with inverter-interfaced users," in *2013 IEEE Grenoble Conference PowerTech, POWERTECH 2013*, 2013, pp. 1–5.